POLITECNICO DI TORINO

Master of Science in Automotive Engineering

Master Thesis

Numerical analysis of the direct injection and combustion processes in a spark ignition hydrogen internal combustion engine

Supervisors:

prof. Federico MILLO

prof. Andrea PIANO

Candidate:

Matteo GRITTI

October 2023

Ringraziamenti

Desidero ringraziare in primis mia Mamma e mio Papà per tutti i sacrifici che hanno fatto per permettermi di scegliere dove e come indirizzare la mia vita; sarà mio piacere e orgoglio poterveli ripagare uno ad uno. Non avete mai smesso di credere in me e così facendo mi avete dato la forza necessaria per andare sempre avanti, anche quando le situazioni non erano delle migliori.

Un grazie lo devo pure alla mia "sorellina", sebbene non siamo soliti ad essere troppo affettuosi tra di noi, sappi che sei stata fondamentale per la mia crescita personale, perché ho sempre cercato di essere il miglior esempio possibile di fratello maggiore per te; spero di esserci riuscito.

Grazie Sem, per essere te, non cambiare mai.

Grazie Belle, per i consigli dati, per le chiacchierate fatte e per l'esempio di sorella maggiore che sei sempre stata quando serviva.

Un ringraziamento va anche a tutto il resto della mia famiglia (Nonna Lorenza, Nonna Marisa, Nonno Elia, Zia Manuela, Zio Roberto, Zia Stefania, Andre), che è da sempre il mio porto sicuro.

Grazie a tutti i miei amici, dal primo all'ultimo, perché sempre disponibili a regalarmi attimi di distrazione quando necessario. In particolare grazie dal profondo del cuore Achi, Berto, Dado e Rolle; voi più di chiunque altro vi siete subiti i miei momenti più "no" per poi darmi la forza per uscirne. Siete, e sempre sarete, le persone che vorrò al mio fianco per festeggiare i miei traguardi così da renderli ancora più belli.

Grazie Antonio, Francesco, Jacopo e Nicola per aver reso leggeri gli anni della magistrale e per avermi accompagnato in questo viaggio che senza di voi non sarebbe stato lo stesso.

Infine un grazie speciale al prof. Federico Millo che mi ha dato la possibilità di collaborare con lui per l'attività di tesi. In contemporanea desidero ringraziare anche il prof. Andrea Piano, Francesco Pucillo e Salvatore Roggio per avermi costantemente seguito durante l'attività permettendomi di imparare tanto. Un grazie in generale va a tutto il gruppo e3 che mi ha accolto e fatto sentire a mio agio fin da subito.

Grazie davvero a tutti, a chi c'è sempre stato e a chi non c'è più, vi porto nel cuore.

Ora si cambia capitolo, quindi tocca rimboccarsi le maniche e "a TUTTA", pota!

Index

Abstract

In the current context of actions needed to counter climate change, the continuous tightening of CO_2 and criteria pollutant emissions limits is considered to be a pivotal challenge to the mobility sector. Different potential technological solutions are being explored to face this scenario. The vast research area ranges from the implementation of electrification in powertrains, also considering exclusively electrified ones, to the continuous development of the internal combustion engine (ICE) hardware. Focusing on the latter, among the technological solutions investigated, different fuel typologies are currently under examination to substitute fossil-derived fuels. In this environment, hydrogen is recognized to be particularly interesting, thanks to its combustion properties: high flame propagation speed and wide flammability range, which allow lean combustion, and good knock resistance. However, its low density and high diffusivity imply that the evolution of the in-chamber injection process is well controlled to obtain the best possible mixture conditions at the spark plug surroundings to guarantee relevant efficiency and power levels minimizing nitrogen oxide (NOx) emissions.

In this context, the present study aims to analyze the potentialities of a direct injection hydrogen-fueled internal combustion engine. The engine in exam was derived from a 6-cylinder, 3 L diesel engine, equipped with a new dedicated piston bowl according to the results obtained from previous studies.

First, the activity focused on the simulation and analysis of the injection and combustion processes of a set of operating points in a 3D-CFD environment by means of the *CONVERGE CFD* software. After that, the results, analyzed to understand the effect of different injection timings and lambda values on the mixture homogenization and the combustion process, allowed the calibration of a turbulence model and subsequently of a predictive combustion model (*SI-Turb*) in a 1D-CFD environment using the *GT-SUITE* software.

Sommario

Nell'attuale contesto di azioni necessarie per fronteggiare il cambiamento climatico, il continuo restringimento dei limiti di emissioni di CO_2 e inquinanti è considerato una sfida chiave per il settore della mobilità. Diverse potenziali soluzioni tecnologiche sono in fase di esplorazione per affrontare questo scenario. L'ampia area di ricerca spazia dall'implementazione di elettrificazione nei powertrains, considerando anche quelli esclusivamente elettrificati, al continuo sviluppo dell'hardware del motore a combustione interna (MCI). Focalizzandosi su quest'ultimo, tra le soluzioni tecnologiche investigate, diverse tipologie di carburanti sono attualmente esaminate per sostituire i combustibili fossili. In questo contesto, l'idrogeno è riconosciuto come particolarmente interessante, grazie alle sue caratteristiche di combustione: un'alta velocità di propagazione della fiamma e un ampio range di infiammabilità, che garantiscono una combustione magra, e una buona resistenza al knock. Tuttavia, la sua bassa densità e alta diffusività implicano che l'evoluzione del processo di iniezione in camera sia ben controllato per ottenere le migliori condizioni possibili di carica nei dintorni della candela per garantire importanti valori di efficienza e potenza minimizzando le emissioni di ossidi di azoto (NOx).

In questo contesto, il presente studio ha lo scopo di analizzare le potenzialità dell'iniezione diretta in un motore a combustione interna alimentato a idrogeno. Il motore in esame è stato derivato da un motore diesel 6-cilindri 3 L, equipaggiato con una nuova geometria del pistone come conseguenza dei risultati ottenuti da studi precedenti.

In primis, l'attività è stata focalizzata sulla simulazione e analisi dei processi di iniezione e combustione di un set di punti operativi in un ambiente 3D-CFD utilizzando il software *CONVERGE CFD*. In seguito, i risultati, analizzati per capire l'effetto di differenti timing di iniezione e valori di lambda sull'omogeneizzazione di carica e il processo di combustione, hanno permesso la calibrazione di un modello di turbolenza e successivamente di un modello di combustione predittivo (*SI-Turb*) in un ambiente 1D-CFD grazie al software *GT-SUITE*.

Acronyms

ATDC	After Top Dead Centre
BEV	Battery Electric Vehicle
BMEP	Brake Mean Effective Pressure
CFD	Computational Fluid Dynamics
CPOA	Cylinder Pressure Only Analysis
DI	Direct Injection
FF	Flame Front
EGR	Exhaust Gas Recirculation
EOS	End Of Simulation
H_2-FC	Hydrogen Fuel Cells
H_2-ICE	Hydrogen Internal Combustion Engine
HEV	Hybrid Electric Vehicle
ICE	Internal Combustion Engine
Normalized LS	Normalized Length Scale
NOx	Nitrogen Oxides
PFI	Port Fuel Injection
PHEV	Plug-in Hybrid Electric Vehicle
PID	Proportional Integral Derivative

PLIF	Planar Laser-Induced Fluorescence
RANS	Reynolds-Averaged Navier Stokes
RMSE	Root Mean Square Error
SCR	Selective Catalytic Reducer
SOI	Start Of Injection
TDC	Top Dead Centre
TKE	Turbulent Kinetic Energy
TPA	Three Pressure Analysis
VVT	Variable Valve Timing
WP	Working Point

Figures index

Tables index

1 Introduction

1.1 Background

The main focus of the transport sector in the last decades has been related to the noxious emissions. Each Country is developing some specific laws to reduce the emissions caused by this sector. The development of new vehicles and propulsion systems is now entirely driven by these laws whose main objectives are the reduction of Green House Gases (GHGs), with particular focus on carbon dioxides (CO_2) emissions, and Criteria pollutants, such as carbon monoxides (CO), hydrocarbons (HC), nitrogen oxides (NOx) and particulate matter (PM), that are harmful to the entire planet being responsible for the air quality.

The pollutants listed are the products of a fossil fuel combustion process. In 2019, the EU approved the Green Deal, an investment plan whose aim is to grant energetic independence from fossil fuels by 2050. A series of new legislations have then moved towards this direction. This year, the new Euro 7 legislation has been approved. It has been intended to be applied both to passenger cars and heavy-duty vehicles, but after some concerns of different states on the impact on the former industry, the European Commission decided that its tightenings will be more stringent only for the heavy-duty class [1]. It will come into effect starting from the 1st of July 2025 and it will introduce more stringent limits for pollutant emissions with respect to the in-place Euro 6 legislation. Plus, limits will be introduced for previously un-considered pollutants such as ammonia (NH_3) and nitrous oxide (N_2O). New regulations will also be applied to other kinds of emissions as the brakes' particles and the tires' microplastic ones. Other new regulations will be related to the testing procedure. Still, the most challenging aspect introduced will be the technological and fuel neutrality, meaning that all the limits on the emissions will be imposed regardless of the type of powertrain or fuel used [2]. To pursue the Green Deal, this year in March, the "Fit for 55" legislation has been approved by the EU; its goal is to reduce by at least 55% the greenhouse gas emissions within 2030 and to consequently achieve the complete decarbonization of the EU by 2050 [3].

Figure 1.1: Euro 7 legislation characteristics [2]

To face this scenario appeared in the last two decades, new technologies have been studied and developed. The ones having a faster and more direct impact on the mobility sector are related to the electrification (BEV, PHEV, HEV) of the powertrains. However, other types of fuels are being studied; among them, bio/synfuel and hydrogen appear to be the most promising ones. Focusing on the latter, the interest in this source of fuel is mainly driven by the absence of carbon; as a consequence, from its combustion process no product related to carbon, such as CO_2, is produced, guaranteeing a clean combustion process.

Battery electric, H_2 and bio/synfuel powertrains are considered the four true zero-emissions technologies to power vehicles. Each technology has its advantages and disadvantages, which make them more or less suitable for different vehicle types [4].

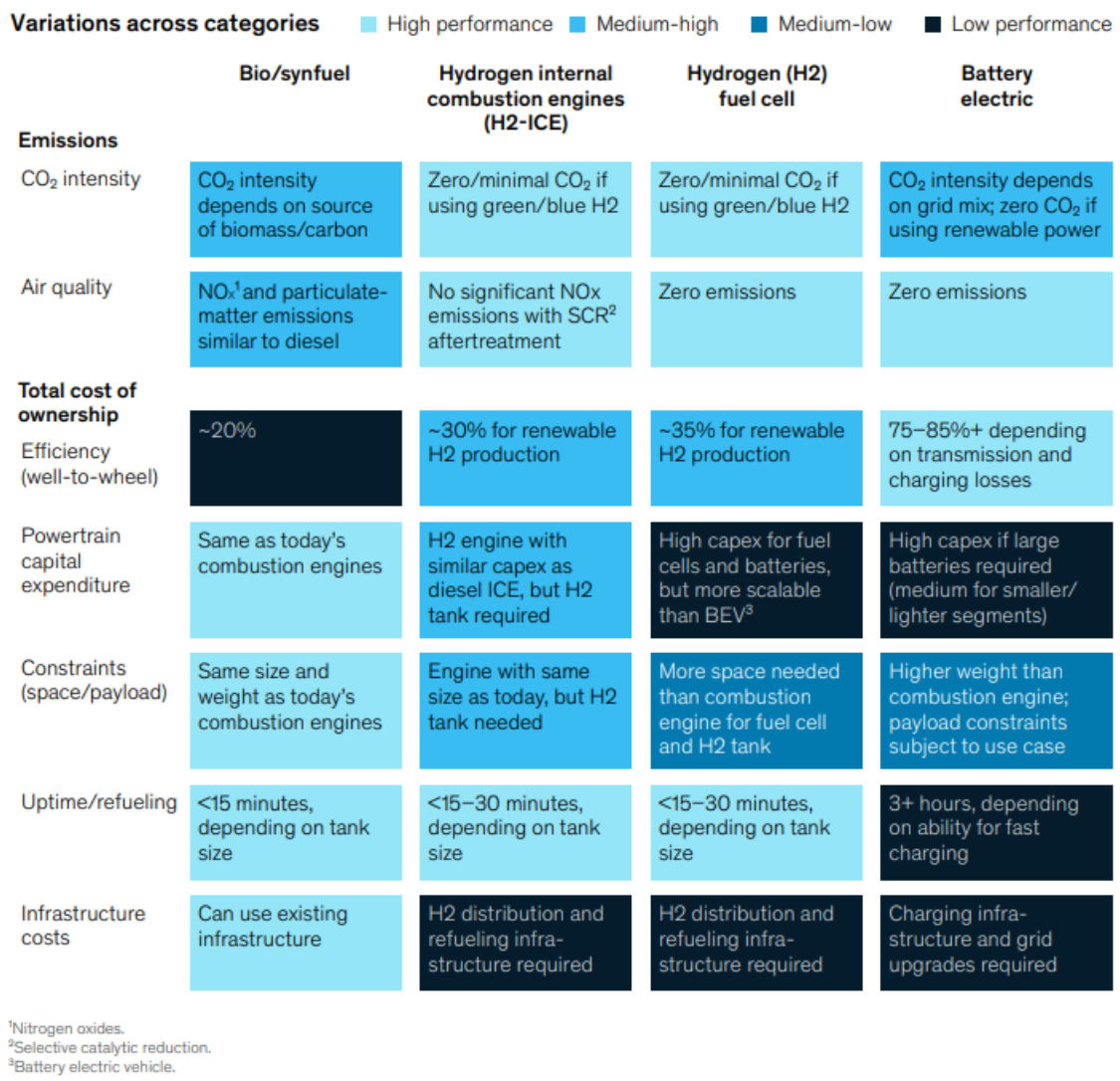

Figure 1.2: Comparison between the four true zero-emission technologies [4]

As highlighted in Figure 1.3, it is always essential to have a clear picture of the entire process needed to produce a specific fuel. In the case of the hydrogen, three different roads can be followed [5]:

- Green hydrogen: It is produced using renewable energy sources such as wind, solar or hydropower. An electrolysis mechanism is used to split water into hydrogen and oxygen. In this way, a clean and emission-free hydrogen is obtained that can be used to power applications requiring a clean energy source.
- Blue hydrogen: It is produced using natural gas feedstocks instead of water. The first part of the process consists of converting the natural gas into hydrogen and carbon dioxide through a process called steam methane reforming (SMR). The carbon dioxide part obtained is then captured and stored underground using a

process known as carbon capture, utilization and storage (CCUS). This process allows preventing the immediate release of carbon dioxide into the atmosphere. However, considering that for the production of 1 kg of H_2 are needed 1-3 kg of carbon dioxide, the stored volumes of CO_2 will be very high when released. With respect to the production of green hydrogen, blue hydrogen is cheaper due to the usage of natural gas feedstocks instead of renewable energy sources.

- Grey hydrogen: It is produced using fossil fuels or natural gases without CCUS. The fossil fuel is converted into H_2 through high-temperature gasification. For the production of 1 kg of H_2, around 10 kg of carbon dioxide is needed. The very high emissions associated with this type of hydrogen make it the least desirable among these three.

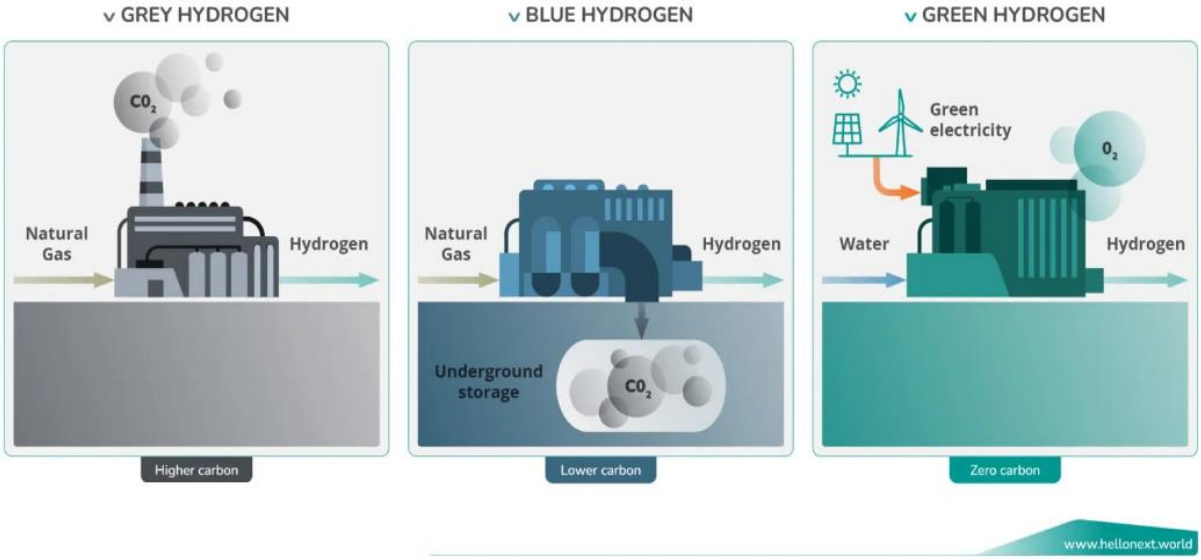

Figure 1.3: Grey, blue and green hydrogen production [5]

Hydrogen can be exploited with different technologies in the mobility sector, among which H_2-FC and H_2-ICE are the principal ones. The former uses hydrogen as fuel in packs of fuel cells to obtain electric energy to power an electric motor; the latter instead uses hydrogen as fuel in an ICE. The possibility of leaning on an existing technology and using a popular hardware component, allowed the H_2-ICE to gain interest in the last decade.

This technology can be further divided into two different applications. The port fuel injection (PFI) application in which the fuel is injected in the intake duct and mixed with

air before being aspirated in the combustion chamber, and the direct injection (DI) application in which the fuel is directly injected into the combustion chamber. The latter application grants the possibility to reach higher power density outputs with respect to the former, but it needs more controls. In fact, if from one side the risk of backfire, typical of PFI applications, is brought to 0 and the power density is also increased, on the other side, it is necessary to control the fuel stratification into the combustion chamber to guarantee the best possible conditions around the spark plug; to do so, different parameters must be checked and also the piston geometry plays a fundamental role in the way in which the fuel spreads into the combustion chamber.

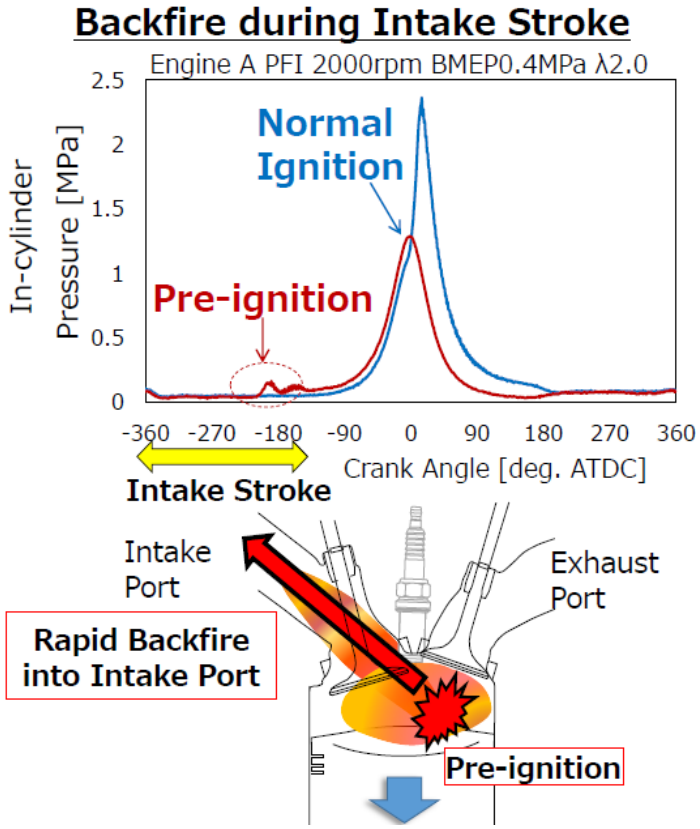

Figure 1.4: Illustration of backfire and pre-ignition phenomena [6]

Not having a huge quantity of physical engines fueled with hydrogen, to have a better understanding of how varying parameters such as the start of injection (SOI) or the quantity of fuel injected influences the injection and combustion processes, it is necessary to pass through simulation softwares. These simulations can be mainly run in two different environments, a 3D-CFD and a 1D-CFD one. The former allows us to have a

deeper understanding of the in-cylinder phenomena granting us the possibility to see how the charge moves, but it is generally restricted to a single engine cylinder because it results very costly in terms of memory and computational time to be simulated. On the other hand, the latter turns out to be less memory and time costly with a less detailed possibility of understanding the in-cylinder movements and phenomena more in general.

What is done to have the clearest picture possible is to work with both environments in a synergetic way. For this purpose, the 6-cylinder starting model used for this thesis activity was created in a 1D-CFD software and was used to recover the boundary conditions necessary to build up the 3D-CFD one. The 3D-CFD simulation, carried out on a single-cylinder model, was run to have a visual understanding of the in-cylinder charge motion and to retrieve the necessary parameters to create a Three Pressure Analysis (TPA) and a Cylinder Pressure Only Analysis (CPOA) models in a 1D-CFD environment. For the purpose of the activity, the 3D-CFD model was also used to calculate with different approaches the value of lambda on the flame front (FF). The final part of the activity was completed in a 1D-CFD environment where, after having obtained a calibrated turbulence model and good burn rate profiles, the combustion was calibrated and the performance parameters were extrapolated and analyzed.

1.2 Recent studies and applications

In the last twenty years, many researches have focused on the possibility of finding new solutions to create a more sustainable mobility; furthermore, the increasingly stringent legislations have pushed this process. The technologies studied comprehend battery electric vehicles (BEV), plug-in hybrid electric vehicles (PHEV), hybrid electric vehicles (HEV), and the internal combustion engine (ICE); the wide variety of technologies studied is the consequence of the lack of a single one able to bring on all the advantages of the mentioned ones. Focusing on the ICE, different fuels have been and are being tested to find the one able to grant adequate performances and to fulfill the legislations requirements. For this purpose, hydrogen has been and is being studied.

Hydrogen combustion characteristics, as highlighted by C.M. White & others in [7], allow H_2-ICEs to burn cleanly and operate efficiently allowing ultra-lean operations with very low NOx production and efficient low-load working points. Considering the wide flammability range of H_2 ($0.1 \leq \phi$ [equivalence ratio] ≤ 7.1), highly diluted mixtures also allow stable operating conditions and consequently low emission values. The combination of high flame velocities and low lean-flammability limit grants the possibility to operate unthrottled, reducing the pumping losses and increasing the efficiency, as well as having higher exhaust gas recirculation (EGR) tolerance. However, the limiting characteristic of H_2 engines is represented by the preignition effect, a consequence of the very low ignition energy, which doesn't allow them to reach the same peak power and performance as the equivalent gasoline ones. For this reason, instead of the port-fuel injection (PFI) solution, which is more subject to this limiting factor, recent studies have focused on the direct injection (DI) one. The latter allows for achieving higher volumetric efficiencies eliminating the injection of hydrogen in the intake ports and avoiding preignition thanks to the possibility of controlling the injection timing.

Fuel properties at 25 °C and 1 atm

Property	Hydrogen	CNG	Gasoline
Density (kg/m^3)	0.0824	0.72	730[a]
Flammability limits (volume % in air)	4–75	4.3–15	1.4–7.6
Flammability limits (ϕ)	0.1–7.1	0.4–1.6	≈ 0.7–4
Autoignition temperature in air (K)	858	723	550
Minimum ignition energy (mJ)[b]	0.02	0.28	0.24
Flame velocity (m s^{-1})[b]	1.85	0.38	0.37–0.43
Adiabatic flame temperature (K)[b]	2480	2214	2580
Quenching distance (mm)[b]	0.64	2.1[c]	≈ 2
Stoichiometric fuel/air mass ratio	0.029	0.069	0.068
Stoichiometric volume fraction %	29.53	9.48	≈ 2[d]
Lower heating value (MJ/kg)	119.7	45.8	44.79
Heat of combustion (MJ/kg$_{air}$)[b]	3.37	2.9	2.83

[a]Liquid at 0 °C.
[b]At stoichiometry.
[c]Methane.
[d]Vapor.

Figure 1.5: Characteristics of different fuels [7]

The possibility of controlling this further degree of freedom has been studied in different papers. T. Wallner & others [8,9] have focused their studies on the influence of the start of injection (SOI), combined with other factors such as the injector design or configuration, on engine efficiency and emissions. Their studies are both based on an experimental engine manufactured by the Ford Motor Company and run with the same operating conditions; the hydrogen injection pressure is held constant at 100 bar while a load and SOI sweep are considered.

Engine manufacturer	Ford Motor Company
Displacement (l)	0.5
Compression ratio	11.5:1
Bore/Stroke (mm)	89/79.5
Valve Train	4V Dual Overhead Cam (DOHC)
Intake Valve Timing	IVO=15º CA BTDC, IVC=35º CA ABDC
Exhaust Valve Timing	EVO=45º CA BBDC, EVC=10º CA ATDC
Max Torque (Nm)	30
Speed Range (RPM)	800-6000
Hydrogen measurement	Micro-motion Coriolis Meter
Injector – Direct Injection	Westport

Figure 1.6: Experimental engine characteristics [8,9]

In [8], it is also considered the possibility of having two different injector locations, so that the nozzle configurations studied are:

- 6-hole injector in a central location
- 6-hole injector in a lateral location
- 5-hole injector in lateral location pointing towards the spark plug
- 5-hole injector in lateral location pointing towards the piston top

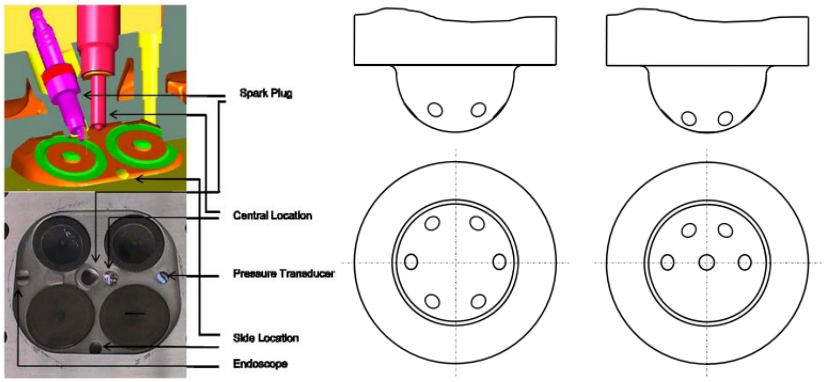

Figure 1.7: Cylinder head and injector tips design [8]

What is observed, analyzing low and high-load working conditions is that in the former the nozzle design has a significant impact on the indicated thermal efficiency while in the latter it doesn't, but in both working conditions it appears that the injectors on the lateral location show higher efficiencies values. NOx emissions appear independent of the injector nozzle design and increase with late SOI for low-load operating conditions, while increasing the load they show a decreasing trend, and pointing the jet towards the spark plug results in higher NOx emissions.

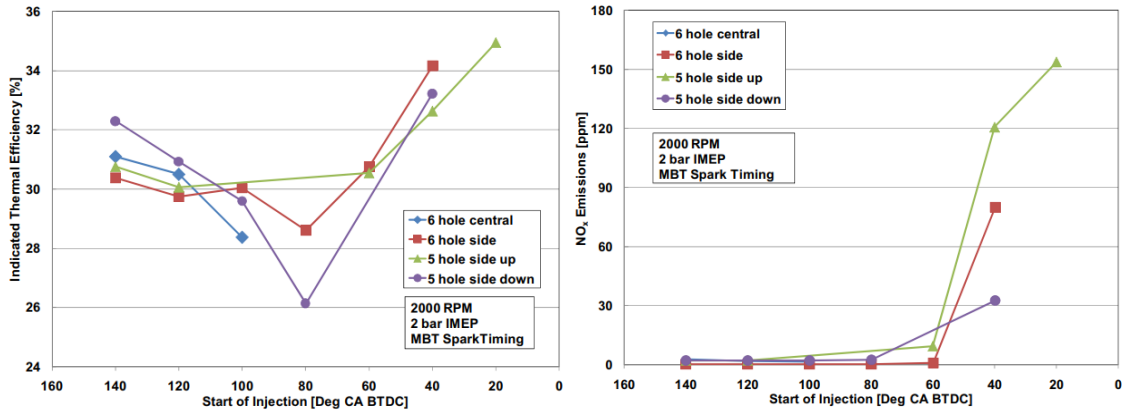

Figure 1.8: Indicated Thermal Efficiency and NOx Emissions at low-load [8]

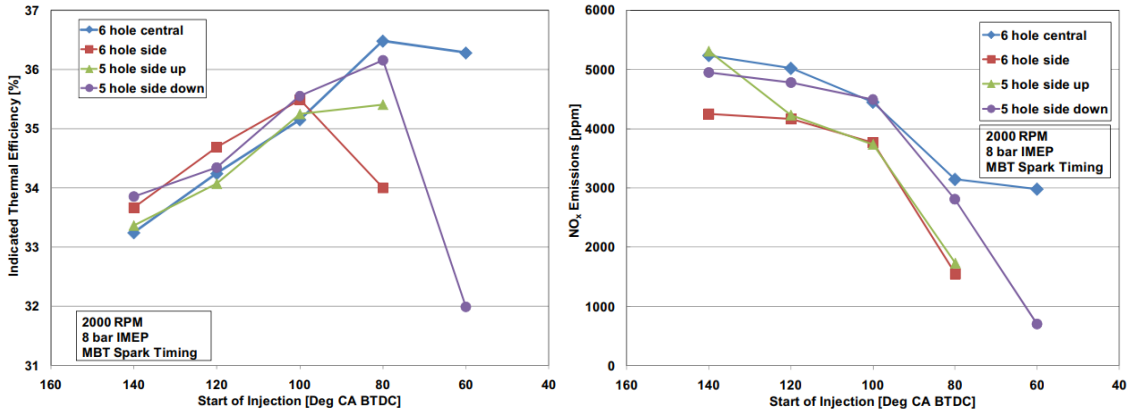

Figure 1.9: Indicated Thermal Efficiency and NOx Emissions at high-load [8]

The focus of the paper [9] is directed toward the injection strategy intended as a combination of injection angle and SOI. To simplify the setup and avoid complex phenomena such as jet-to-jet interactions, a single-hole injector configuration is selected with a 1.375 mm diameter. The injection directions analyzed are:

- φ = 0°, towards the spark plug
- φ = 45°, towards the intake valves
- φ = 90°, towards the intake quenching zone
- φ = 180°, away from the spark plug
- φ = 270°, towards the exhaust quenching zone
- φ = 315°, towards the exhaust valves

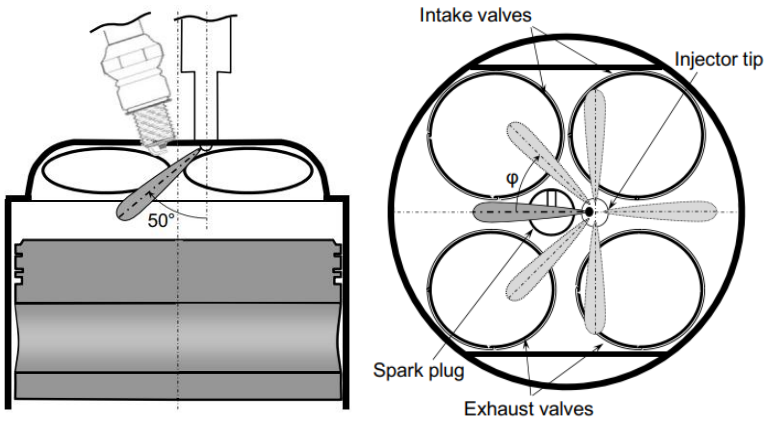

Figure 1.10: Combustion chamber detail and injection directions [9]

The low and high-load working points behave in almost the opposite way for what concerns both the indicated thermal efficiency and the NOx emissions. It must be considered that the ϕ values used, ϕ=0.25 and ϕ=0.8 for the low-load and high-load working points respectively, might be the cause of unfavorable stratification around the spark plug mainly for the lower value; which is the reason for the absence of values in the low-load maps.

The injection direction appears to be the higher influencing factor for the efficiency, but it must be considered together with the SOI. Injecting towards the spark plug results in obtaining higher efficiency values if operating at low load, while the high-load working condition behaves oppositely.

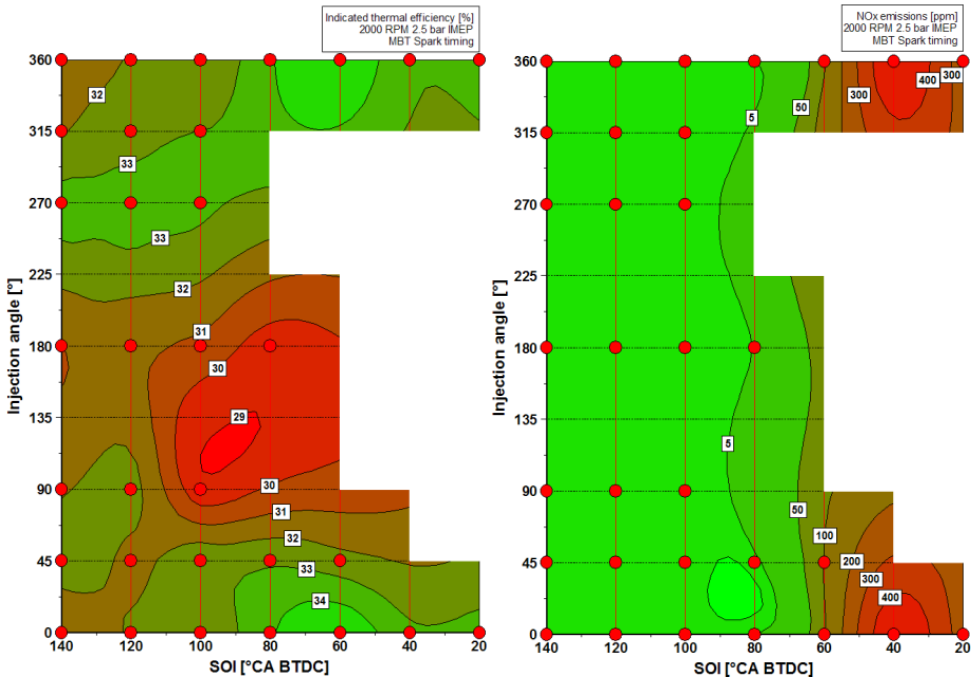

Figure 1.11: Low-load ITE and NOx Emissions maps [9]

SOI occurs to be the most influencing factor for NOx emissions, but it must be strictly considered with respect to the working point analyzed. Early SOI timings allow for reducing NOx emissions at low-load operating conditions, while increasing the load it is preferred to adopt late SOI timings.

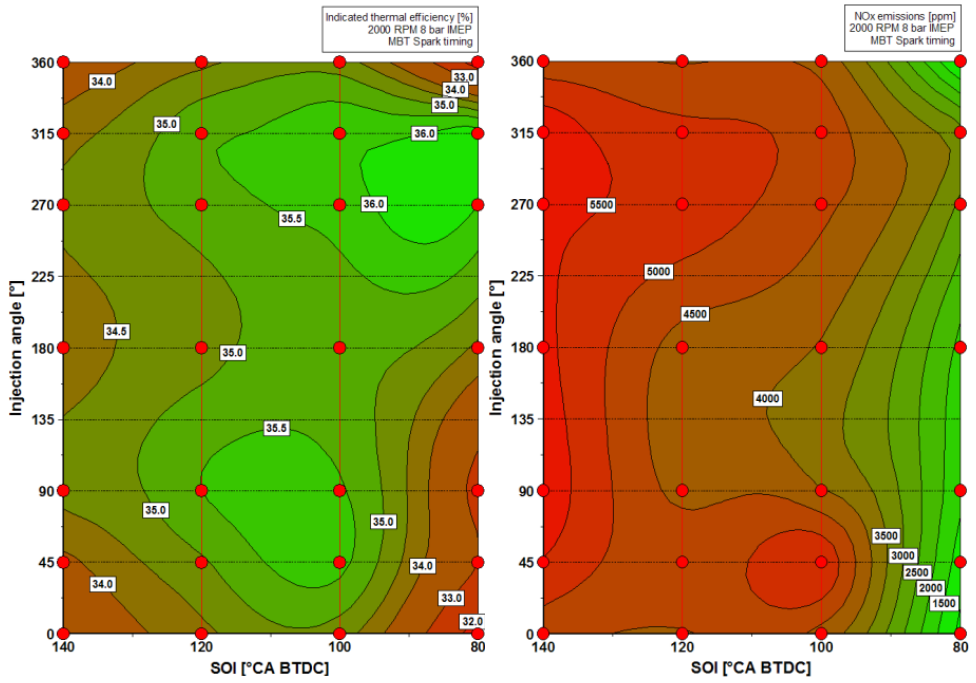

Figure 1.12: High-load ITE and NOx Emissions maps [9]

It is clearly shown how an optimization only based on one parameter isn't able to lead to the best output results, but it is necessary to find a compromise between parameters for each operating condition considered.

V.M. Salazar & others [10] analyzed the influence of the same parameter studied in [8] and [9], SOI and injector location and geometry, using a different engine and a specific technique called Planar Laser Induced Fluorescence (PLIF) on the mixture preparation.

Bore	92 mm
Stroke	85 mm
Displacement	560 cm^3
Compression ratio	11
Speed	1500 rev/min
Intake pressure	1 bar
Fired IMEP	2.5 bar
Global equiv. ratio	≈ 0.25
Injection pressure	80 - 116 bar (depending on injector)
Injection duration	18.5 – 22 °CA (depending on injector)
Intake valve timing[1]	IVO: 346° CA / IVC: -140° CA
Exhaust valve timing	EVO: 130° CA / EVC: -356° CA

Figure 1.13: Engine characteristics [10]

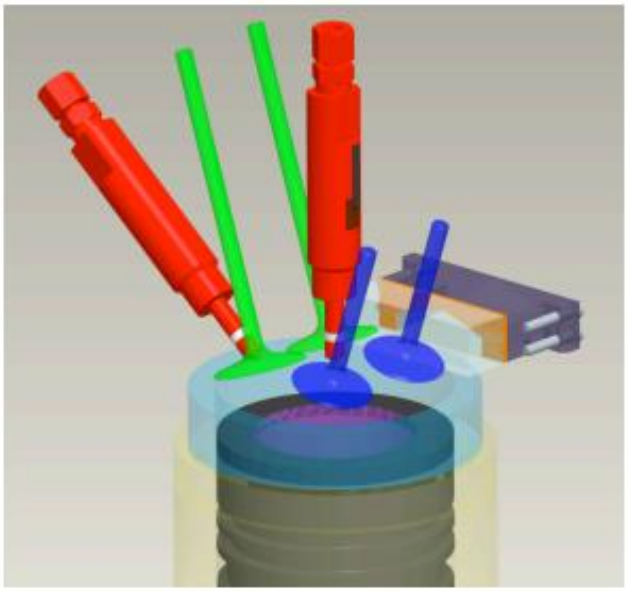

Figure 1.14: Cylinder configuration [10]

The configurations examined in this paper with the PLIF methodology are:

- single-hole injector in a central location pointing toward the spark plug
- 6-hole injector in a lateral location
- 6-hole injector in a central location
- 5-hole injector in a lateral location pointing towards the spark plug
- 5-hole injector in a lateral location pointing towards the piston top
- 13-hole injector in a central location

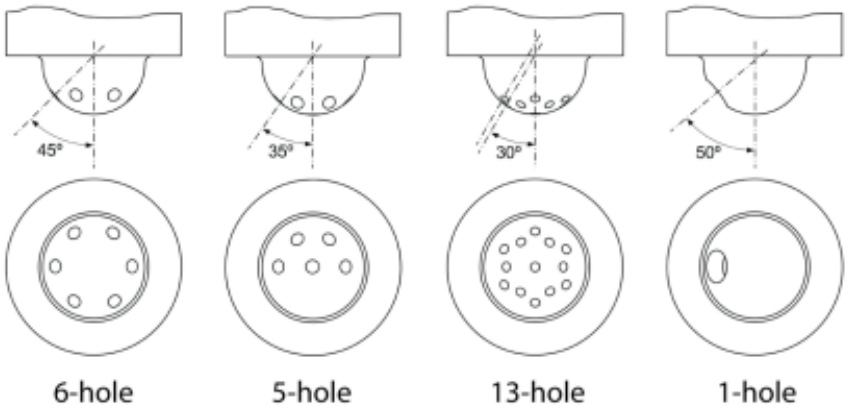

Figure 1.15: Injector tip designs [10]

What is observed is that fast jet penetration and long available time make jet-to-jet and jet-to-wall interactions are the dominating mechanisms in mixture preparation for early and intermediate time injections. Curiously, considering the SOI=-80° CA, the fuel distribution at ST is similar for all the multi-hole injectors and it results unfavorable in all cases; this distribution is a consequence of the downward jet momentum interacting with the piston top, spreading the jet into the squish zone without sufficient time to re-emerge into the center of the combustion chamber.

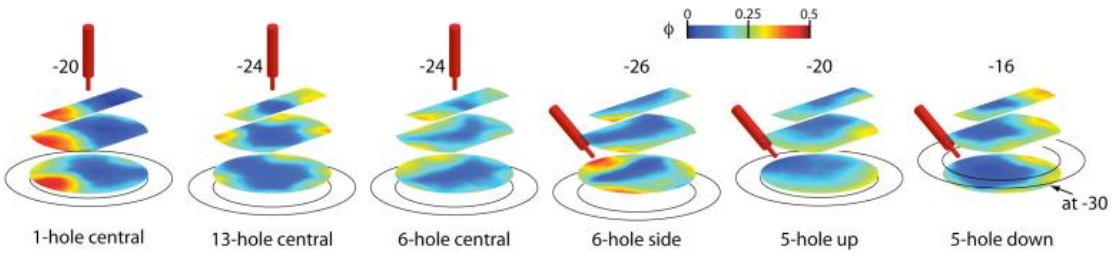

Figure 1.16: Fuel distribution comparison at ST for SOI = -80 deg aTDC [10]

Unfortunately, there are no big datasets available on hydrogen combustion because this technology requires specific engine adaptations, so it is important to exploit numerical models that can help in reducing experimental timings while having an understanding of the phenomena examined.

When numerical models are used, a variety of degrees of freedom typical of the model used come into play. For this purpose, R. Scarcelli & others wrote a paper, [11], in which they analyzed the influence of SOI and injector geometry and direction on engine efficiency and combustion stability. The engine and operating conditions used as reference are the same as [9], and the results are compared to the ones obtained with the PLIF mechanism on an accessible engine as in [10].

The numerical simulations of the in-cylinder mixture formation are obtained from the software *Fluent*. Two different computational grids are used, one for the full engine geometry and one for the reduced one, which comprehends a smaller in-cylinder volume, and they focus on different approaches; the former on the flow-field development during the gas-exchange phase, the latter on the compression stroke and injection process.

These considerations led to a model able to predict the state of the fuel-air mixing at ST with reasonable accuracy, obtaining the same conclusions as papers [9] and [10].

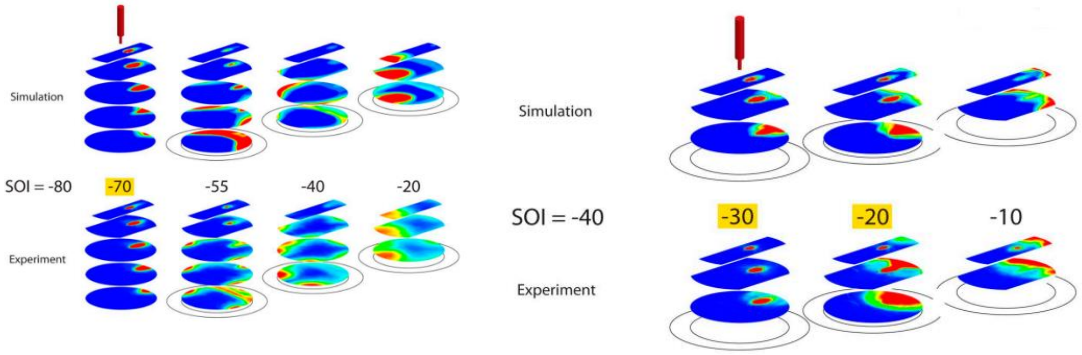

Figure 1.17: Fuel distribution evolution with SOI = -80 deg aTDC and SOI = -40 deg aTDC [11]

A deeper understanding of the influence of parameters specific to the numerical models can be achieved through another paper written by R. Scarcelli & others [12], in which a parametric analysis of the influence of numerical grid resolution and turbulence model on jet penetration and mixture formation is performed.

The *Fluent* code with a Reynolds-Averaged Navier Stokes (RANS) approach is used to model the in-cylinder turbulence. The two turbulence models selected and compared are the k-eps RNG and the k-eps realizable ones; for the latter different values of the Schmidt number, responsible for affecting the fuel dispersion, are studied to overcome the under-prediction in fuel dispersion of the k-eps RNG model.

It is noted that the turbulent models and their settings have no influence on jet penetration, but they hold some improvements in terms of fuel dispersion.

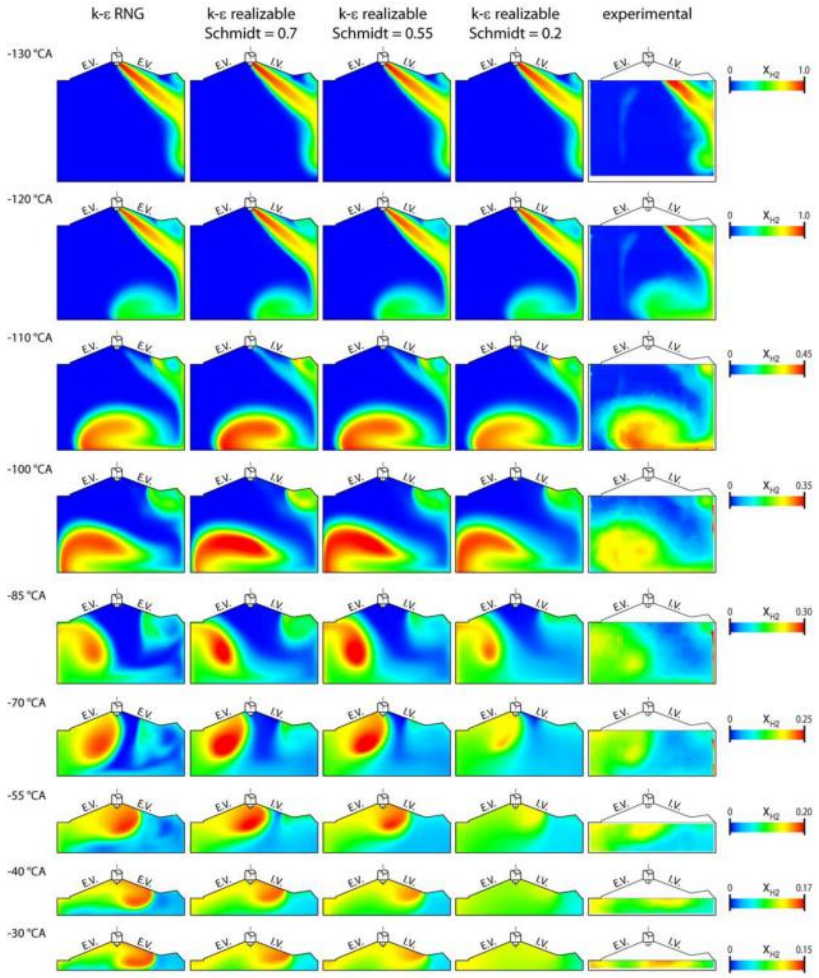

Figure 1.18: Turbulence model influence on jet penetration and fuel dispersion [12]

The influence of the grid resolution on jet penetration and mixture formation is analyzed considering three different computational grids, from a coarser up to a finer value.

Contrary to the turbulence models, grid evolution has a significant influence on jet penetration and no effect on fuel dispersion.

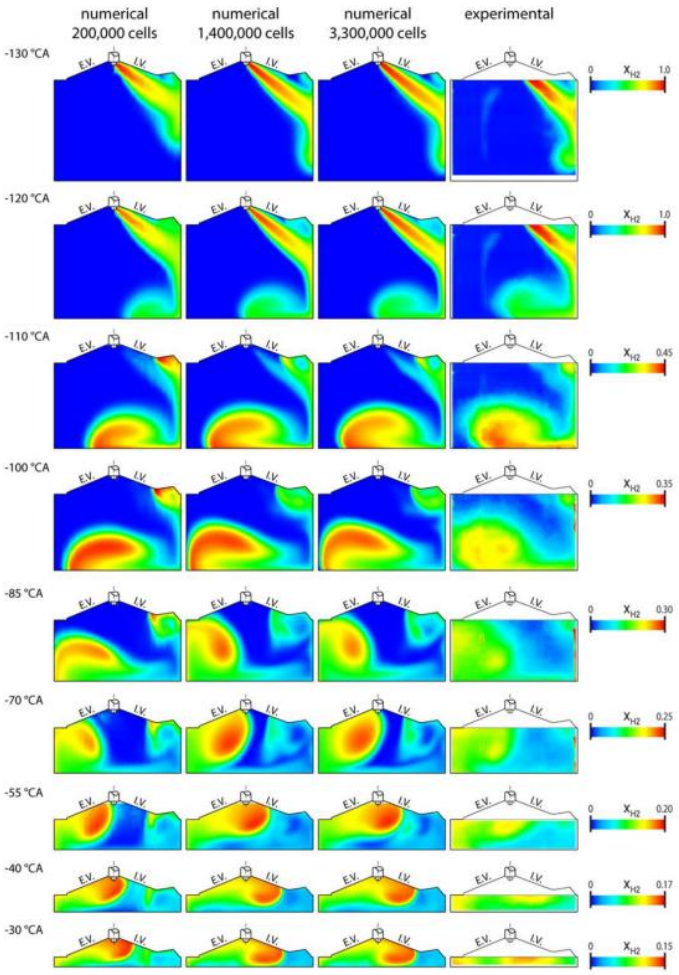

Figure 1.19: Grid evolution influence on jet penetration and fuel dispersion [12]

The overall conclusion of the paper holds that in general numerical and experimental data show a remarkable agreement in terms of jet penetration, wall impingement and overall mixture evolution.

1.3 Aim of the activity

This thesis activity has aimed at calibrating a predictive combustion model for a DI H_2-ICE able to take into account the phenomenon of stratification. A synergetic approach between 0/1/3D-CFD environments has been used to evaluate and analyze the possibility of exploiting the use of hydrogen as fuel supplied with direct injection in an internal combustion engine. The fulcrum of the analysis was to understand the injection event varying two parameters strictly related to this technology, such as the injection timing and the lambda value, and the following influence these have on the combustion evolution. The common point found in analyzing different operating conditions was related to the importance of the fuel distribution in the chamber and its level of stratification around the spark plug, being the most critical parameter influencing the following combustion process. The piston top geometry used during this thesis activity was the follow-up of previous studies, as it was considered an important parameter to take into account for the fuel distribution evolution inside the combustion chamber [13].

To develop such activity, 1D-CFD and 3D-CFD analysis have been exploited; for this purpose, *GT-Suite* and *Converge Studio* have been the softwares used, respectively. The results of the 3D-CFD analysis have been used to extrapolate the profiles of lambda on the flame front, to calibrate the turbulence and subsequently the combustion mechanisms in the 1D-CFD model.

It is essential to highlight how the 3D-CFD model has been analyzed considering three specific operating conditions. These have been labeled as Working Point 1 (1500 rpm x 3 bar BMEP), Working Point 2 (2500 rpm x 8 bar BMEP) and Working Point 3 (3500 rpm x 10 bar BMEP) to cover a range of operating conditions sweeping from low-speed low-load up to high-speed high-load. The calibrations performed on the 1D-CFD model have been made on these points to extend the validation to the entire dimensional plan in future studies.

2 Engine test case and simulation methodology

2.1 Test case

The engine used in this activity is a 3.0L 6-cylinder derived from a diesel application. The geometry of the bowl is an evolution of the more classical lobe-shaped one, studied in a previous activity [13], and is hemispherical. The hydrogen injector is placed in the cylinder head in an asymmetric position while the spark plug where was originally placed the diesel injector, in the center of the combustion chamber.

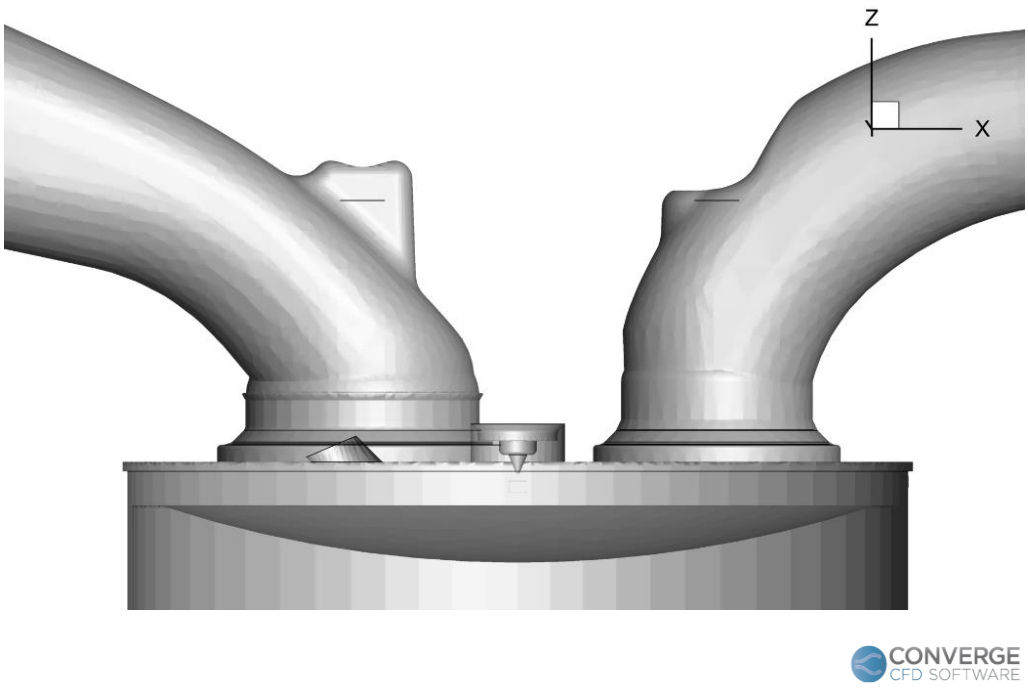

Figure 2.1: Combustion chamber detail

Attribute	Unit	Object value
Bore	mm	83
Stroke	mm	90.4
Connecting Rod Length	mm	145
Compression Ratio	-	11.78
TDC Clearance Height	mm	1

Table 2.1: Engine geometric characteristics

Attribute	Unit	Object value
Injection pressure	bar	20
H_2 mass flow	g/s	10

Table 2.2: Injector characteristics

2.2 1D-CFD model setup

The engine assembly is made up of other components. The turbo-compressor group, in which the compressor's maximum speed is limited to 200 krpm and the turbine is controlled by acting on the rack position, being of the variable geometry type. The air filter and the Selective Catalytic Reducer (SCR) are modeled as ducts able to impose a pressure drop to the flow, of air entering the compressor and of exhaust gases exiting from the turbine; in the latter, no chemical reaction occurs since it is not the aim of this activity to obtain and analyze specific chemical reactions and mechanisms. The intercooler, placed immediately after the turbo-compressor group to have a better cooling of the compressed air, is modeled using a table that takes into consideration its cooling efficiency.

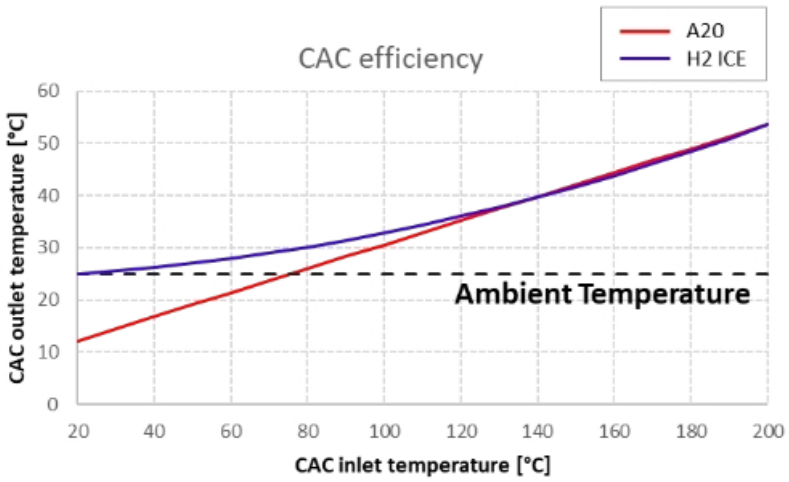

Figure 2.2: Intercooler cooling efficiency plot

A high-pressure EGR circuit is placed downstream of the cylinders. The high flammability range of the hydrogen requires controls on the intake temperatures since otherwise auto-ignition phenomena might occur. It is important to have a very efficient cooling system for the EGR circuit. In this case, specific data on the intercooler efficiency were not given, it has then been decided to fix the temperature for the gases at the exit of the EGR circuit equal to 100°C (373.15 K). The value chosen is the consequence of a supposition made on a previous activity ([13]), in which it had been considered that the influence of this specific parameter on a global analysis is minimal; nevertheless, for more

specific studies or models it would be necessary to consider this.

The intake and exhaust valve lift profiles are kept as the same and fixed for the entire map. The possibility of implementing a variable valve timing (VVT) system is postponed to future analysis, in which it will be possible to evaluate the effectiveness of implementing this system with DI.

The in-cylinder charge motion is evaluated taking into account the bowl shape and the parameters used to model it have been calibrated on the 3D-CFD model. The most important parameter in a DI engine is the Spray/Jet Multiplier which refers to the turbulence created in the combustion chamber from the fuel injection event itself. All of the four parameters have been calibrated looking for a single value for each of them for the entire dimensional plan.

The 1D-CFD model is implemented with a series of different controllers that manage its functioning. The aim of these controllers consists of selecting the best possible value for the model operating parameters to match the desired targets given as input respecting the imposed constraints. Seven constraints on different components are considered and imposed as limits not to exceed. The entire turbo-compressor group has an imposed limit on the maximum rotational speed of 200 krpm. Focusing on the single turbo-compressor components the imposed limits are:

- a 5% error on the surge value (calculated with respect to the corrected mass-flow rate) and a T_2 (compressor exit) value of 180°C for the compressor
- a maximum T_3 (turbine in) value of 850°C and a maximum p_4 (turbine in) value of 4 bar for the turbine

The two remaining limits are imposed on the maximum in-cylinder pressure and the knock. The former is imposed at p_{max} = 140 bar and the latter is calculated as time necessary to end the combustion pre-reactions following the Douaud-Eyzat model. This model is based on specific tables able to give as output the autoignition time varying lambda and EGR values, an integration is then performed until the end of combustion. In this way when the integration reaches a value equal to 1, it means that all pre-reactions have been completed and autoignition will occur.

These limits imposed are managed by the controllers to reach the desired value of the operating parameters. Two types of operating parameters are considered: the imposed ones, for which the desired value is imposed and considered as a specific value towards which the model must converge, and the variable ones, which vary to reach the desired

value of the imposed parameters. In the model used, the former are represented by the brake mean effective pressure (BMEP), the lambda value, the rotational speed, the SOI and the % of EGR, while the latter, which are the ones managed by the controllers, by the EGR and throttle valves opening, the rack positioning and the ST.

The controllers act each time a constraint isn't respected on the parameters with the higher influence on the not respected constraint; in the case more constraints aren't respected at the same time, it is always considered the one which exceeds the most from the limit value. When an error is detected, the first controller to receive a signal is the one related to the rack, which will try to match the desired load value. This works in combination with other two controllers:

- one acting on the throttle valve to match the desired BMEP value
- one acting on the EGR valve to match the desired %EGR value

The fourth controller acts on the spark timing and tries to set the MFB50 (angular value at which the mass fraction burned is equal to 50%) at the optimal value of 8° after top dead center (aTDC). Whenever it appears that at the optimal MFB50 value knock occurs, the controller shifts the ST value until knock won't occur; in this situation, the MFB50 value will be a consequence of the combustion evolution with the new ST value.

The only controller that isn't taken from the GT-Suite library is the knock one. In that case, a PID (Proportional Integral Derivative) controller has been selected and its gains have been imposed in a previous study [13].

2.3 3D-CFD model setup

A 3D-CFD model has been used to have a better understanding of the in-cylinder phenomena and the general engine behavior, while at the same time, it has been needed to compare the results of the 1D-CFD model.

The 3D-CFD model has been analyzed in CONVERGE CFD v3.0.14. The discretizations of space and time have been carried out by selecting a second-order central difference scheme and a first-order implicit Euler scheme respectively; to minimize the effect on simulation time without compromising too much the simulation accuracy, a variable time-step has been used. A base grid size equal to 2 mm has been exploited, but for some specific regions a fixed embedding or an Adaptive Mesh Refinements (AMR) technique have been employed; the minimum value of grid size reached has been 0.25 mm. For the turbulence modelling, the Reynolds-Averaged Navier-Stokes (RANS)-based Re-Normalization Group (RNG) k-ε model has been used; while the turbulent heat transfer prediction has been relied on the O'Rourke and Amsden model. Regarding the combustion modelling, the Well-Stirred Reactor (WSR) approach has been selected; as a consequence, being based on this approach, the SAGE detailed chemistry combustion model has been adopted. The reaction mechanism ruling the combustion that has been selected is the one proposed by Zhang et al. [14].

The 3D-CFD model is made of the intake and exhaust ports, the injector channel, the spark plug and the cylinder (head, piston, liner). The simulations have been performed along a crank angle interval of 600°, starting from 260°, while the exhaust phase is ending, and ending at 860°, at the exhaust valves opening of the following cycle; in this way, it was possible to simulate the entire intake phase and consequently to obtain the turbulence values directly from the 3D-CFD model instead of from empirical reasonings.

To better exploit the synergy between the 3D-CFD and 1D-CFD model, the former has been divided into five main regions for which the boundary conditions have been determined from the 1D-CFD simulation. This is necessary to avoid problems related to the temperature values of some sharp and small areas such as the valve seats, for which the 1D-CFD model isn't able to predict with enough precision their values. The analyzed regions are the intake ports, the exhaust ports, the head, the piston and the liner. The temperature, pressure and chemical composition values at the boundary are imposed equal to the ones of the 1D-CFD model and varying in time.

All the characteristic parameters of a 3D-CFD model setting have been defined in a previous activity [13].

2.4 Dataset

The dataset analyzed in this thesis activity consist of 48 different cases divided into 3 working point (WP) to cover different punctual operating conditions; a low-load low-speed condition represented by WP1 and characterized by a rotational speed of 1500 rpm and a target load of 3 bar BMEP, a medium-load medium-speed condition represented by WP2 and characterized by a rotational speed of 2500 rpm and a target load of 8 bar BMEP, and a high-load high-speed condition represented by WP3 and characterized by a rotational speed of 3500 rpm and a target load of 10 bar BMEP. For each working point, the influence of SOI and lambda is studied. Four different values of both these parameters are studied:

- SOI values [aTDC]: -150 deg, -110 deg, -70 deg, -35 deg;
- Lambda values [-]: 2, 2.25, 2.5, 2.75.

It is important to highlight that the different values of lambda are obtained as a combination of injected fuel and boost pressure values; increasing the lambda will result in a decreased value of efficiency so a higher amount of fuel will be needed, as a consequence the quantity of air introduced in the combustion chamber, ruled by the boost pressure, will be given by the fuel quantity injected to obtain the desired lambda value.

To avoid other situations that might help or not the combustion process, it is decided to keep the ST for every case studied at 720°, which corresponds exactly to the top dead center (TDC).

	Speed [rpm]	**BMEP target [bar]**	**SOI [deg aTDC]**	**ST [deg aTDC]**	**λ [-]**	**EGR [%]**
WP 1	1500	3	-150 ÷ -35	0	2 ÷ 2,75	0
WP 2	2500	8	-150 ÷ -35	0	2 ÷ 2,75	0
WP 3	3500	10	-150 ÷ -35	0	2 ÷ 2,75	0

Table 2.3: Working Points considered

The range covered by the values of SOI is on purpose very wide and wants to help in having a better understanding of the in-cylinder fuel motion as a consequence of the available time before the spark. The different values selected for lambda instead are used to understand if a richer or leaner mixture will affect the in-cylinder charge motion and other parameters such as its diffusivity or penetration.

From the analysis of the 3D-CFD results, the dataset used to analyze the combustion process has then been restricted to 24 considered cases since only the ones with normal or slow combustion have been handled, while all the other cases with too-fast combustion or misfire have been considered useless for the extrapolation of the lambda value on the flame front (FF) and so for the calibration of the stratification mechanism and the combustion model. In particular, 10 cases for WP1, 6 cases for WP2 and 8 cases for WP3 have been considered.

	Case	**SOI [deg aTDC]**	**EOI [deg aTDC]**	**λ**
WP1	1	-110	-105.45	2
	2	-150	-145.45	2
	3	-70	-65.45	2
	4	-35	-30.5	2.25
	5	-110	-105.5	2.25
	6	-150	-145.5	2.25
	7	-110	-105.6	2.5
	8	-150	-145.6	2.5
	9	-110	-105.6	2.75

	10	-150	-145.6	2.75
WP2	11	-110	-96.5	2
	12	-150	-136.5	2
	13	-110	-96.5	2.25
	14	-150	-136.5	2.25
	15	-150	-136.4	2.5
	16	-150	-133.7	2.75
WP3	17	-110	-86.8	2
	18	-70	-46.7	2.25
	19	-110	-86.7	2.25
	20	-150	-126.7	2.25
	21	-70	-45	2.5
	22	-110	-85	2.5
	23	-150	-125	2.5
	24	-110	-80.2	2.75

Table 2.4: Dataset of the cases used for the turbulence calibration

3 Results and discussion

3.1 3D-CFD results

The charge distribution into the chamber is of pivotal importance to obtain a good and stable combustion. The way in which it evolves in time depends on parameters such as piston bowl design, injection timing and average lambda value. Considering the former, this study already implements a modified version of the original piston bowl that was directly derived from the diesel engine used as a reference and which has now a hemispherical shape instead of the re-entrant one. The bowl's geometry directly influences the charge distribution in the combustion chamber since its design can modify how the charge trajectory is deflected when it encounters the combination of piston top design and piston upward movement. The simpler bowl geometry implemented in this study allows to have lower values of piston top impingement and charge trajectory modification with respect to a classical re-entrant bowl, as analyzed in [13].

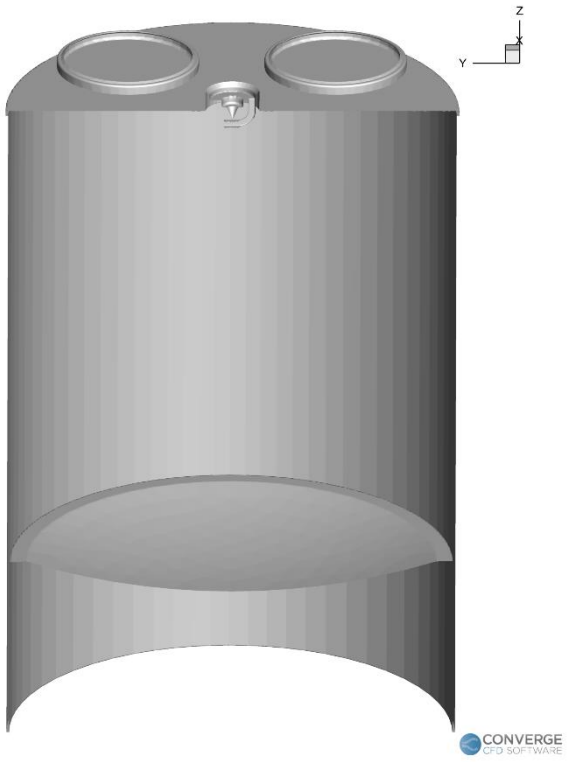

Figure 3.1: Combustion chamber section - bowl detail

3.1.1 Injection timing influence

The importance of injection timing lies in the fact that having a direct injection configuration requires a well-done monitoring of the hydrogen distribution in the combustion chamber since it isn't homogeneous, as it happens in a Port Fuel Injection (PFI) configuration. The easiest way to do that is by correctly phasing the injection event for each operating point. If from one side some characteristics of the hydrogen, such as the high diffusivity, help in filling the combustion chamber, on the other side it isn't easy to obtain the optimal conditions around the spark plug at the spark timing due to the in-cylinder phenomena. Furthermore, it is necessary to guarantee an adequate charge stratification on the entire angular interval of the combustion. The final goal would be to obtain an optimal combustion in terms of efficiency, performance and emissions. In this case, the best possible charge distribution condition in the combustion chamber would require to have a richer charge in the spark-plug region and a leaner one at the walls, with respect to the average value. Clearly, a trade-off between performance and NO_x emissions must be considered since it is not possible to increase one without increasing the other.

The injection event development is a direct consequence of the injector positioning since this will influence the trajectory of the charge injected. The engine used in this study is equipped with a direct injector placed between the intake valves. It is important to highlight that the injector positioning hasn't been optimized for this specific application, but it is the consequence of the easiest retrofitting approach. Furthermore, this injector positioning implies that the injection event will develop in a non-symmetrical way into the combustion chamber, thus the interaction with the piston top has also been analyzed since it will evolve differently in the examined planes.

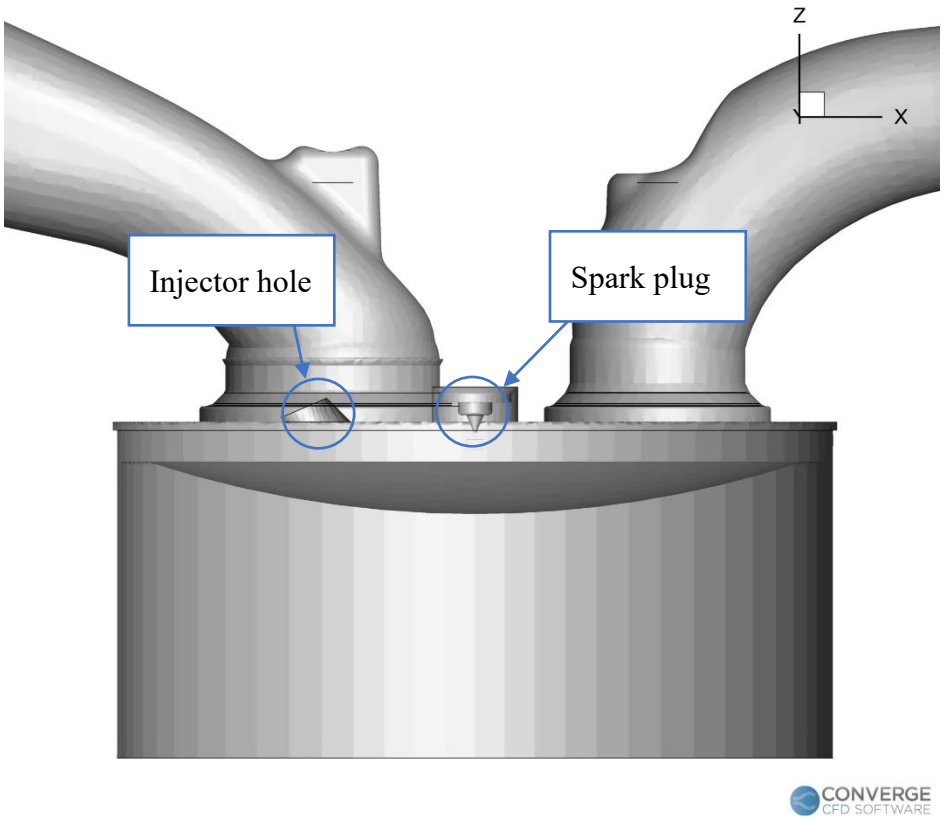

Figure 3.2: Combustion chamber detail

Four different injection timings were considered for each working point. The injection timings taken into consideration cover a wide angular window in order to have a complete picture of the influence of this parameter on the charge evolution in the combustion chamber. The earliest injection timing will be more subject to wall impingement, while the latest one will have more difficulties in filling the combustion chamber and granting a good distribution of charge around the spark plug suitable for the combustion. These different scenarios will be better analyzed in the following.

It must be considered that the solution adopted is a consequence of the transformation and adaptation processes of a diesel engine into a hydrogen one. These processes could be the object of interest and optimization for future studies which will need to find the trade-off between a configuration that can guarantee the best possible performances and one that can keep the manufacturing costs as low as possible.

To analyze the injection event, the post-processing software TECPLOT has been used. Three different planes all perpendicular among them have been created to section the combustion chamber. An X plane passes through the center of the chamber between the

intake and exhaust valves; a Y plane sections the chamber in between the intake and exhaust valves, parallel to the injected jet of hydrogen. A further Z plane has been used to section the chamber passing through the spark plug electrode.

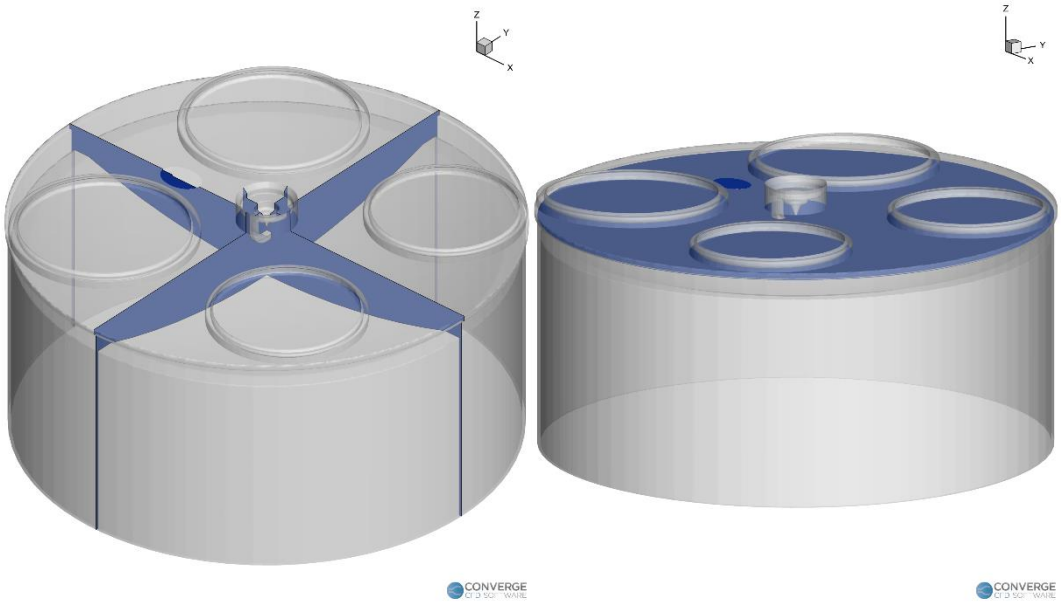

Figure 3.3: X, Y and Z sectional planes representation

The hydrogen characteristics combined with the direct injection could create charge distributions not particularly favourable for the combustion event. A very lean charge mixture in the spark plug region could lead to a low-speed initial combustion phase followed by a slow process evolution, or a very rich charge mixture around the spark plug could result in a very high-speed combustion development process. The worst possible scenario in terms of combustion process is represented by a too-lean charge mixture in the spark plug region that could lead to a misfire.

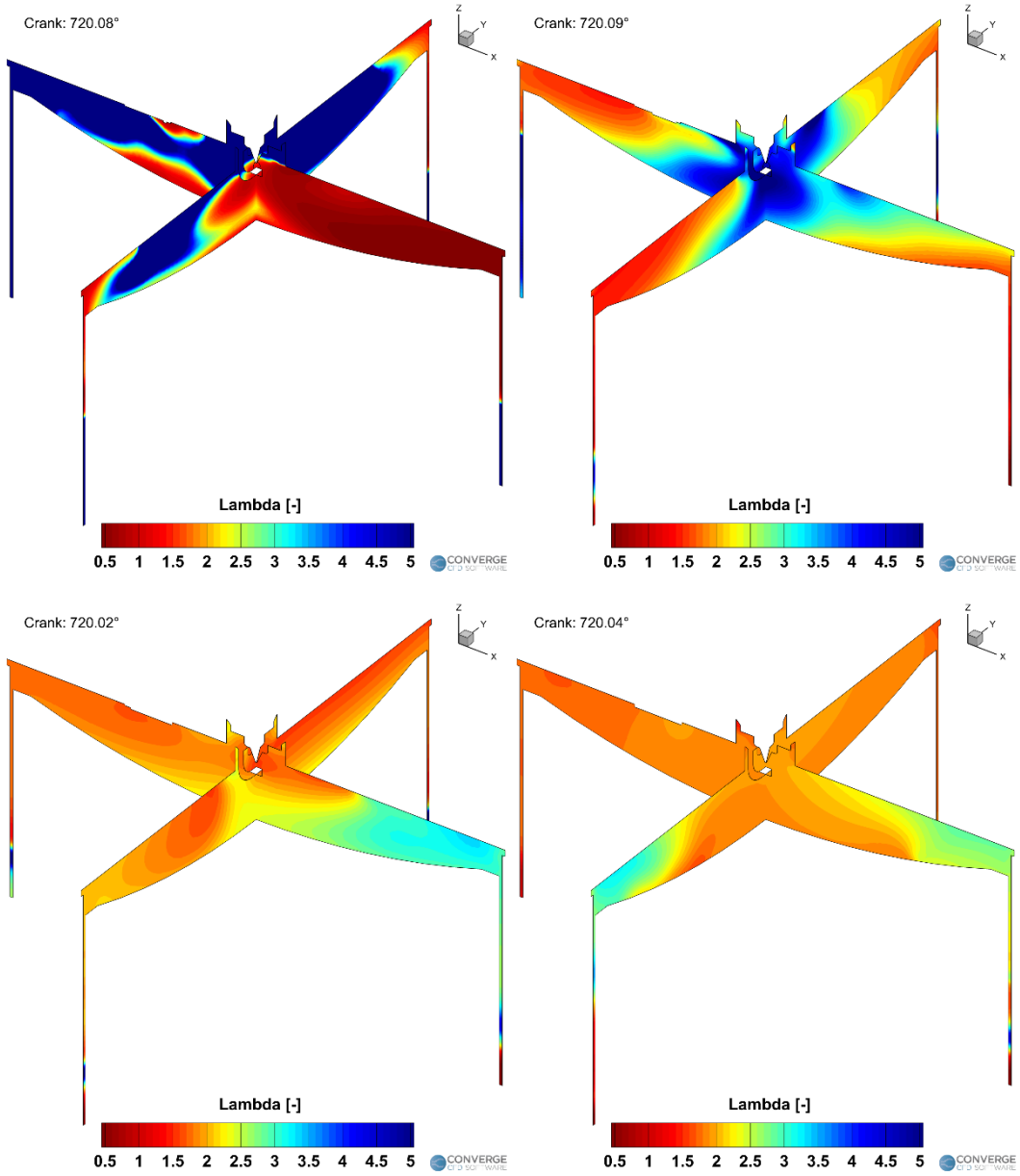

Figure 3.4: WP 1 ST frames at λ=2 and SOI = -35° (top left), SOI = -70° (top right), SOI = -110° (bottom left), SOI = -150° (bottom right) [aTDC]

At low-load low-speed operating conditions, early SOI timings help in obtaining an almost homogeneous charge in the combustion chamber at ST thanks to the high amount of time available before reaching TDC. Unfavorable charge distributions are instead obtained with late SOI timings because of the combination of reduced time available before TDC and in-cylinder flux movements; injecting at SOI = -35 deg aTDC results in a too-rich charge distribution around the spark plug which will develop in a too-fast combustion event, while injecting at SOI = -70 deg aTDC results in a too-lean charge distribution around the spark plug which will lead to a late and slow combustion process.

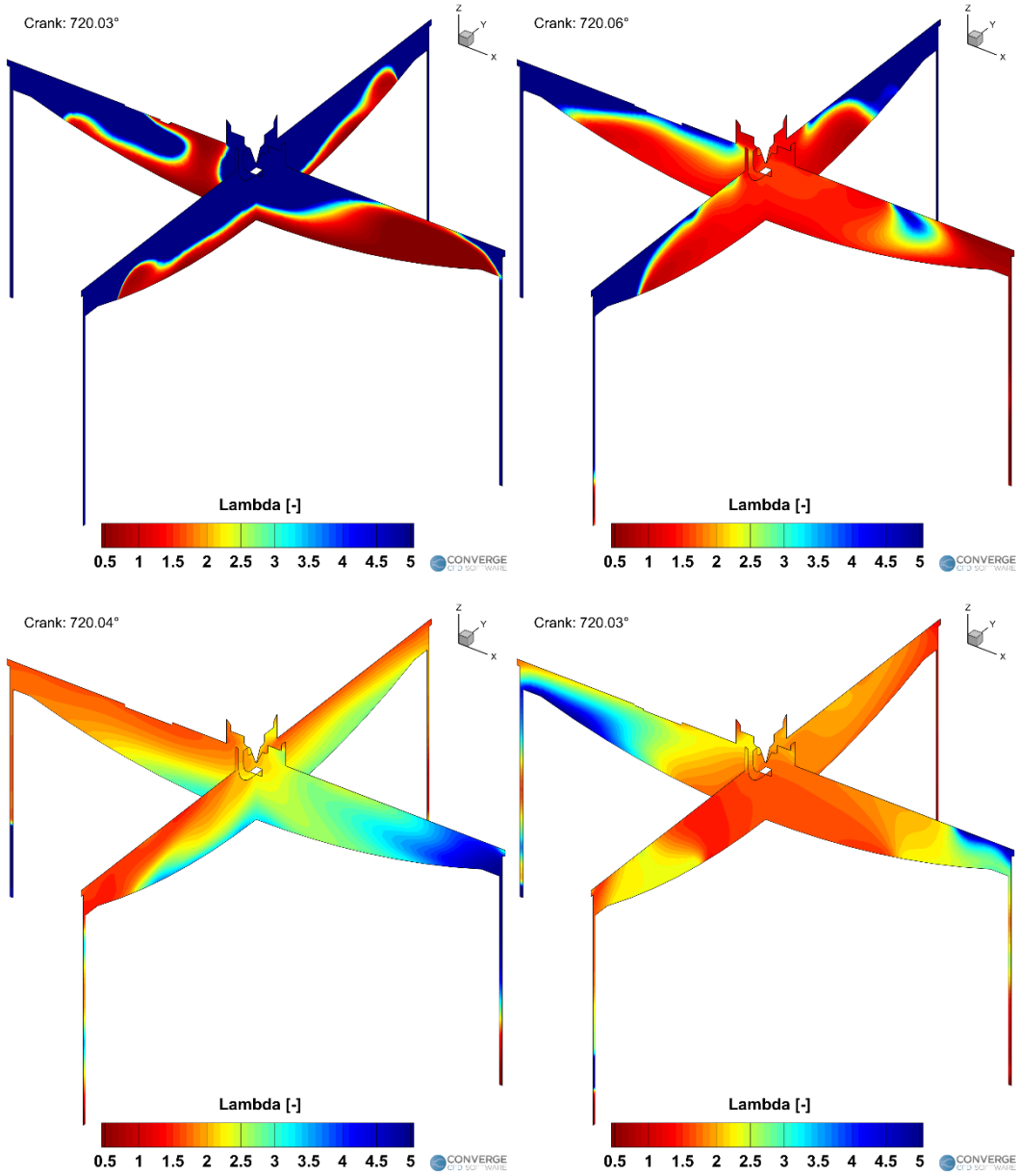

Figure 3.5: WP 2 ST frames at λ=2 and SOI=-35° (top left), SOI = -70° (top right), SOI = -110° (bottom left), SOI = -150° (bottom right) [aTDC]

Very similar charge distributions with respect to WP 1 are obtained with WP 2. Late SOI timings develop unfavorable charge distributions around the spark plug, but in this case, with the latest SOI timing the injected hydrogen has almost no time to spread into the combustion chamber and to mix with air; with SOI = -70 deg aTDC, at ST it is formed a too-rich charge cloud which will lead to a too-fast combustion process. The charge homogeneity of the earliest SOI timings is less pronounced concerning the cases of WP 1.

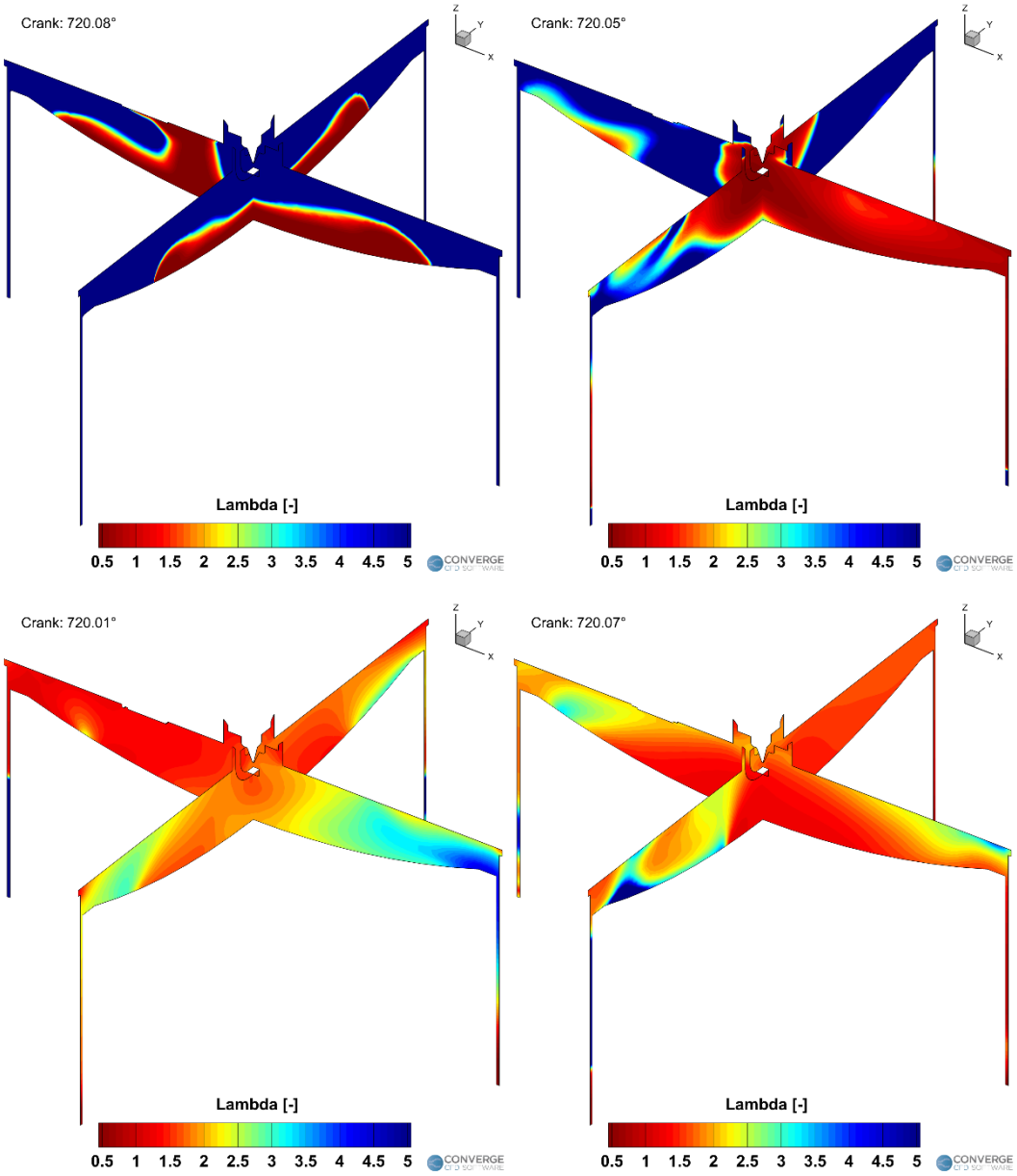

Figure 3.6: WP 3 ST frames at λ=2 and SOI = -35° (top left), SOI = -70° (top right), SOI = -110° (bottom left), SOI = -150° (bottom right) [aTDC]

The consequence of the increase in load and speed of WP 3 develops in a general overall lower lambda value in the combustion chamber as the effect of a very small amount of time available before TDC for the hydrogen to be mixed with air for early SOI timings. The cases with SOI = -35 deg aTDC and SOI = -70 deg aTDC behave as the same ones of WP 2.

The injection timing influence is directly connected to the working point at which the engine is operating. However, it can be stated that the latest injection timing examined, SOI = -35 deg aTDC, is the one that brings up unfavorable charge distributions at ST.

The small amount of time between the End Of Injection (EOI) and ST doesn't allow the hydrogen to properly distribute and mix in the combustion chamber.

To analyze the injection event, three cases, one for each WP, have been selected as examples and considered representative of all cases; in particular, they are all characterized by a SOI = -110 deg aTDC and a lambda = 2.

The high-speed high-load case analyzed is the one in which the injection lasts longer in CA since the engine speed is higher.

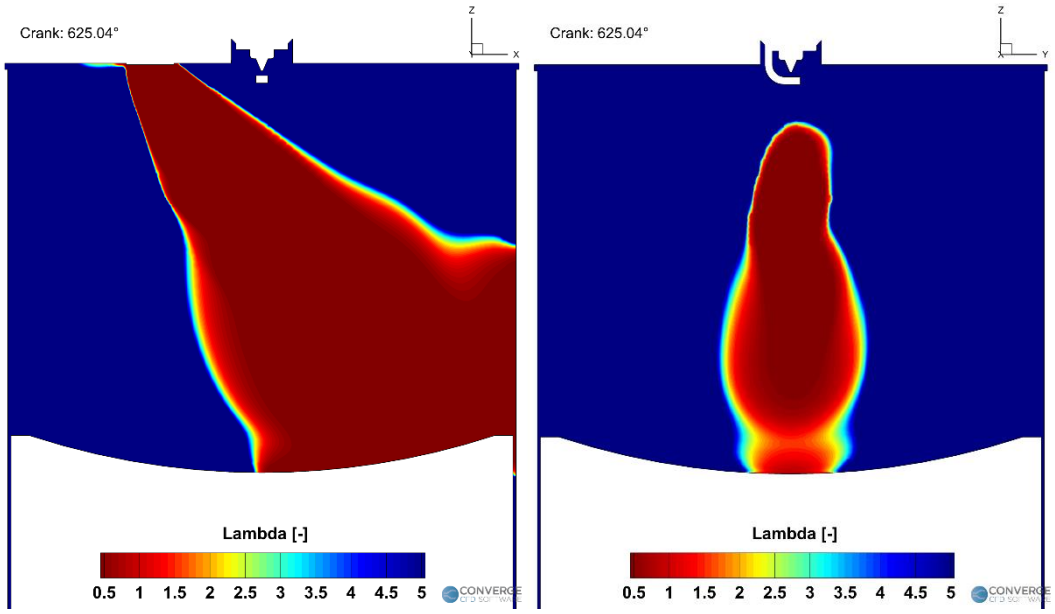

Figure 3.7: WP 3 injection evolution on Y-plane (left) and X-plane (right), CA = SOI +15°

The injection on the Y-plane is strongly asymmetric due to the injector positioning and injection direction, while in the X-plane it appears slightly asymmetric towards the left side of the chamber. After only 15° post-SOI, the hydrogen jet has already reached the piston top; its trajectory is modified as a consequence of the combination of the impact with the piston top and the upward movement of the piston.

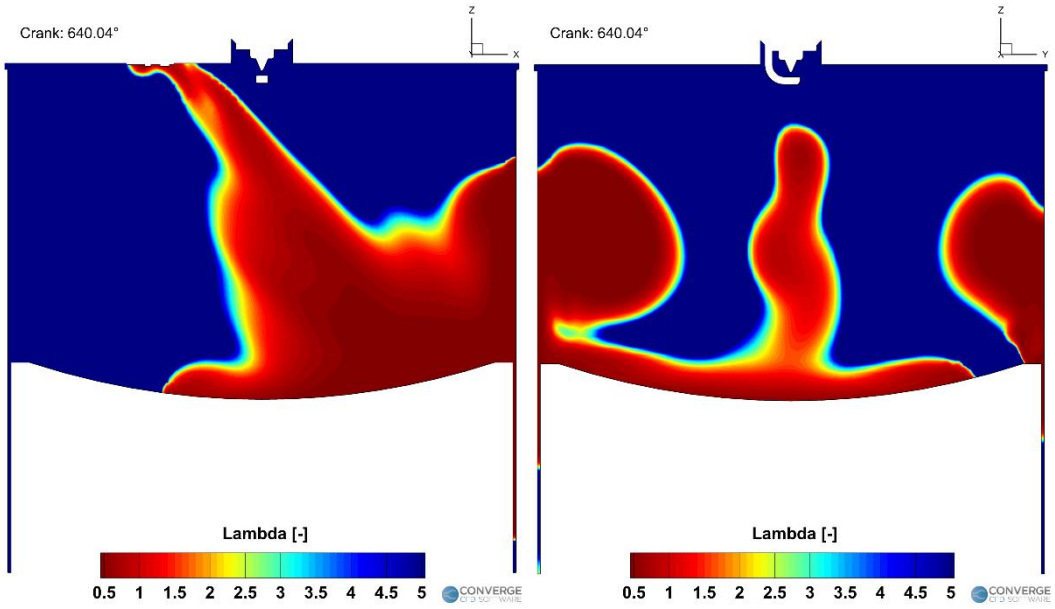

Figure 3.8: WP 3 injection evolution on Y-plane (left) and X-plane (right), CA = SOI +30°

As depicted, on the Y-plane, all the injected hydrogen concentrates in the bottom right zone of the combustion chamber. The slight asymmetry noted after 15° post-SOI on the X-plane leads to a higher amount of fuel trapped in the left lobe created after impacting with the piston top.

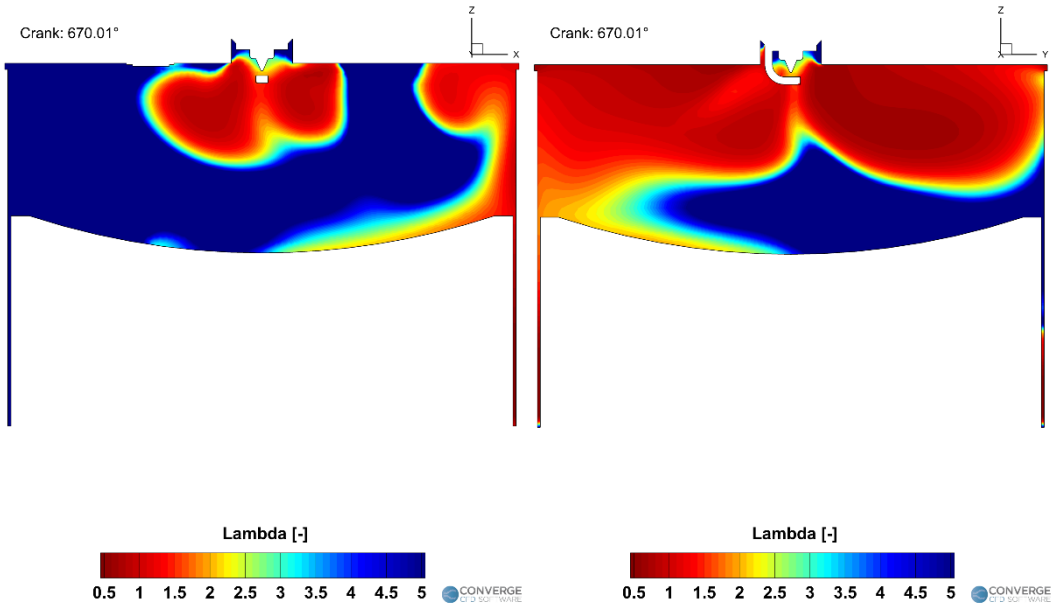

Figure 3.9: WP 3 injection evolution on Y-plane (left) and X-plane (right), CA = SOI +60°

The upward movement of the piston pushes the hydrogen fraction towards the roof of the chamber imposing to it an anti-clockwise motion in the Y-plane. Instead, in the X-plane, the two lobes meet at the chamber roof creating a very rich cloud of fuel in the spark plug region while leaving a very lean cloud near the piston top.

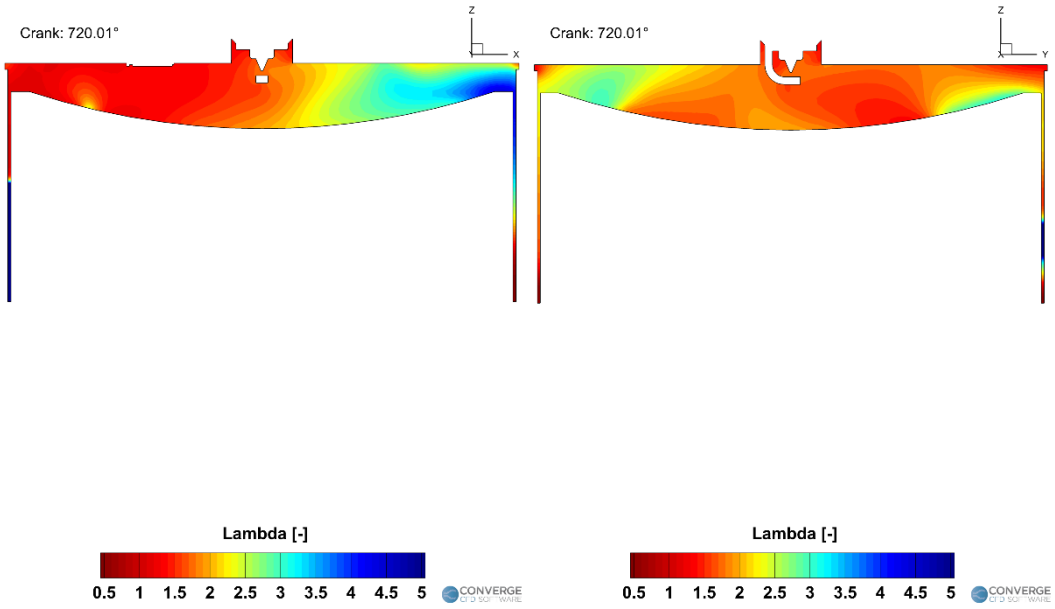

Figure 3.10: WP 3 injection evolution on Y-plane (left) and X-plane (right), CA = ST

At ST, CA = 720°, it is possible to appreciate how on the Y-plane the charge distribution in the combustion chamber is divided into two zones. The left side is richer with respect to the right side. On the contrary, the charge distribution highlighted in the X-plane appears to be more homogeneous, even though with still the presence of leaner pockets.

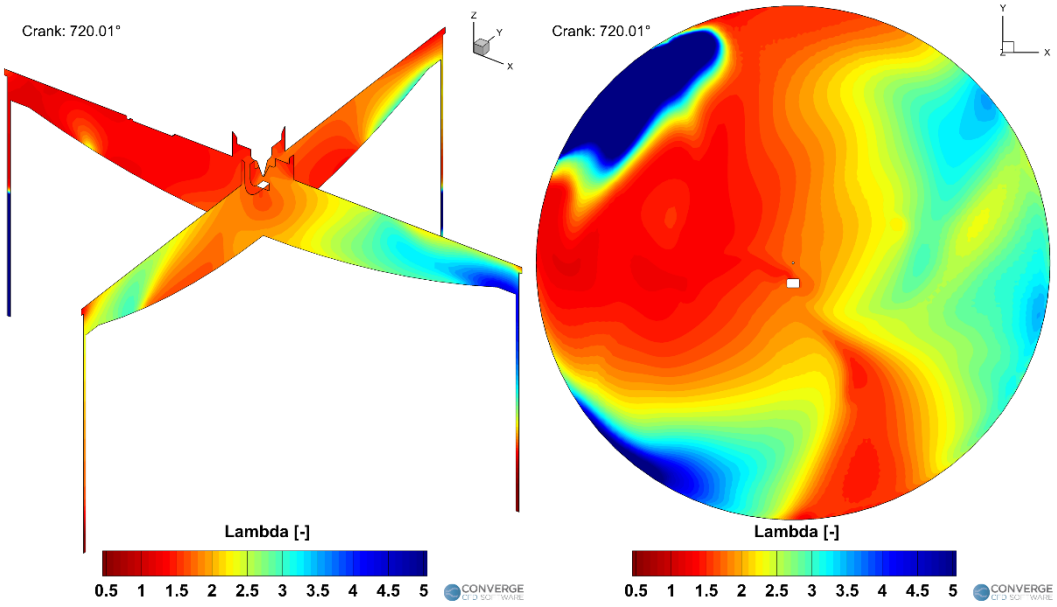

Figure 3.11: WP 3 injection evolution on chamber detail (left) and Z-plane (right), CA = ST

In Figure 3.11 it is possible to appreciate more clearly the charge distribution in the combustion chamber. The charge isn't homogeneously distributed and it is easily identified a preferential direction towards which the flame will propagate, which will be towards the richer zones. The leaner pockets could slow down the flame propagation near the walls.

By reducing the speed and the load, a shorter injection duration will be obtained.

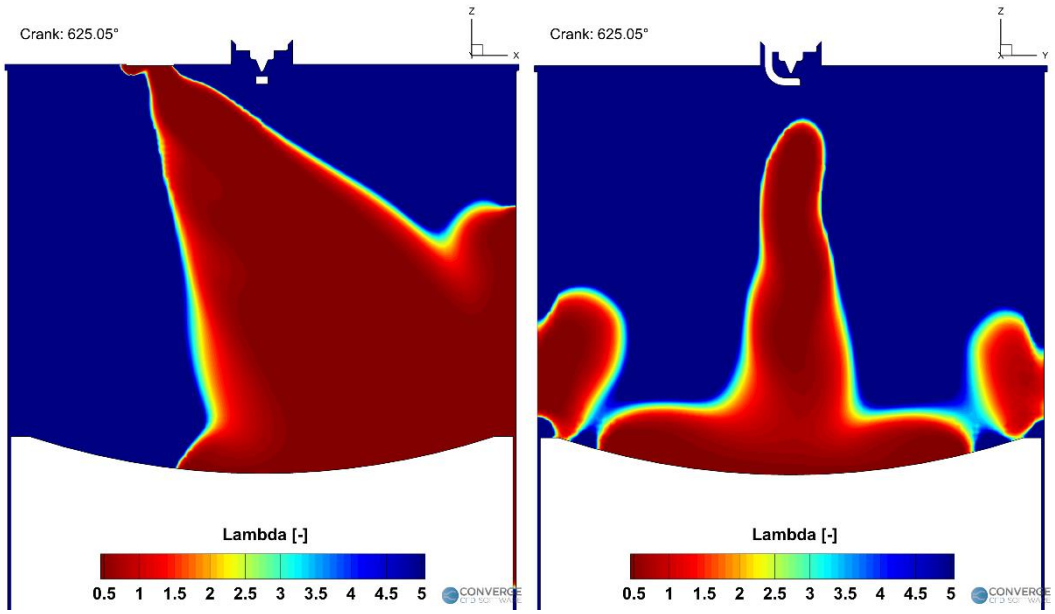

Figure 3.12: WP 2 injection evolution on Y-plane (left) and X-plane (right), CA = SOI +15°

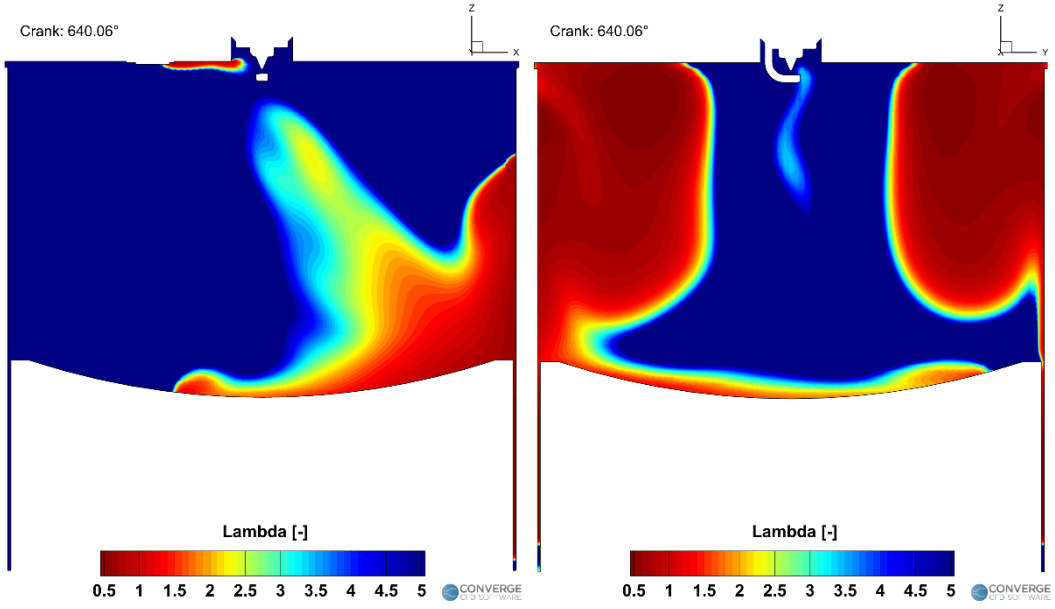

Figure 3.13: WP 2 injection evolution on Y-plane (left) and X-plane (right), CA = SOI +30°

In Figure 3.13, the injection event has already ended and in the Y-plane it can be noted how all the hydrogen fraction is distributed in the bottom right corner of the combustion chamber. On the X-plane, the impact with the piston top divides the jet into two lobes; a

light asymmetry is still present in favor of the left one.

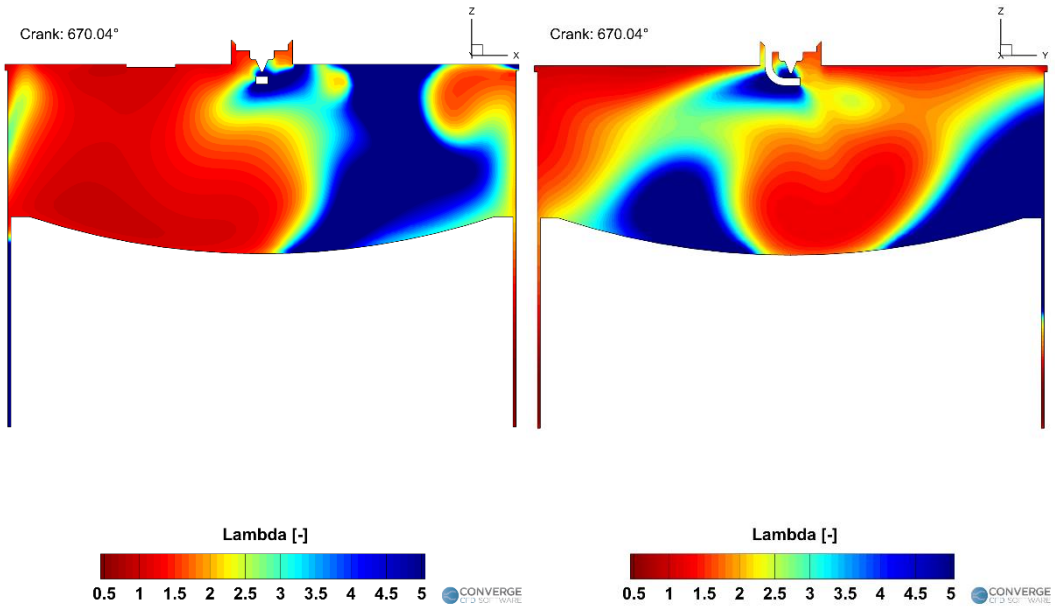

Figure 3.14: WP 2 injection evolution on Y-plane (left) and X-plane (right), CA = SOI +60°

Differently from the previous WP, at CA = SOI +60° in the Y-plane, the charge has had more time to move inside the combustion chamber and the anti-clockwise motion imposed by the piston upward movement allowed the charge to reach past the spark plug; the chamber is divided into a rich left side and a lean right one. Instead on the X-plane, the merge of the two lobes has created two richer pockets, one in the middle and the other in the top left angle of the combustion chamber.

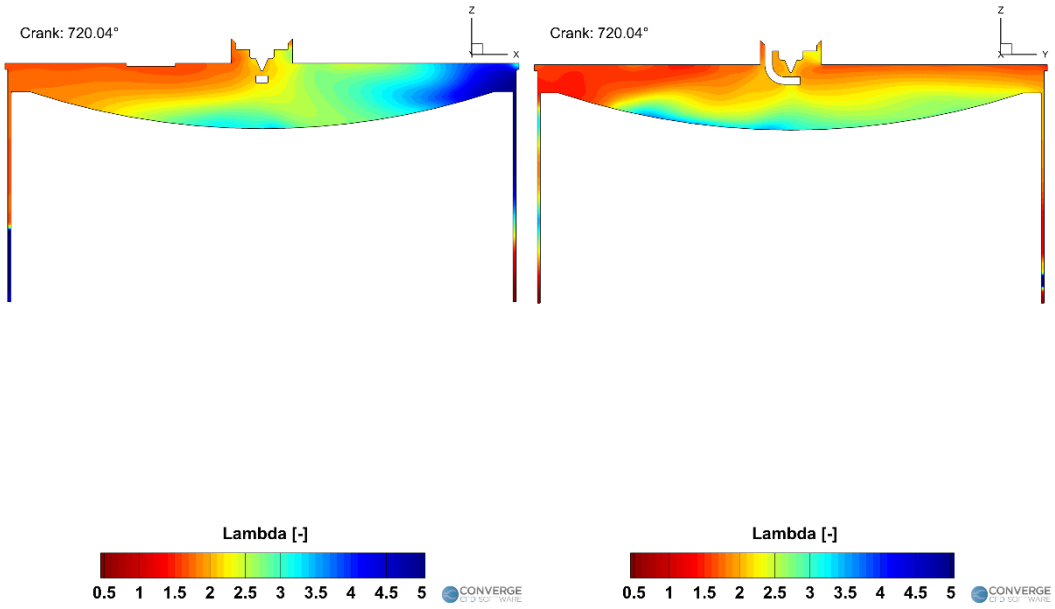

Figure 3.15: WP 2 injection evolution on Y-plane (left) and X-plane (right), CA = ST

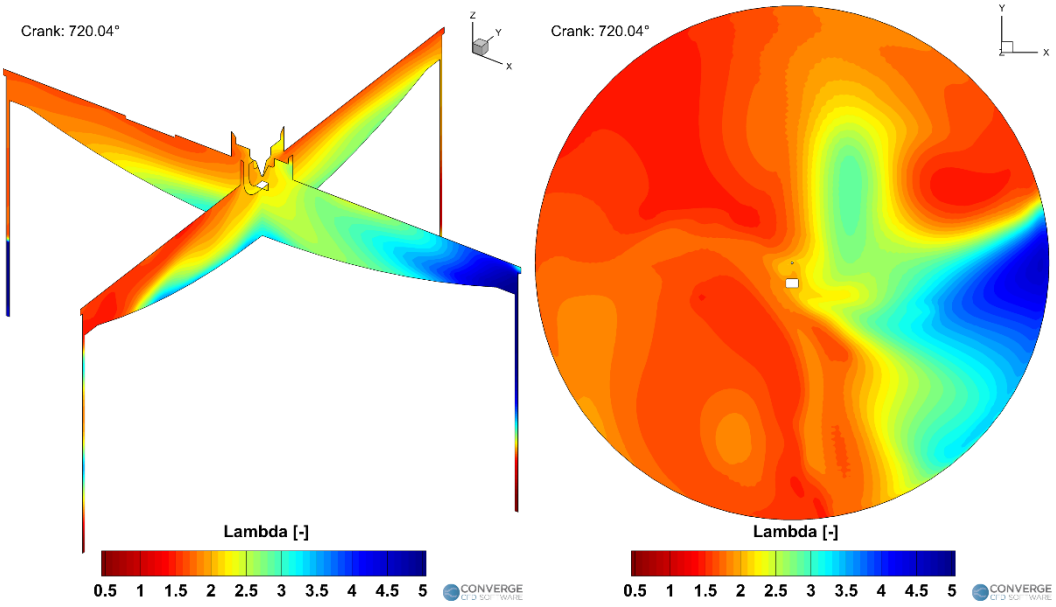

Figure 3.16: WP 2 injection evolution on chamber detail (left) and Z-plane (right), CA = ST

Figure 3.15 and Figure 3.16 depict the charge distribution in the combustion chamber at ST. A very lean pocket is present in the right zone of the X-plane, but overall the distribution appears to be quite homogeneous. However, it must be noted how the charge distribution is spread along the Z-axis; a richer zone is developed towards the combustion chamber roof and a leaner one towards the piston top.

A further decrease in speed and load allows a better charge distribution and mixture at ST.

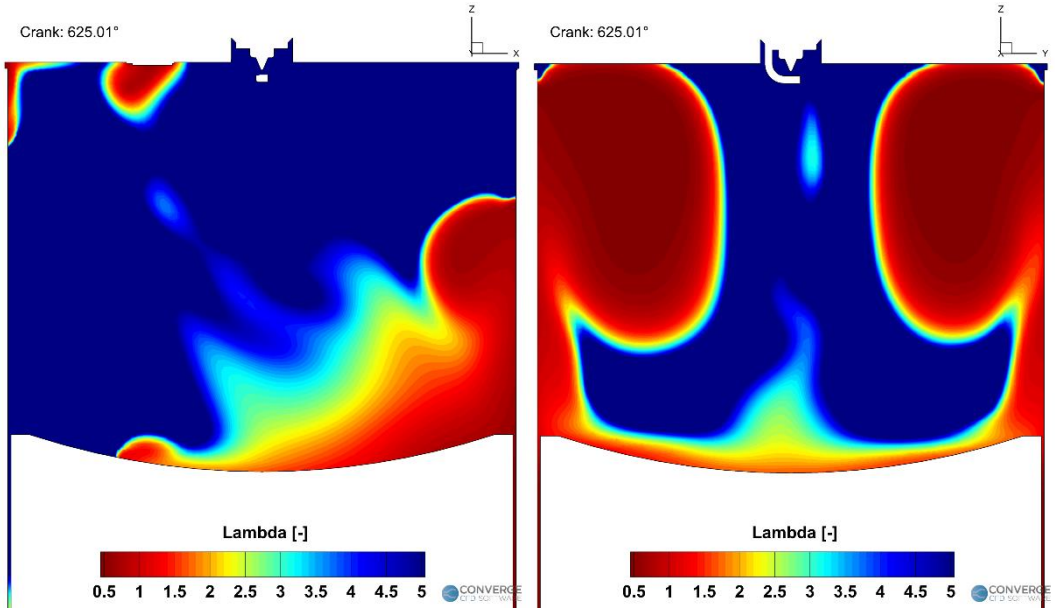

Figure 3.17: WP 1 injection evolution on Y-plane (left) and X-plane (right), CA = SOI +15°

After 15° post SOI all the fuel has already been injected into the chamber and has already condensed in the bottom right zone of the combustion chamber in the Y-plane. In the X-plane, the lobes created after the jet impact on the piston top appear to be almost perfectly symmetric; the slight asymmetry of the jet during the injection event has essentially disappeared.

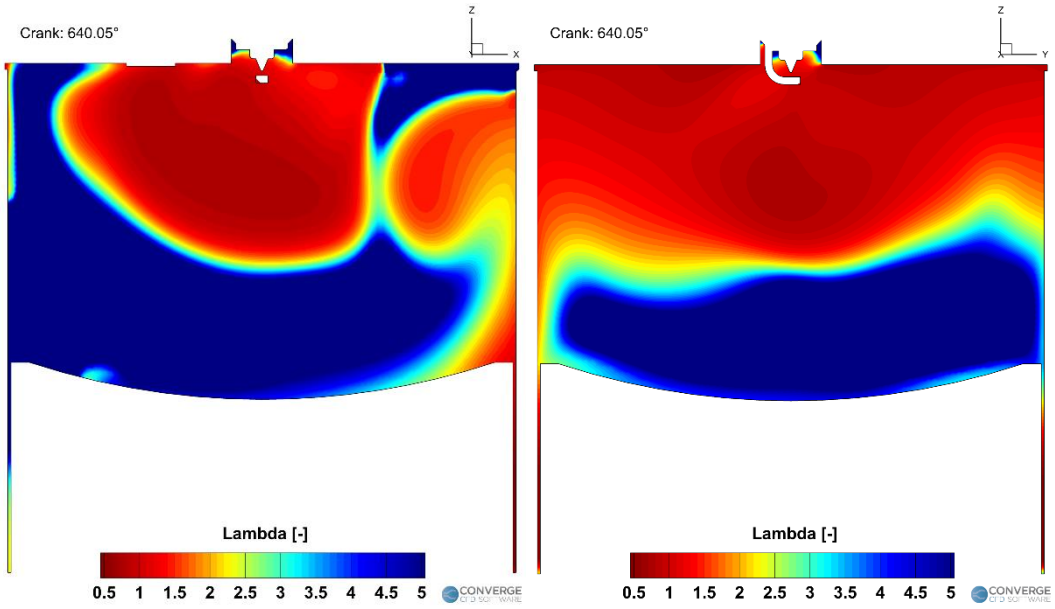

Figure 3.18: WP 1 injection evolution on Y-plane (left) and X-plane (right), CA = SOI +30°

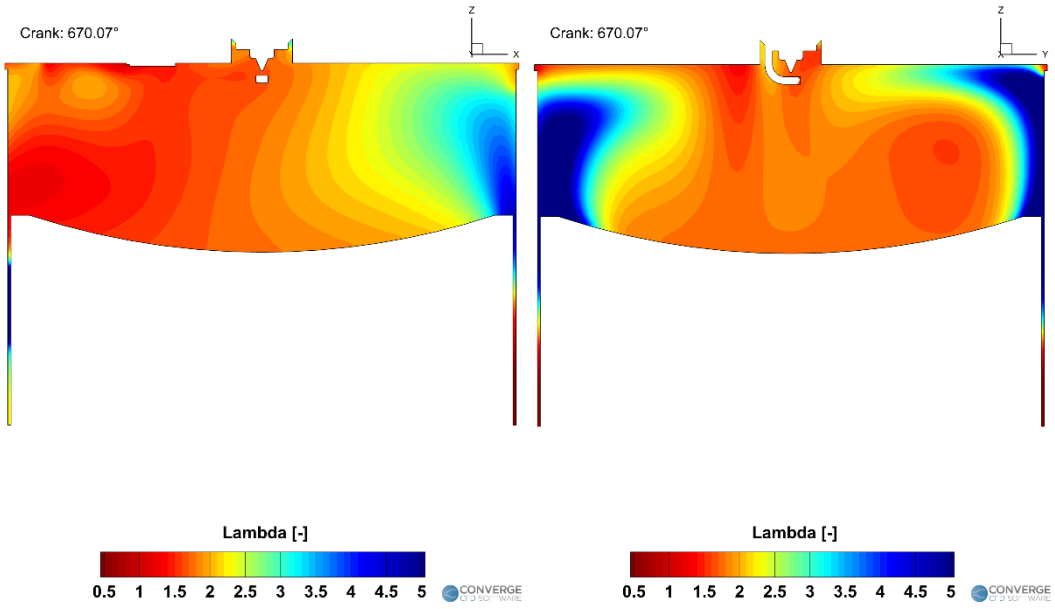

Figure 3.19: WP 1 injection evolution on Y-plane (left) and X-plane (right), CA = SOI +60°

The charge distribution in the Y-plane of Figure 3.19 is a direct consequence of the counter-clockwise motion imposed from the piston top to the charge. The higher available amount of time before ST allows the lobes on the X-plane to condense in a bigger richer zone in the middle of the combustion chamber.

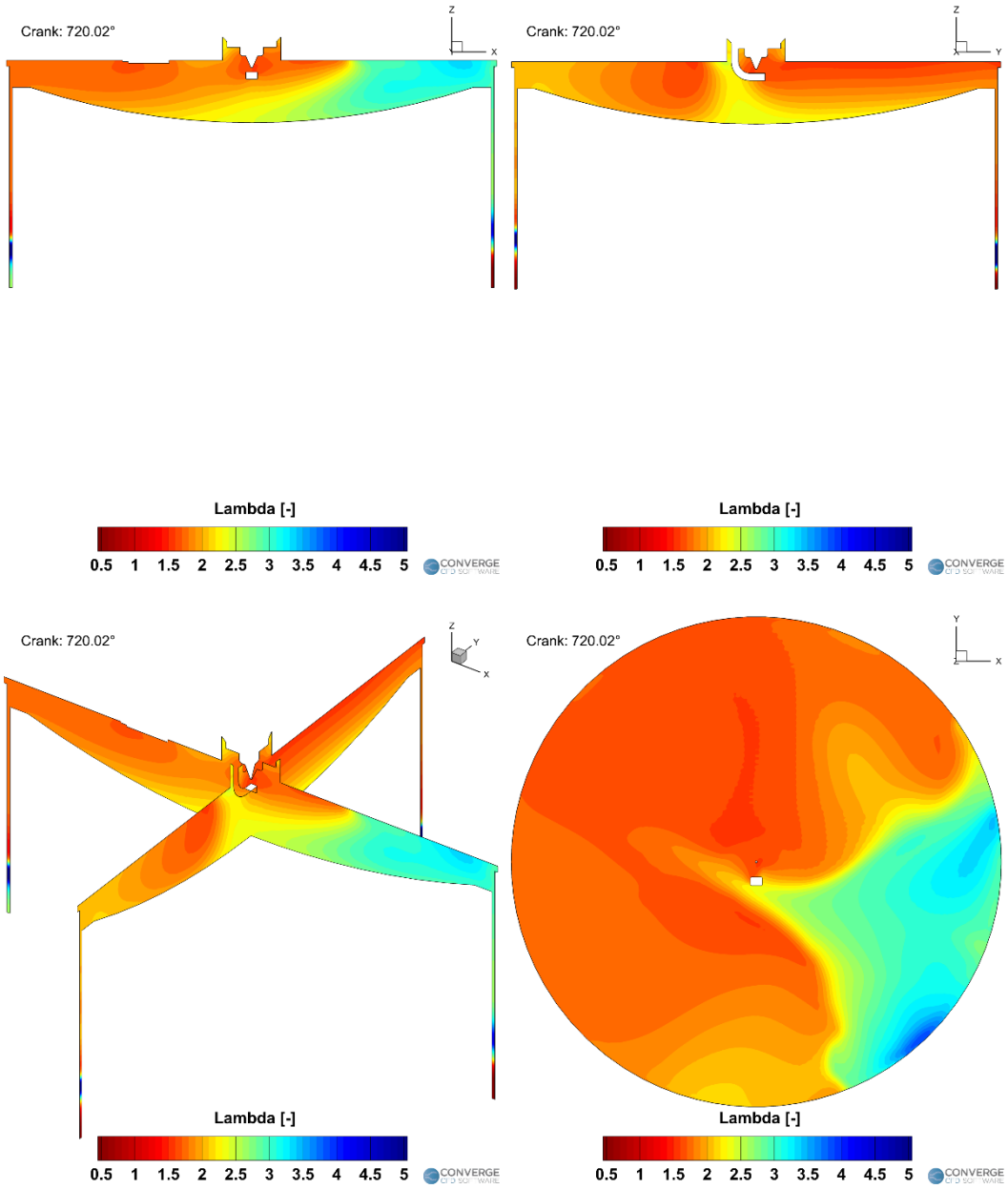

Figure 3.20: WP 1 injection evolution on Y-plane (top left), X-plane (top right), chamber detail (bottom left) and Z-plane (bottom right), CA = ST

Eventually, an overall homogeneous charge distribution is obtained at ST. Still, a leaner pocket is present on the right side of the Y-plane; this could influence flame propagation by slowing it down.

3.1.2 Lambda value influence

The wide range of flammability of hydrogen allows it to operate with high lambda values. In this study, four different situations have been analyzed, starting from a lambda value equal to 2 and moving up to a lambda value equal to 2.75 with steps of 0.25. Increasing the lambda average value resulted in obtaining overall leaner charge distributions at ST. It must be considered that the increment in value for the lambda parameter has been obtained through a combination of an increase in both fuel mass injected and boost pressure; increasing the lambda will result in a decreased value of efficiency so a higher amount of fuel will be needed, as a consequence the quantity of air introduced in the combustion chamber, ruled by the boost pressure, will be given by the fuel quantity injected to obtain the desired lambda value.

The four lambda conditions of the WP 3 cases with SOI = -110 deg aTDC have been selected by way of example.

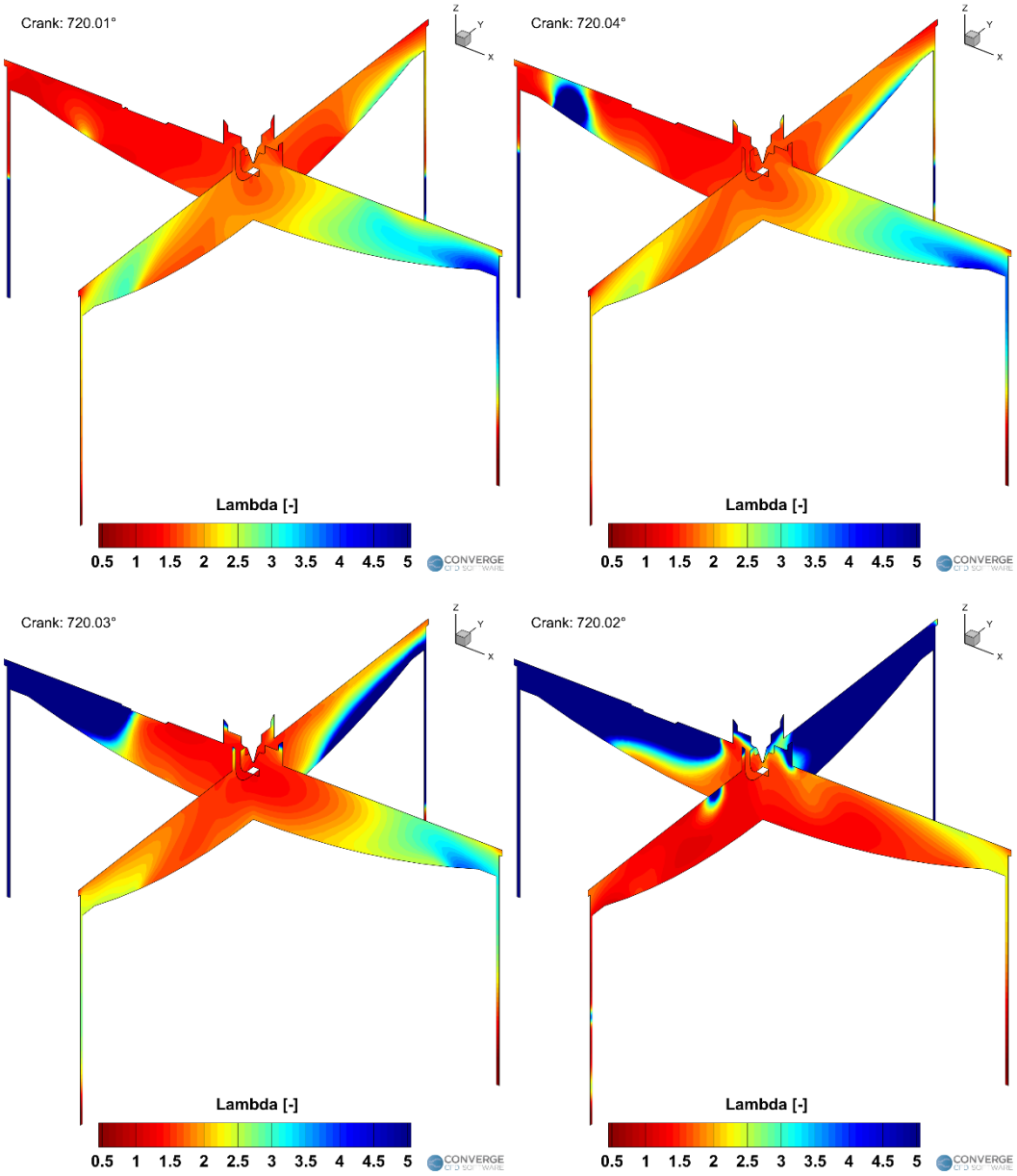

Figure 3.21: WP 3 ST frames of case 17 [λ=2] (top left), case 19 [λ=2.25] (top right), case 22 [λ=2.5] (bottom left), case 24 [λ=2.75] (bottom right), CA = ST

All of the four cases displayed in Figure 3.21 exhibit good combustion because the lambda conditions around the spark plug at ST are always favorable, even though the overall lambda values are different. This highlights the importance of obtaining a good charge distribution around the spark plug at ST.

3.1.3 Lambda extraction process on the flame front

The monodimensional approach used by GT-SUITE implements a specific command that allows the model to take into consideration the stratification phenomenon, otherwise only accurately repeatable in a 3D-CFD model. The laminar combustion speed of the *SI-Turb* model is regulated by the profile of the equivalence ratio over the mass fraction burned (function of the flame front) which is given as input to the command. To recover the profile needed, it is necessary to properly analyze the results obtained from the 3D-CFD simulations using the post-processing software TECPLOT. However, the desired profile isn't already present in the 3D-CFD results, so two different approaches have been used to try to extract this profile in the best possible way. The logic behind the selection of these two approaches lies on the consideration that the flame front, while progressing inside the combustion chamber, will excite some specific chemical reactions and will modify the thermodynamic state of the burned gas zone with respect to the unburned one.

The first approach, which could be considered more physical, lies on the verified assumption that the combustion progression triggers a temperature rise. It has been selected a specific value of temperature of 1500 K as a threshold between the burned and unburned zones. The value of lambda has been then averaged on the iso-surface at T = 1500 K for each crank angle.

However, this approach hasn't proved to be very effective because the distinction between the burned and unburned zones results very difficult to predict. In fact, during the expansion phase when the piston moves down, the burned gases are cooled and, in this way, this approach ends up considering also burned gas regions in the iso-surface instead of only the flame front region.

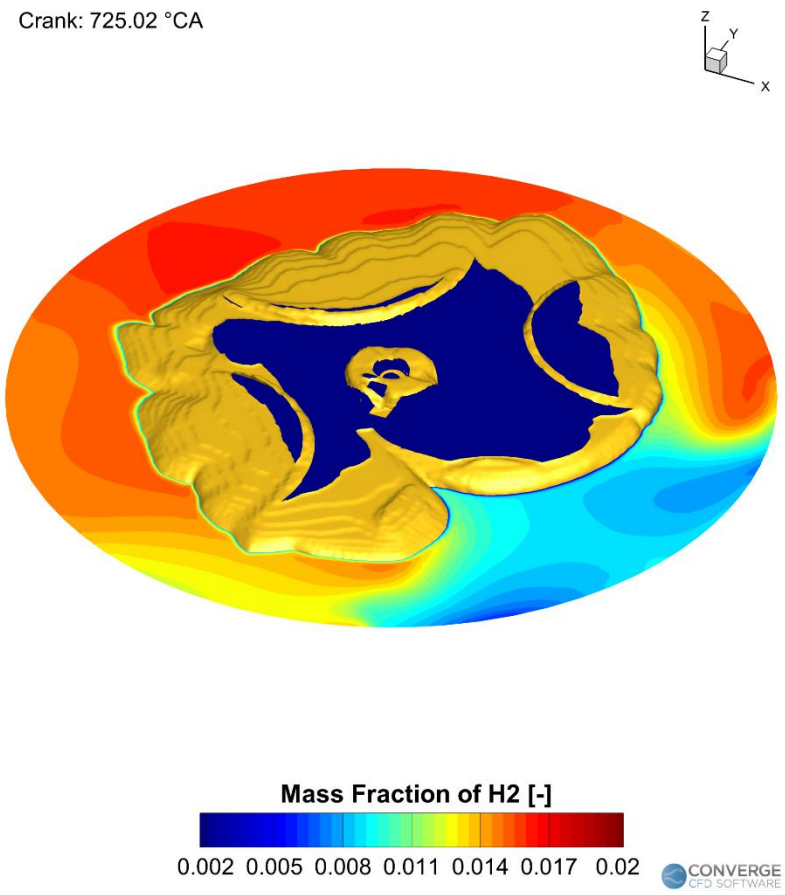

Figure 3.22: Iso-surface at T=1500 K representation (yellow) and Z-plane slices contoured with H_2 mass fraction, CA = ST + 5°, case 1

In Figure 3.22, it can be noted how the iso-surface includes regions where there is no more H_2 available, so no flame could be present. So the average value of lambda obtained won't be the one on the flame front.

For the above-mentioned reasons, a second approach has been implemented. This one is of the chemical type and lies on the assumption that, rather than a single-step process, the combustion is a combination of chemical reactions subdivided into more steps in which different intermediates chemical species are formed and react among them to form the final products of the combustion process. A single chemical species able to help in tracing the flame front has been selected. The H_2O_2 is only present before the combustion, it has been then used as a tracer for all the zones on the verge of combustion and it has also been helpful in identifying the zones of pre-ignition. As for the first approach, the main difficulty lies on the possibility of selecting the correct threshold values for the parameter taken into consideration. The limit of this approach is that the H_2O_2 species are always

present immediately before the flame front towards the unburned gases region; this behavior is highlighted at the end of the combustion process when the fuel fraction that burns is less and so a limited fraction of H_2O_2 is present. With this approach, the lambda value is obtained by averaging it over each angular step after having blanked the regions outside of the threshold limits.

In previous studies [13], the mass fraction of H has also been analyzed and compared to the one of H_2O_2. It has been noted that the presence of H prevailed in the burned gas zone and that imposing a threshold value on this chemical species helped in blanking the unburned zone. However, since the threshold on H only blanked the unburned gas zone and not the burned one, it has been stated that using this threshold wasn't helpful in trying to extrapolate the flame front.

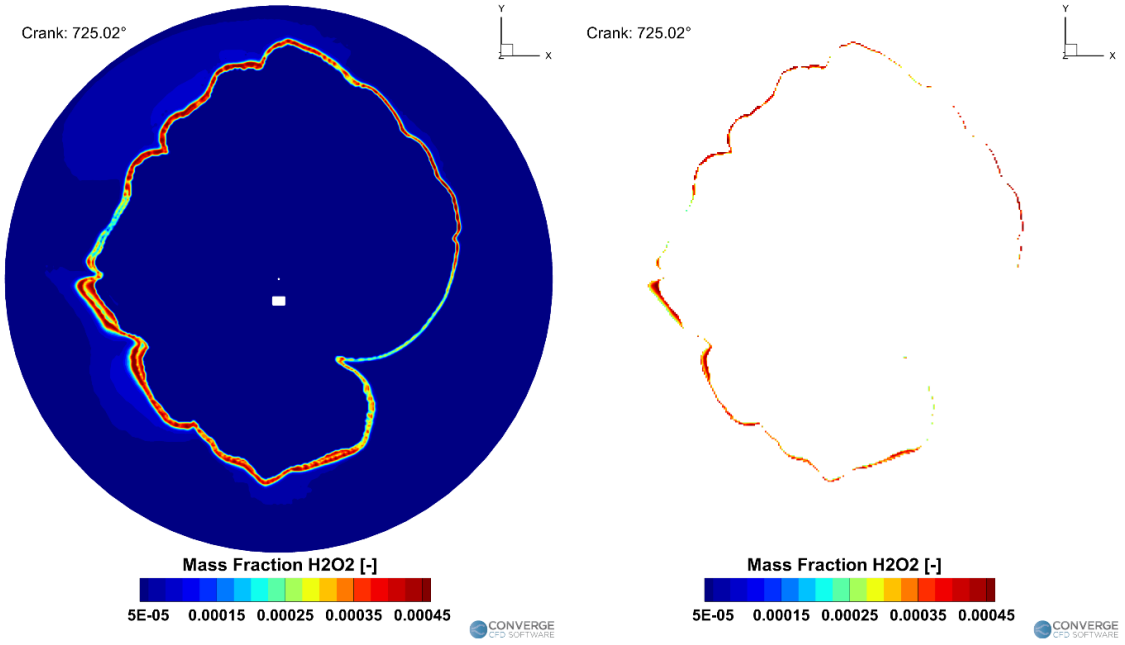

Figure 3.23: H_2O_2 mass fraction on the Z-plane without (left) and with blanking (right), CA = ST + 5°, threshold value H_2O_2 > 0.0002, case 1

As represented in Figure 3.23, imposing a threshold value and blanking the regions out of it helps in removing the burned gas region in a very good way. However, even though in this case the threshold value imposed is already really borderline because too stringent, it remains impossible to perfectly depict the flame front since it isn't possible to know its width; further shrinking the threshold value imposed will only result in the loss of some profile parts in the earliest moments of the combustion process.

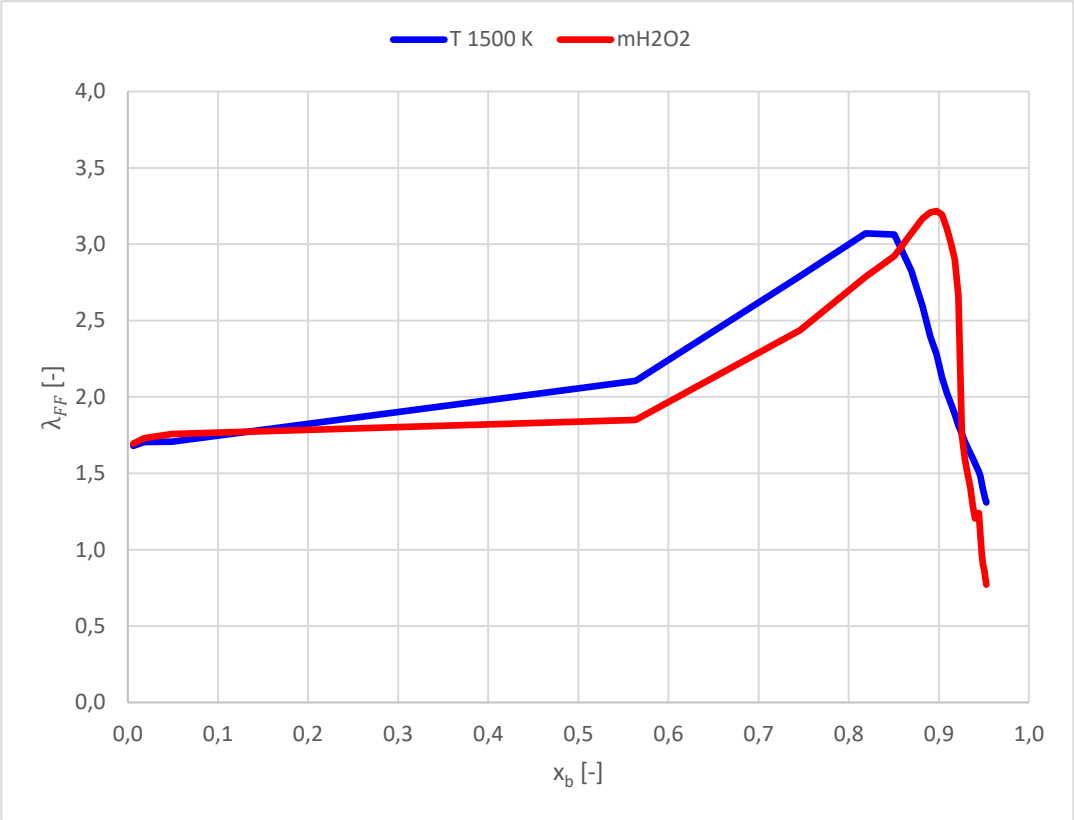

Figure 3.24: λ_{FF}- x_b profiles obtained with the two approaches examined, case 17

The trend generally emerging in the cases analyzed is the one shown in Figure 3.24. The stratification phenomenon is highlighted by the curve trend that could be divided into a first flatter section with an almost constant value of lambda followed by a spike up of the profile towards higher values of it. The lambda value read from the approach based on the iso-surface at T = 1500 K tends to be slightly overestimated, to decrease earlier towards higher values of mass fraction burned and to reach higher values in the interval 0,25 – 0,75 with respect to the approach based on the mass fraction of H_2O_2 as a consequence of the limitation previously explained. Eventually, it was decided to consider for the following steps the value of lambda extrapolated on the flame front with the approach based on the mass fraction of H_2O_2.

3.2 1D-CFD model calibration and validation

Once the 3D-CFD results have been analyzed and the profile of lambda on the flame front has been extracted, a 1D-CFD model has been created and calibrated to evaluate the engine behavior on the entire dimensional plan. The model that has been used to simulate the combustion process in GT-SUITE is the *SI-Turb* one; the combustion process evolution is simulated starting from the turbulence levels, a laminar flame speed model and an estimate of the turbulent combustion speed values. In this thesis activity the laminar flame speed model has been directly selected among the ones present in the GT library; the "*hydrogen*" one has been used.

3.2.1 Turbulence calibration

The first step has been the calibration of the turbulence multipliers for the turbulence model. In the GT-SUITE software, the turbulence is modeled through four parameters:

- Production Term Multiplier: multiplier to the term ruling the production of turbulence from the mean flow;
- Geometric Length Scale Multiplier: multiplier to the representative geometric length scale for the cylinder;
- Intake Term Multiplier: multiplier to the contribution of intake flow through valves to mean kinetic energy;
- Spray/Jet Term Multiplier: multiplier to the contribution of injection flow and pre-chamber nozzle flow to mean kinetic energy [15].

Among the four multipliers the most relevant one in this study, focused on a DI event, has been the Spray/Jet one which is related in a straight line to the turbulence level caused by the injection event of fuel into the combustion chamber. The values of the first three terms were already available from a model previously developed in a PFI configuration and considering that the main difference between a DI configuration and a PFI one is represented by the injection event, these could have been reasonably kept as they were. However, for the sake of completeness and because the intake gases between the two configurations are slightly different, it has been decided to calibrate all four parameters; the already-known values were used as a starting estimate.

The model used for the calibration was made of a single cylinder with the injector and the crank train element; plus, the intake and exhaust boundary conditions were directly taken from the 3D-CFD model.

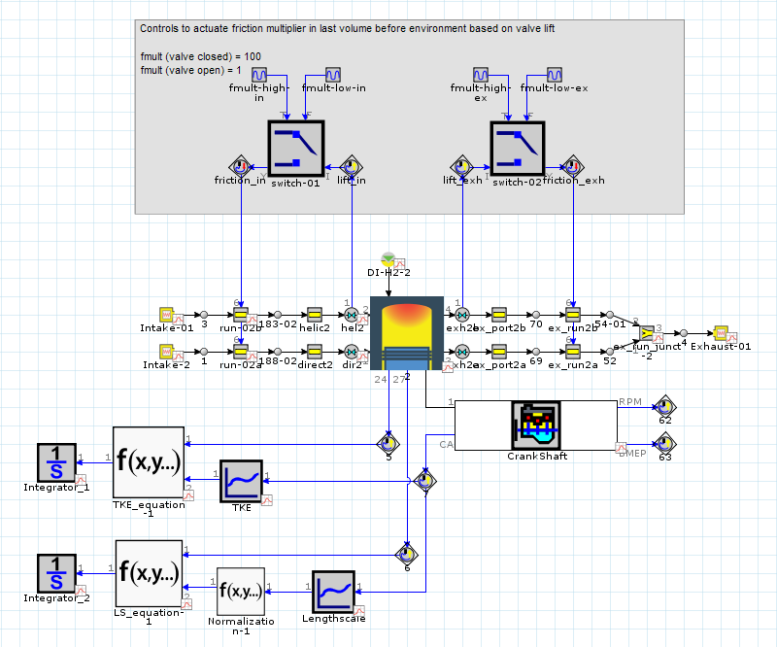

Figure 3.25: Model used for the turbulence calibration

The optimization has been carried out on two quantities, the Turbulent Kinetic Energy (TKE) and the Normalized Length Scale (Normalized LS), that have been optimized in the ST region to obtain the smallest possible relative errors with respect to the 3D-CFD model. The error has been calculated as the square root of the squares' difference of the 1D-CFD and 3D-CFD profiles over the 3D-CFD profile used as reference.

$$error\ TKE = \int_a^b \frac{\sqrt{(TKE_{GT} - TKE_{3D})^2}}{TKE_{3D}} \qquad error\ LS = \int_a^b \frac{\sqrt{(LS_{GT} - LS_{3D})^2}}{LS_{3D}}$$

Equation 1: Equations used to calculate the error between 1D-CFD and 3D-CFD values

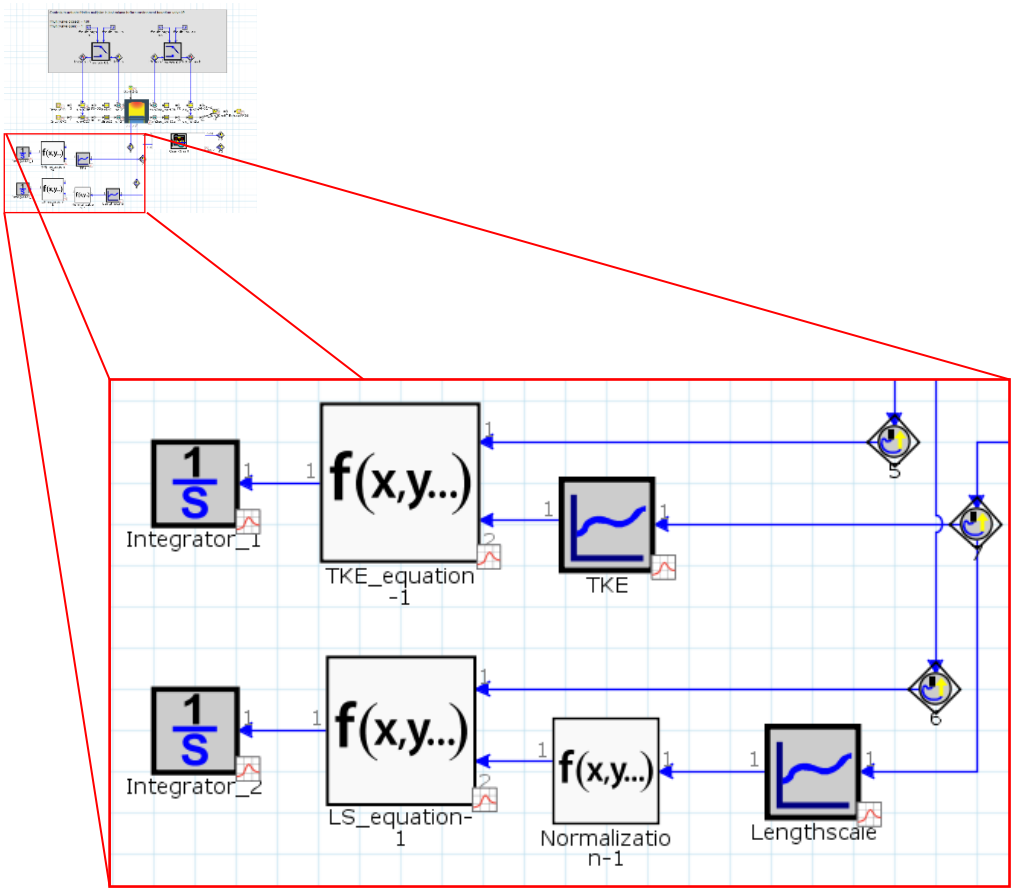

Figure 3.26: Detail of the model used to calculate the errors between 1D-CFD and 3D-CFD results

The procedure has been divided into two steps: the first related to the CA window between -180 deg aTDC and SOI, the second focused on the CA window between -50 deg aTDC and TDC. This procedure has been helpful to calibrate separately the first three parameters and the Spray/Jet Term one; the formers have been calibrated on the first CA window, the latter, having no influence in that same window, on the second one. Furthermore, the turbulence model has been optimized only on one case, case 24, and validated with all the others. The selection of a case with high speed and high load has been made considering that in those operating conditions the turbulence levels introduced are higher with respect to the other two working points analyzed. The optimization objective has been finding a single set of values for all four multipliers to minimize the errors relative to the TKE and the Normalized LS. The values obtained are reported in Table 3.1.

Attribute	*Value*
Production Term Multiplier	0.965
Geometric Length Scale Multiplier	0.851
Intake Term Multiplier	0.536
Spray/Jet Term Multiplier	0.010

Table 3.1: Results of the turbulence calibration processes

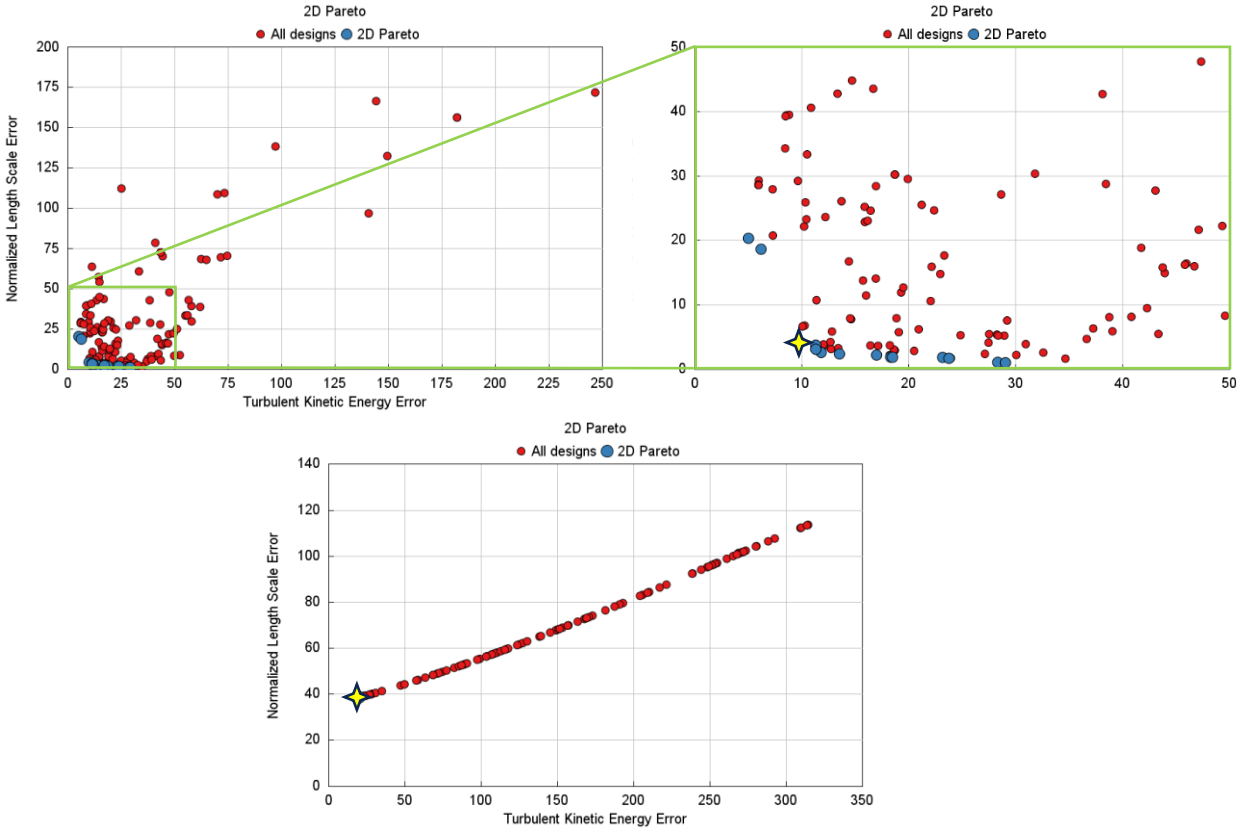

Figure 3.27: Optimizations of the first three Multipliers (top) and of the Spray/Jet Term Multiplier

The following step has been the comparison of the TKE and Normalized LS profiles obtained from the optimized parameters with the ones extracted from the 3D-CFD model. In this way, it has been possible to visually check the differences between these profiles and to analyze them.

It appears very difficult to follow the TKE and Normalized LS profiles extrapolated from

the 3D-CFD analysis along the entire cycle; for this reason, the focus of this activity has been on some CA intervals of interest: the SOI and the angular window [-50 deg aTDC - 0 deg aTDC] immediately before ST.

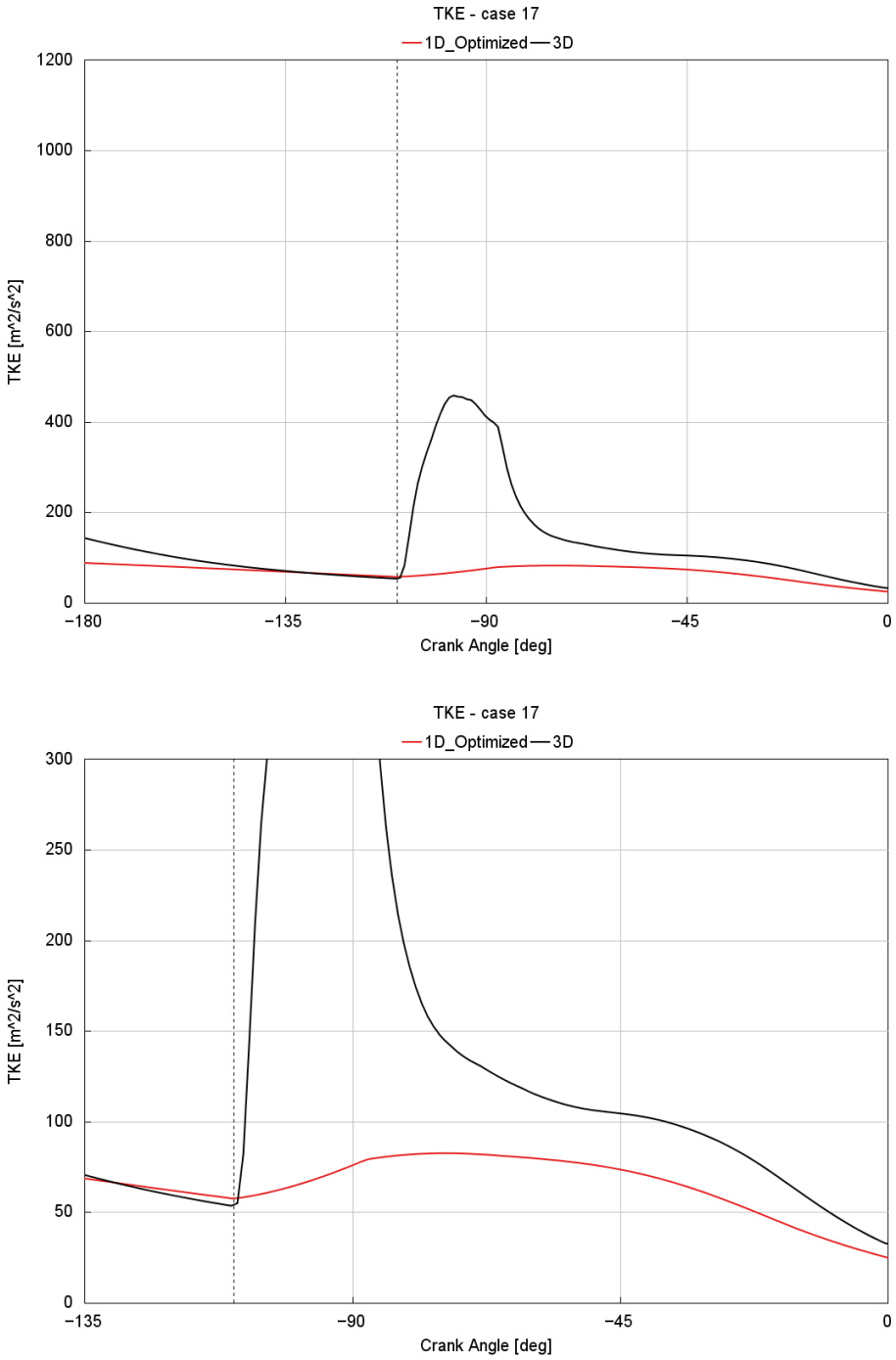

Figure 3.28: TKE case 17 WP3 (top), zoom (bottom)

At high loads, the TKE match between the optimized profile and the 3D-CFD one appears

to be good both at SOI and close to ST. In Figure 3.28 the values of the 1D-CFD profile close to ST are lower than the one of the 3D-CFD ones; this behavior is found in a very limited amount of cases and it has been considered good acknowledging the need to have a single set of values for all the considered cases.

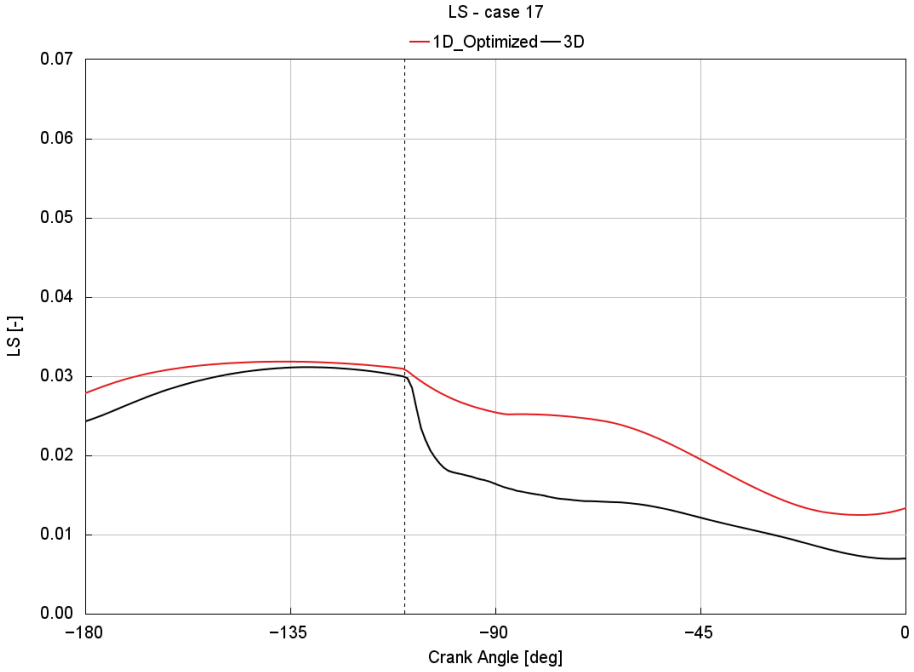

Figure 3.29: Normalized LS case 17 WP3

Focusing on the Normalized LS instead, the trend of Figure 3.29 has been found in every considered case: the very good match between the two profiles at SOI is always followed by a worst one near ST. In particular, the difference between the two profiles at ST increases decreasing the speed and load.

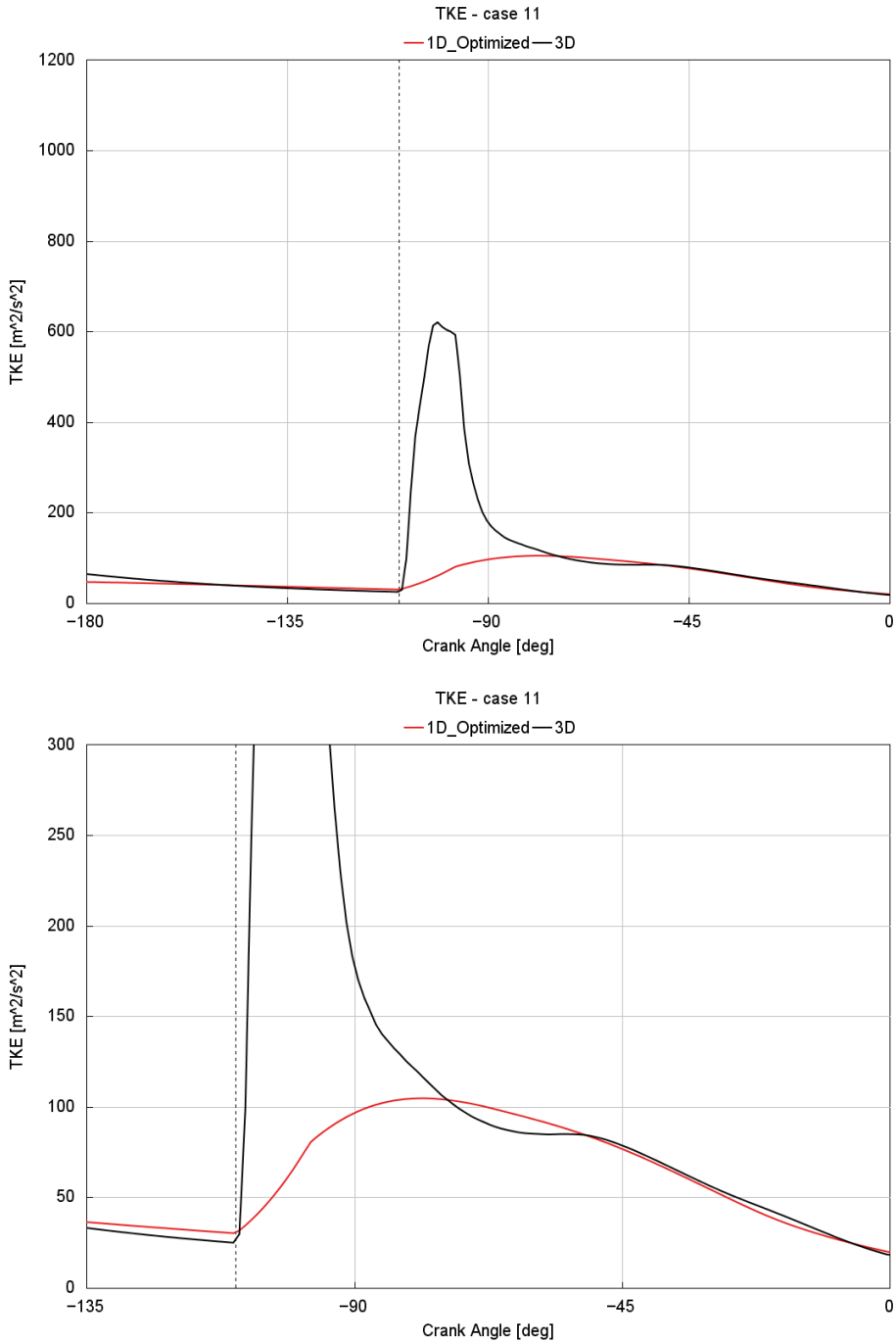

Figure 3.30: TKE case 11 WP2 (top), zoom (bottom)

At WP2, the calibrated turbulence 1D-CFD profile shows a very good match with the 3D-CFD one at SOI and an almost identical one close to ST.

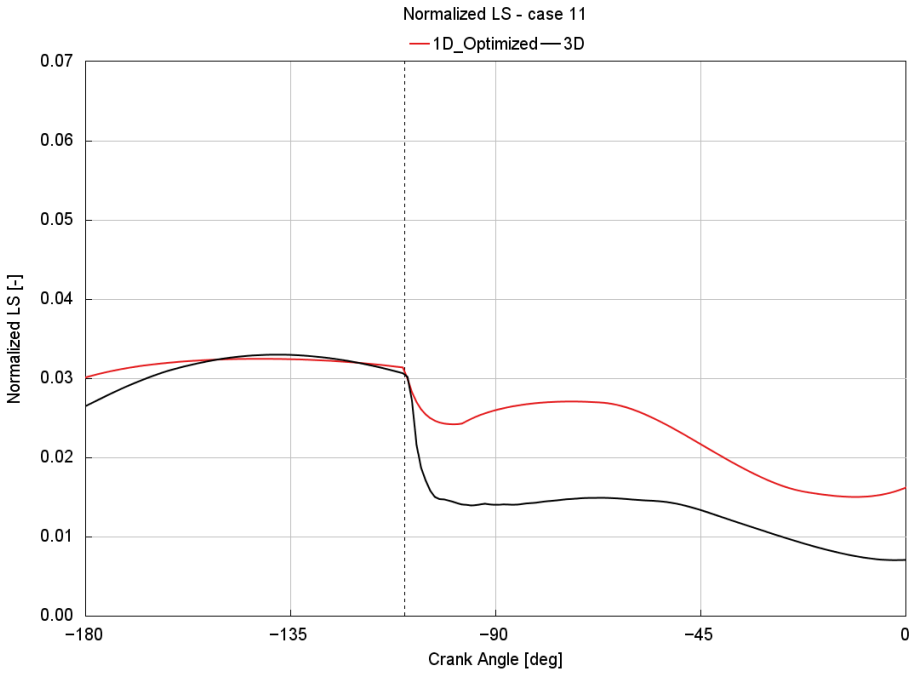

Figure 3.31: Normalized LS case 11 WP2

The same problem experienced with the Normalized LS values in WP3 appears again. The good match between profiles obtained at SOI is followed by a bad match close to ST even though the profiles show very similar trends.

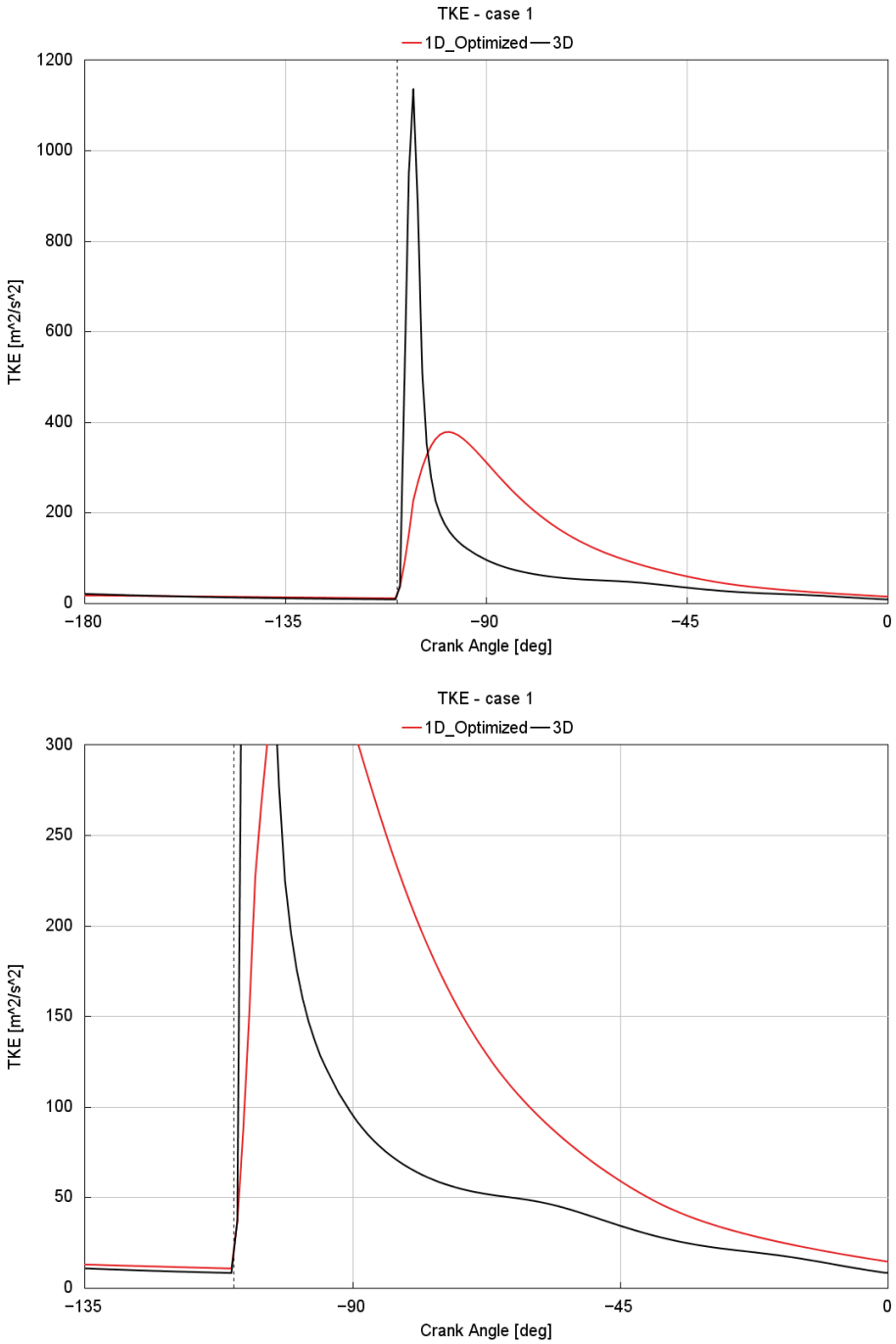

Figure 3.32: TKE case 1 WP1 (top), zoom (bottom)

At the lowest-speed lowest-load working point the match between the optimized profile and the 3D-CFD one at SOI appears to be always very good, while at ST the 1D-CFD profile reaches higher values, overestimating the desired ones.

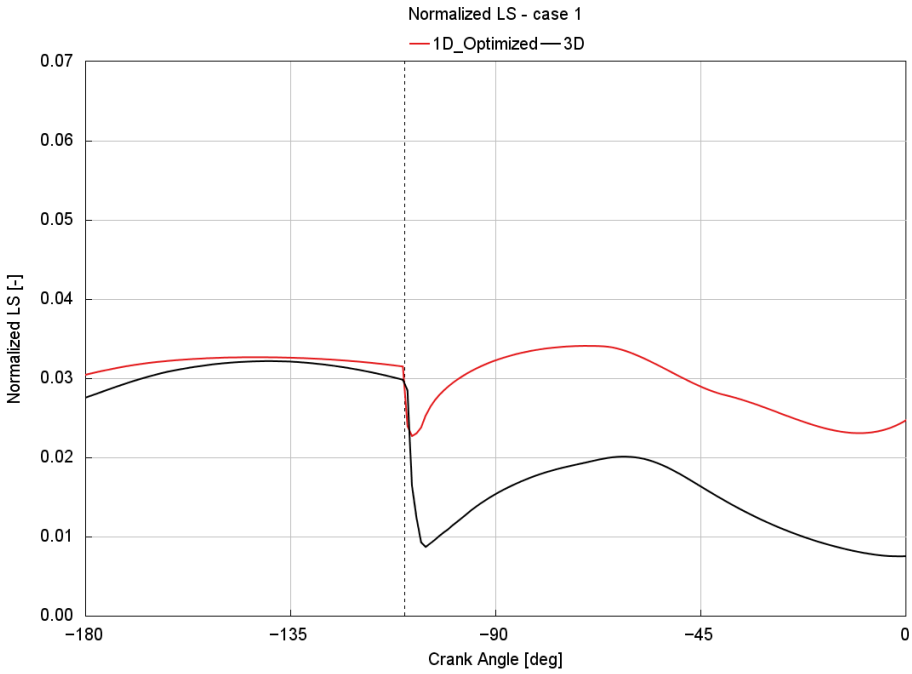

Figure 3.33: Normalized LS case 1 WP1

The Normalized LS discrepancy at ST between the optimized 1D-CFD profile and 3D-CFD one is further increased, while the match at SOI remains good.

It can be concluded that the obtained results both in terms of TKE and Normalized LS can be considered good. The errors that appear close to ST for the TKE have been considered acceptable appraising the impossibility of perfectly reproducing the 3D-CFD results in a 1D-CFD environment where a lot of other uncertainty sources are present. Focusing on the Normalized LS error appearing at ST, it has been considered acceptable taking into account the very low values assumed by that parameter.

3.2.2 SI-Turb model calibration

Once the values of the turbulence parameters have been optimized, the following step has been to evaluate the 3D-CFD results using a Cylinder Pressure Only Analysis (CPOA) method. The CPOA allows to obtain the burn rate profile of each case analyzed requesting the pressure profile and the appropriate boundary conditions as input parameters.

The results obtained from this analysis have been evaluated considering three specific parameters:

- Lower Heating Value (LHV) Multiplier: multiplier to the heating value for the pressure and burn rate profiles match;
- Compression Heat Release (CHR): amount of integrated energy release during compression;
- Fuel injected late: quantity of fuel injected late to support the burn rate.

The CPOA model created is made of three components:

- The analyzed cylinder, in which the temperatures of the head, piston and cylinder are imposed to evaluate the heat exchanges;
- The injector, which imposes the mass-flow rate, the quantity of hydrogen injected and the timing;
- The cranktrain, which simulates the crankshaft mechanism, its frictions and in which the start of the cycle is imposed.

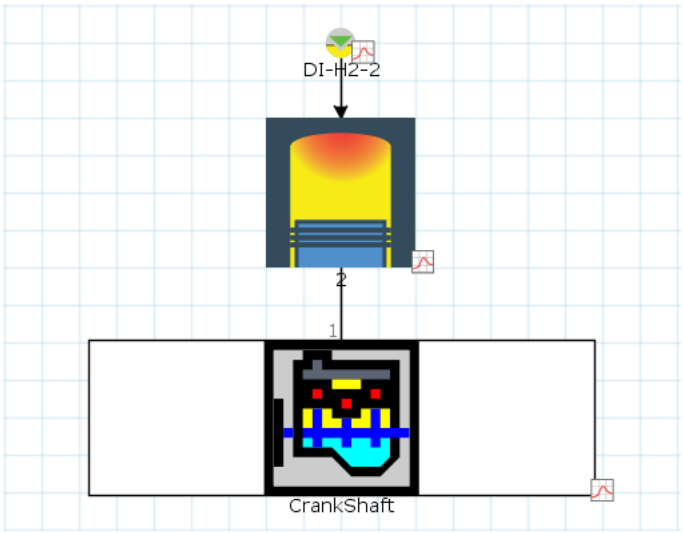

Figure 3.34: CPOA model

The majority of the 3D-CFD simulations have been run in the CA interval 260°-860° and the missing part of the cycle, referred to the initial exhaust phase, has been considered equal to the same of the 1D-CFD cycle used to extract the boundary conditions for the corresponding 3D-CFD simulations. The quantities needed to run the analysis are the initial conditions, such as the thermodynamic and chemical conditions, and the final ones, which are based on the residual fuel mass fraction. The angular moment considered for the initial conditions has been the Intake Valve Closing (IVC), CA = 570,6° already summing up the valve lash, while for the final ones the CA selection has depended on the cases; in fact, the parameter considered to rule the final conditions has been the End Of Simulation (EOS) of each case, since that varied from a minimum of 810° up to a maximum of 860°.

To have a better match between the 3D-CFD and 1D-CFD profiles, in the CPOA the Overall Convection Multiplier has been imposed equal to 1.3 and the CR has been reduced from 11.78 to 11.5 to take into account the possible loss of gases in the combustion chamber due to the blow-by.

From the results of the CPOA, it has been possible to make a comparison with the 3D-CFD profiles of the combustion process. The burn rate and cumulative burn rate profiles have been analyzed and later used as references for the complete 1D-CFD model on the entire dimensional plan.

The final goal of the activity has been the capability of the 1D-CFD model to predict the combustion process on all the points of the dimensional plan. The development of a predictive combustion model led to the selection of the *SI-Turb* combustion model among all the ones available in the GT-SUITE library. The synergetic approach with the 3D-CFD analysis helped in obtaining and using the profiles of λ on the flame front as input. The *SI-Turb* model is based on four parameters that rule the flame front development and the combustion process:

- Flame Kernel Growth Multiplier: multiplier used to scale the calculated value of the growth rate of the flame kernel;
- Turbulent Flame Speed Multiplier: multiplier used to scale the calculated turbulent flame speed;
- Taylor Length Scale Multiplier: multiplier used to scale the calculated value of the “Taylor microscale” of turbulence;
- Dilution Effect Multiplier: multiplier used to scale the effect of dilution (residuals and EGR) on the laminar flame speed; in this activity, it has been imposed as “def (=1)” [15].

The model previously used for the CPOA has been reproposed and updated for the *SI-Turb* calibration process. In fact, the values related to the parameters influencing the turbulence and previously optimized, and the equivalence ratio over mass fraction burned profiles obtained from the 3D-CFD analysis, that considers stratification, have been added to it.

The dataset of 24 cases used to calibrate the turbulence model has been reduced to 15 cases after having analyzed the results coming from the CPOA; it appeared difficult to properly replicate in a 1D-CFD environment the cases that exhibited a too slow combustion very close to a misfire event. To avoid the risk of obtaining combustion results influenced by these cases, it has been decided to remove them from the calibration dataset.

Two optimizations have been performed: one without stratification imposed and the other with stratification imposed. In the latter, the ϕ - x_b profile extrapolated from the 3D-CFD analysis of each considered case has been imposed. The optimization process target has been the Improved Burn Rate RMS Error in both cases. The optimizations have aimed at finding a single set of values able to minimize this error. The obtained values are reported in Table 3.2 and Table 3.3.

Attribute	***Value***
Flame Kernel Growth Multiplier	11.99
Turbulent Flame Speed Multiplier	9.99
Taylor Length Scale Multiplier	5.72

Table 3.2: Results of the optimization without stratification imposed

Attribute	*Value*
Flame Kernel Growth Multiplier	11.99
Turbulent Flame Speed Multiplier	9.99
Taylor Length Scale Multiplier	7.76

Table 3.3: Results of the optimization with stratification imposed

The optimization processes could have been refined by optimizing the set of values for each case separately to obtain the smallest possible error depending on the operating conditions of the case under examination; however, in this activity, it has been taken into account the possibility of finding a single set of values able to minimize the error of all the cases studied.

In the following are reported the results obtained from the optimized combustion models on three different cases, one for each working point, taken as a representative of all.

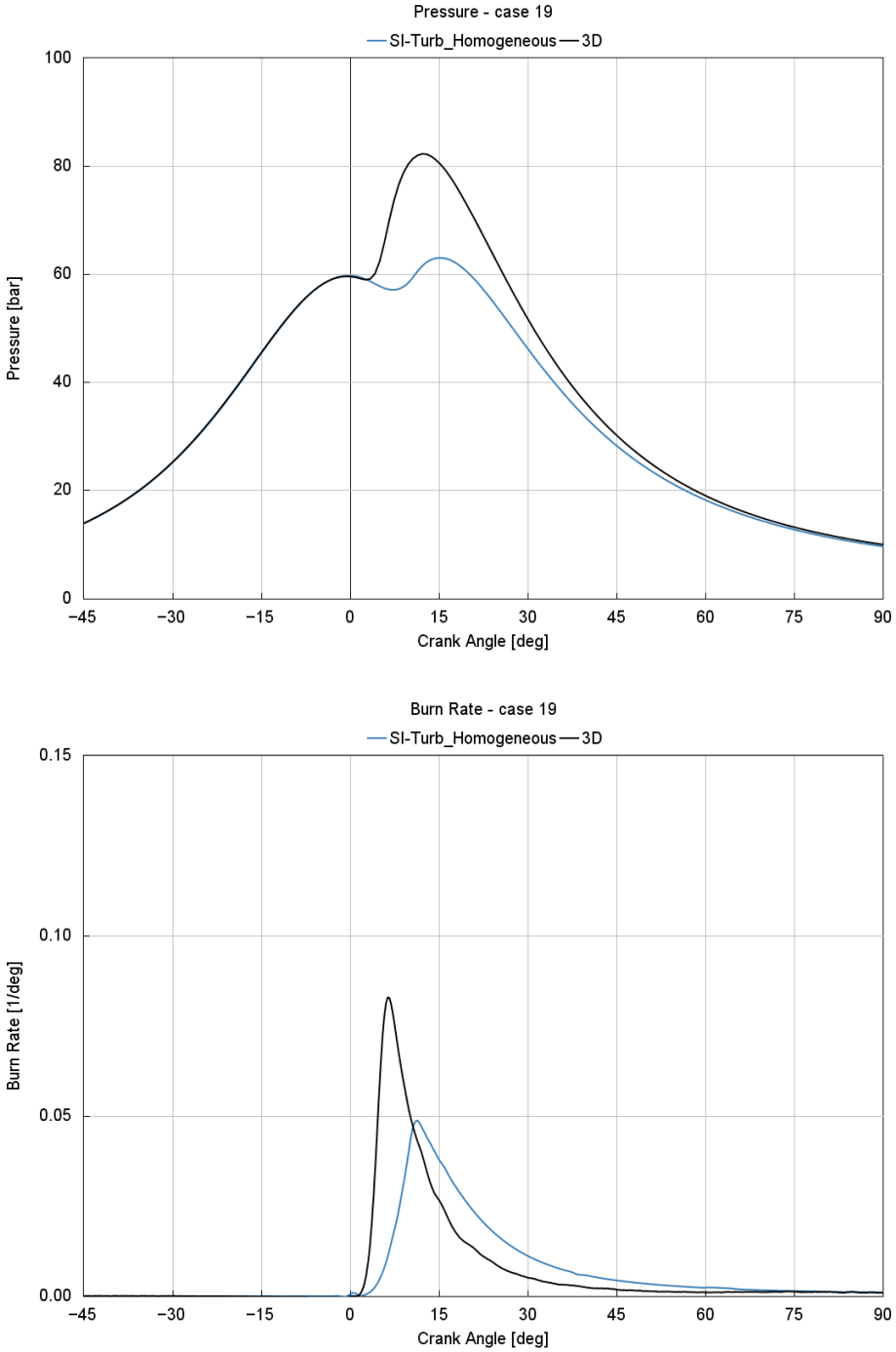

Figure 3.35: Pressure-CA (top) and Burn Rate-CA (bottom) profiles obtained from the optimization without stratification, WP3, case 19

At high-speed high-load conditions, the SI-Turb model without stratification imposed can't follow the trend of the 3D-CFD results and underestimates both the values of pressure and burn rate over crank angle. The latter shows a too-slow value increase and a too-low peak value.

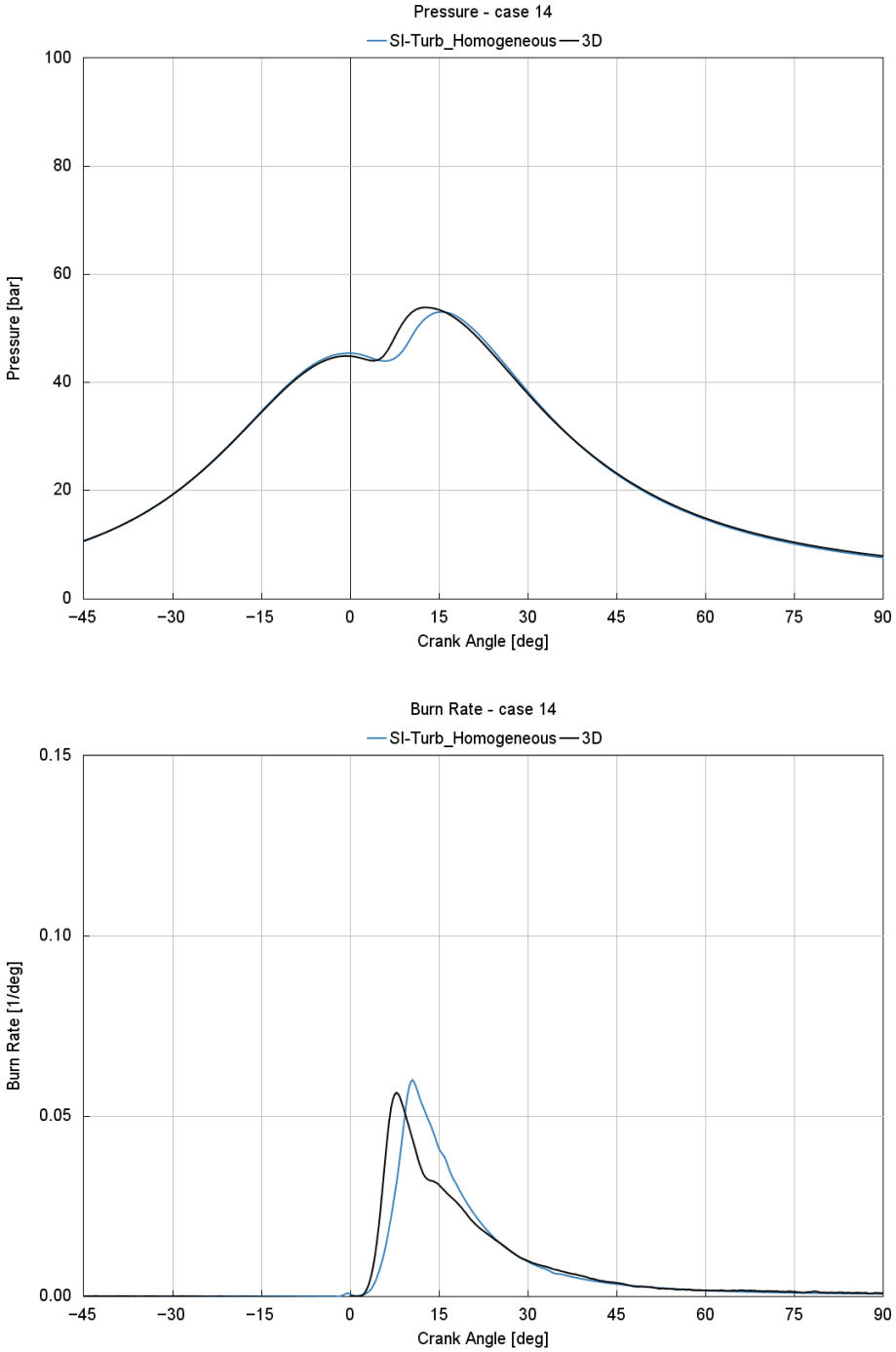

Figure 3.36: Pressure-CA (top) and Burn Rate-CA (bottom) profiles obtained from the optimization without stratification, WP2, case 14

Reducing the speed and the load, the results appear to better match the 3D-CFD profile of both pressure and burn rate over crank angle. The imposed combustion model shows a late pressure ramp-up after ST which is also mirrored in the slower burn rate increase.

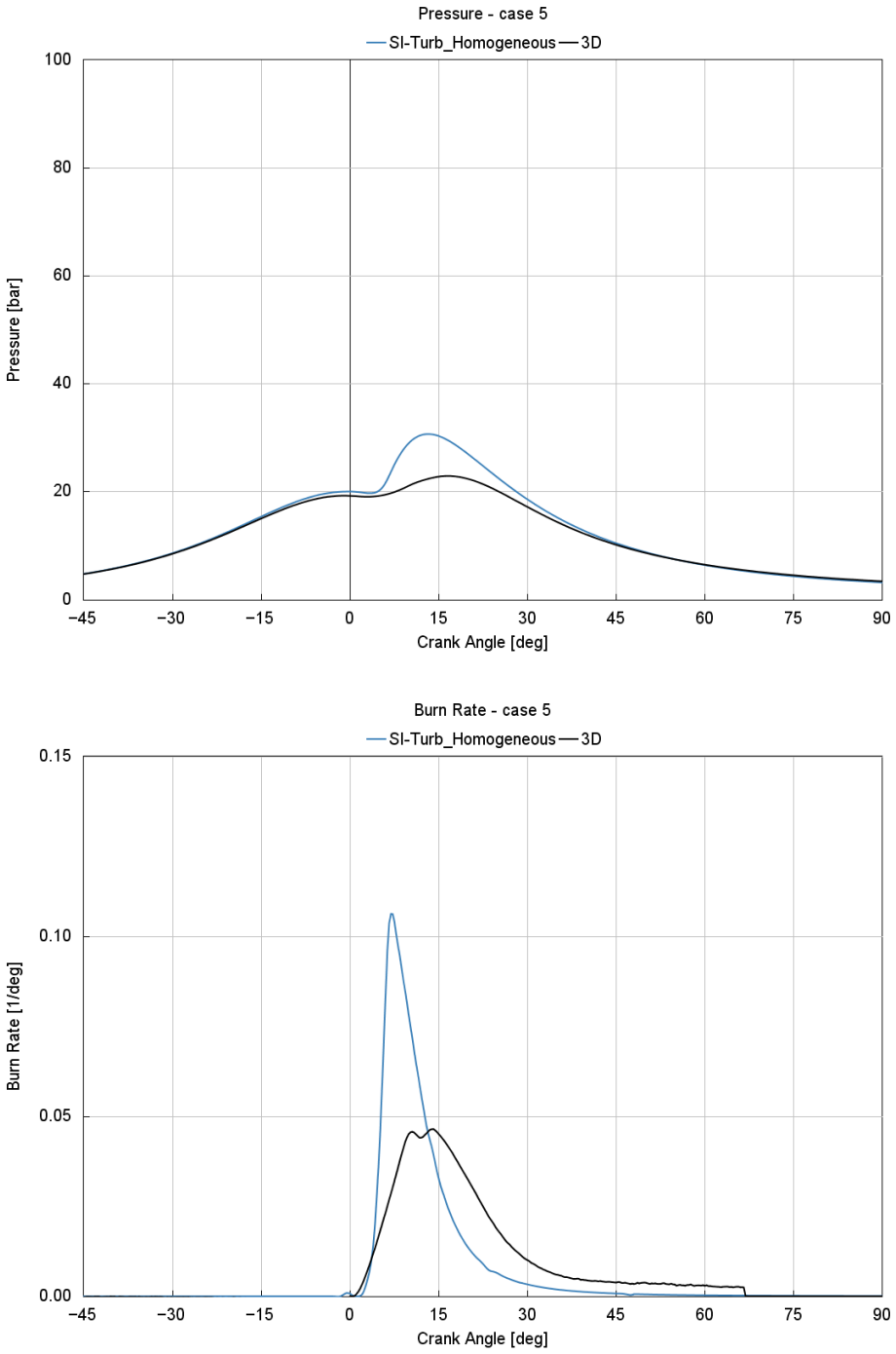

Figure 3.37: Pressure-CA (top) and Burn Rate-CA (bottom) profiles obtained from the optimization without stratification, WP1, case 5

At the lowest-speed lowest-load working point instead, the combustion model behavior is the opposite: it appears not to be able to follow the 3D-CFD profile which exhibits a slow combustion process. The result is an overestimation of the pressure and burn rate over crank angle values.

Once the results obtained with the combustion model without stratification imposed have

been analyzed, the model with the stratification imposed through the ϕ - x_b profile extrapolated from the 3D-CFD analysis has been run and a comparison between the two optimizations has been made.

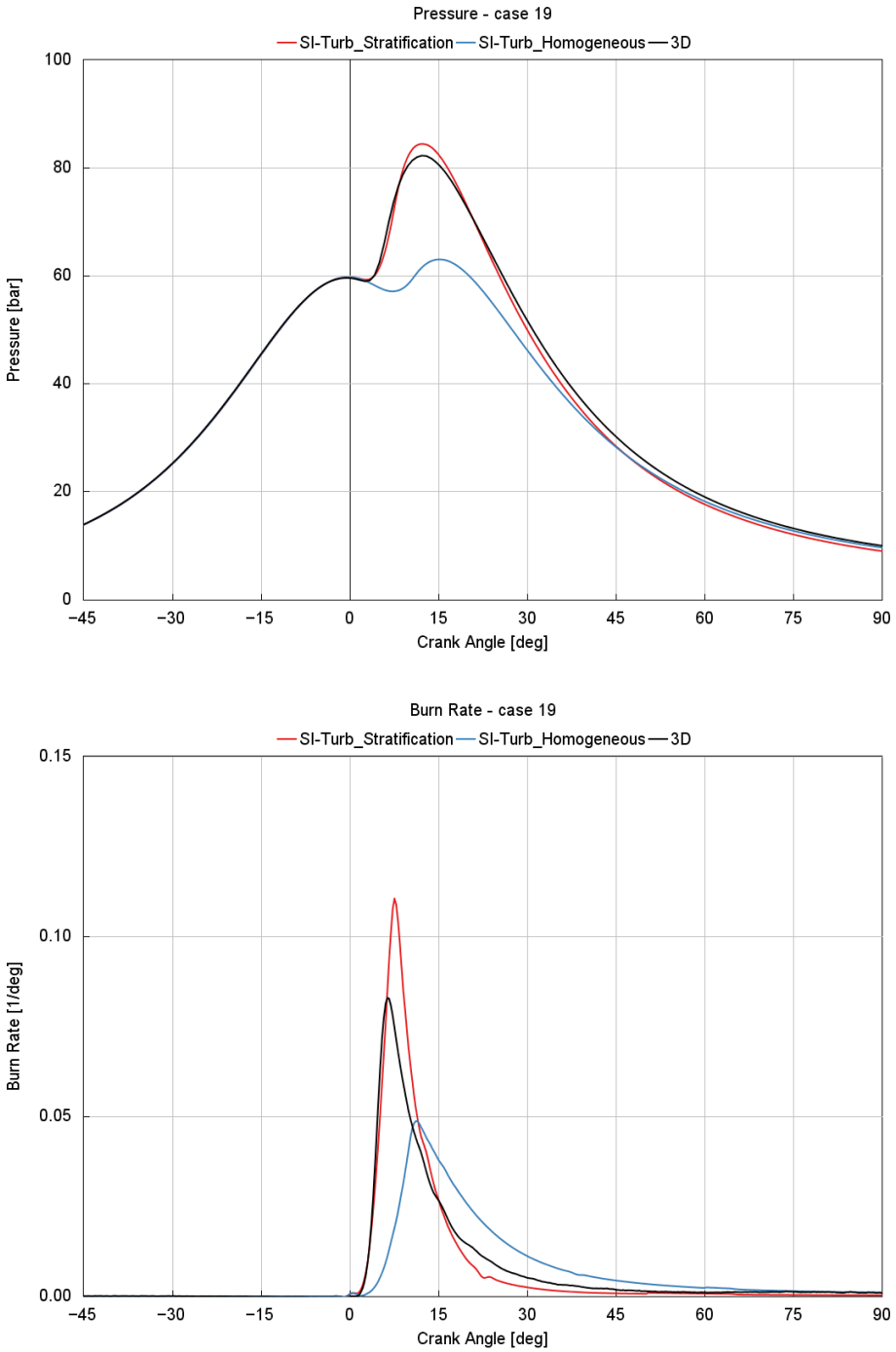

Figure 3.38: Comparisons between profiles obtained without and with stratification on P-CA (top) and BR-CA (bottom), WP3, case 19

The profile of the combustion model with stratification imposed better predicts the trend of the 3D-CFD results at high-speed high-load operating conditions. The match between these two profiles immediately after ST is very good, but the combustion model overestimates the peak value of the burn rate and it reaches a slightly higher value of peak pressure.

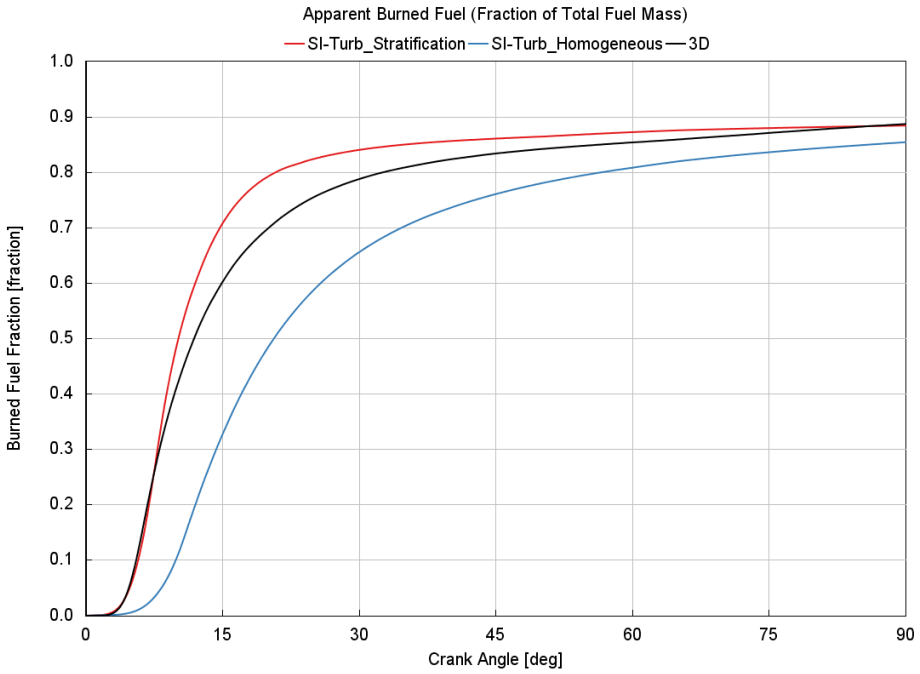

Figure 3.39: Burned Fuel Fraction profiles of the optimizations without and with stratification, WP3, case 19

The burned fuel fraction highlights the behavior of the two different optimizations. It appears to be clear that at this working point the model calibrated with stratification gives back a better match with the 3D-CFD profile with respect to the one without it. This last, in fact, exhibits a lower combustion efficiency. It can be stated that at WP3 the set of values optimized can predict in a good way the combustion process, apprehending that the results will slightly be overestimated around the maximum pressure point.

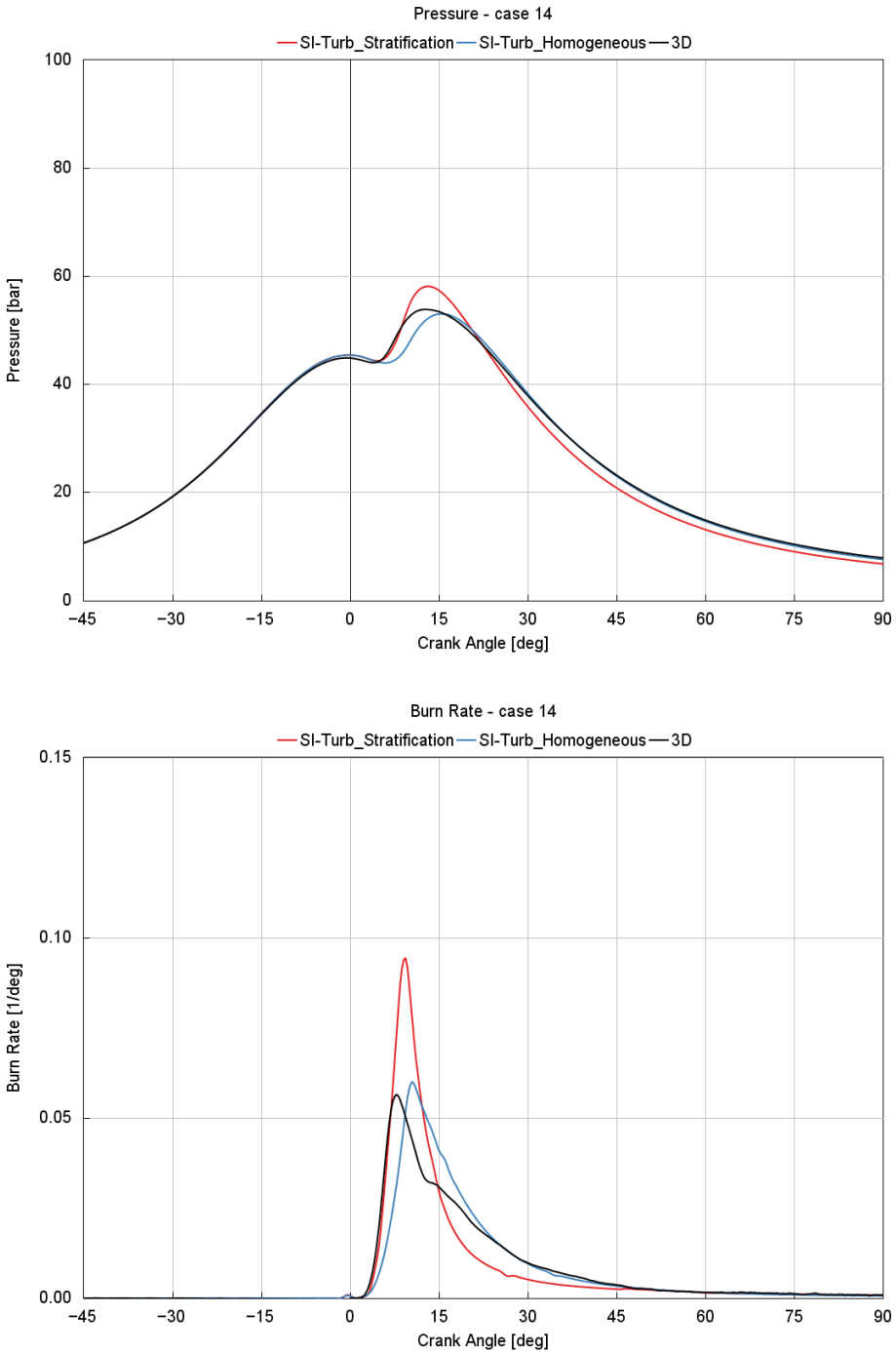

Figure 3.40: Comparisons between profiles obtained without and with stratification on P-CA (top) and BR-CA (bottom), WP2, case 14

At WP2, imposing the stratification to the combustion model doesn't improve the already good results obtained with the model without stratification. The only improvement obtained can be noted in the way in which the profile with stratification matches the ramp-up in pressure immediately after ST; the same match is therefore found in the burn rate where, however, the peak value is overestimated. For this reason, the pressure profile of

the combustion model with stratification exhibits higher values of peak pressure.

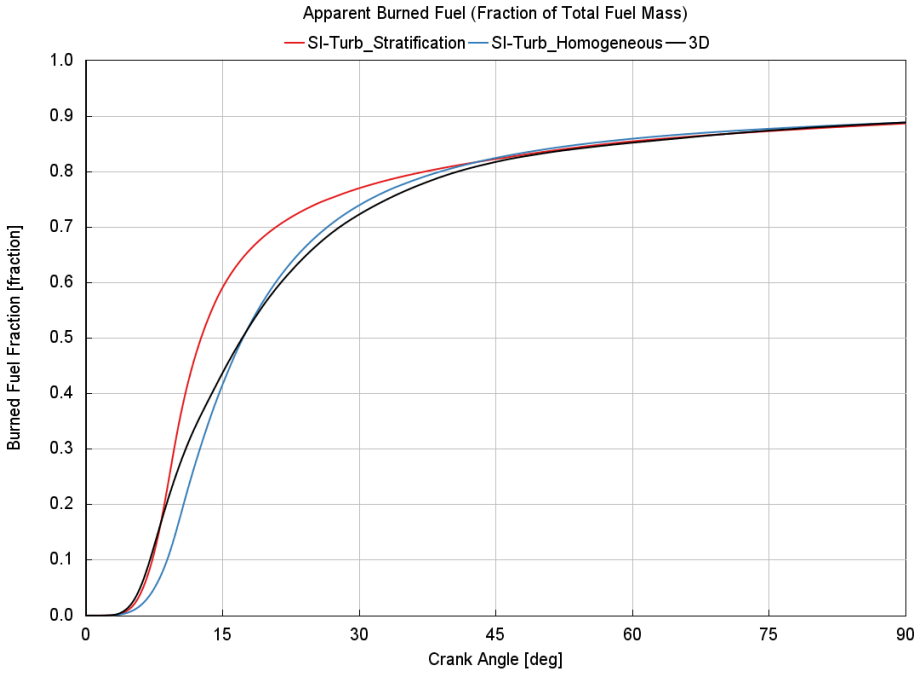

Figure 3.41: Burned Fuel Fraction profiles of the optimizations without and with stratification, WP2, case 14

Figure 3.41 highlights how at WP2 the combustion process trend is better matched by the model without stratification. However, in both cases, the burned fuel fraction values at the end of combustion symbolize a good combustion efficiency in comparison with the results coming from the 3D-CFD analysis.

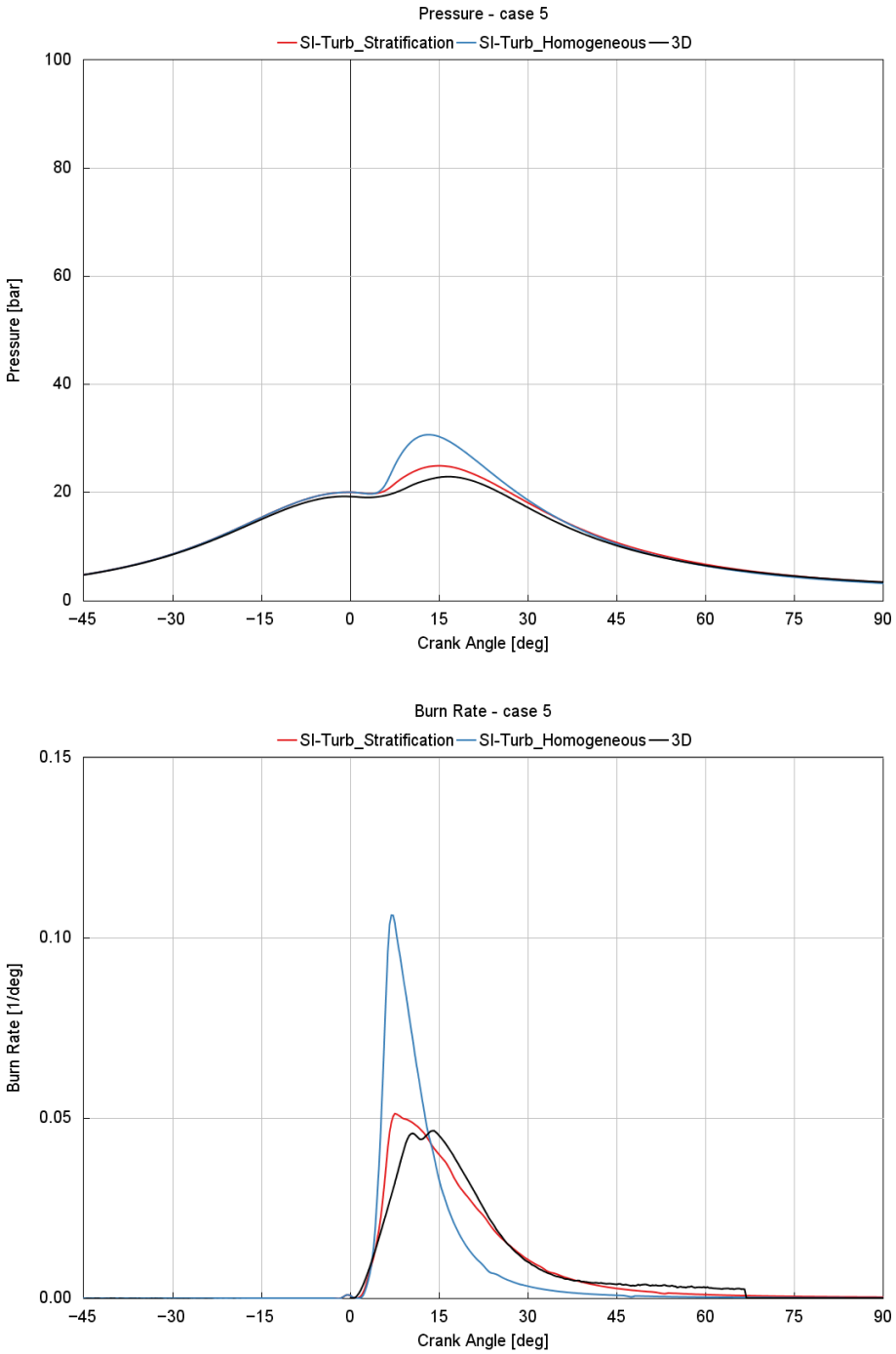

Figure 3.42: Comparisons between profiles obtained without and with stratification on P-CA (top) and BR-CA (bottom), WP1, case 5

At reduced load and speed, the pressure and burn rate over crank angle profiles are better matched by the combustion model implemented with stratification. After an almost equal ramp-up, the combustion model slope is even higher than the one of the 3D-CFD results, but the steeper ramp-up is quickly recovered and the profiles almost match during the ramp-down of the curves.

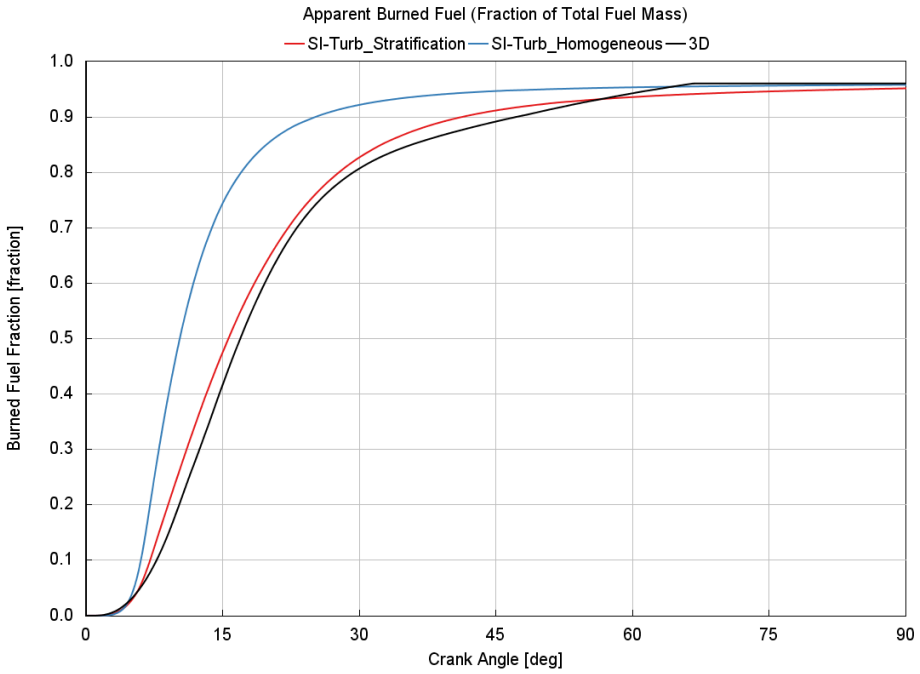

Figure 3.43: Burned Fuel Fraction profiles of the optimizations without and with stratification, WP1, case 5

The model with stratification follows in a very good way the burn rate profile coming from the 3D-CFD analysis highlighting a small overestimation of the same profile, but almost reaching the same value of combustion efficiency near the end of the process.

Comparing the results obtained from the calibrated model with stratification against the ones extrapolated from the 3D-CFD analysis has helped in having a better understanding of the goodness of the calibration performed. However, it has been necessary to extend this kind of analysis to all the cases considered to acknowledge the predictive behavior of the calibrated model. The five descriptive parameters of the combustion over which the goodness of the model has been evaluated are: the maximum pressure, the crank angle at maximum pressure, the crank angle at mass fraction burned at 10% (MFB10), the crank angle at mass fraction burned at 50% (MFB50) and the combustion duration (MFB10-75).

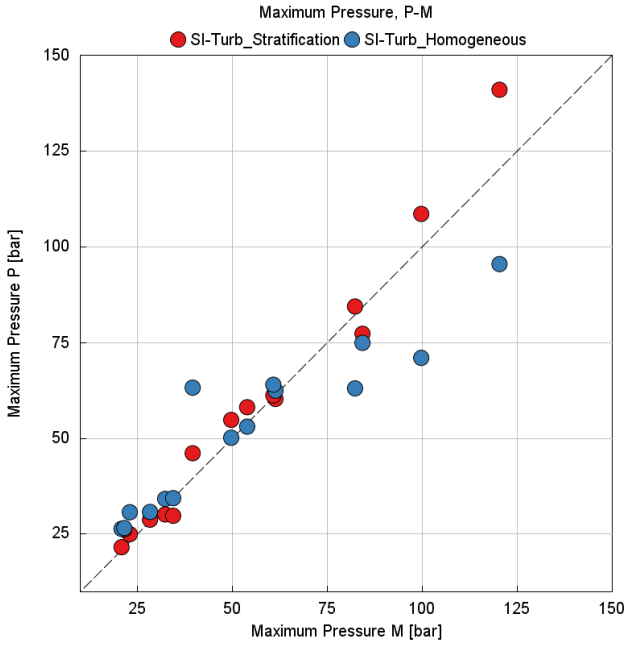

Figure 3.44: Maximum Pressure correlation plot, Predicted-Measured

The comparison between the two models optimized shows the tendency of the case without stratification to underestimate the maximum pressure value at high load conditions, where also the model with stratification gives back not so robust results. At low loads the differences noted have very little influence.

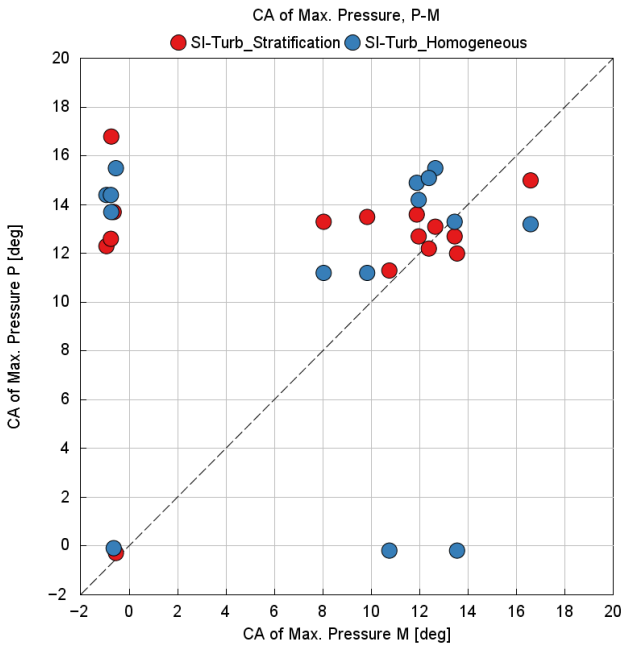

Figure 3.45: CA @ Maximum Pressure correlation plot, Predicted-Measured

Adding the stratification command to the SI-Turb model results in obtaining values of CA at maximum pressure acceptable or only overestimated. The low-speed combustions can be easily noted from the correlation plot.

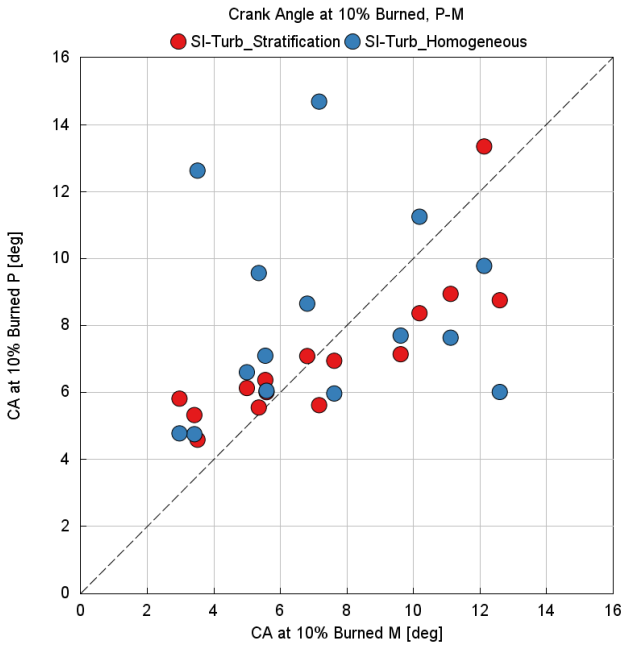

Figure 3.46: MFB10 correlation plot, Predicted-Measured

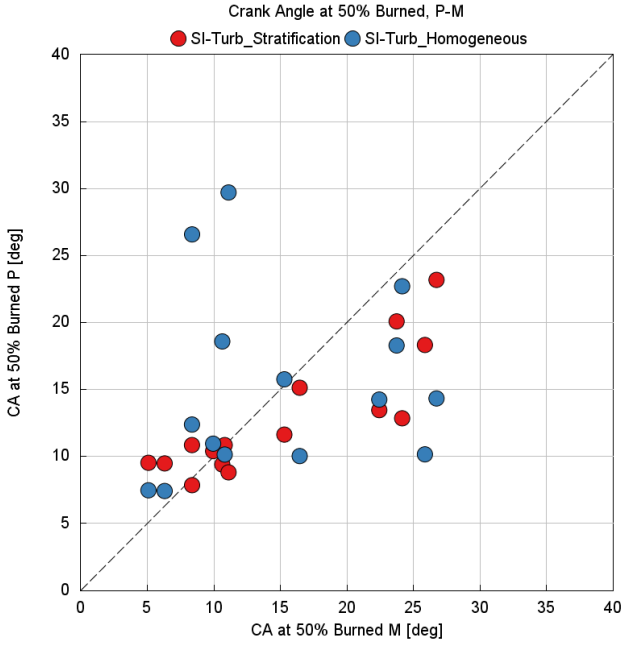

Figure 3.47: MFB50 correlation plot, Predicted-Measured

The correlation plots of MFB10 and MFB50 highlight the improvements obtained from the optimization model with stratification with respect to the one without it. Nevertheless, it must be observed how the results obtained are still far from the ideal bisector line, in particular for the MFB50. In general, the combustion model with stratification develops in slightly faster combustion events.

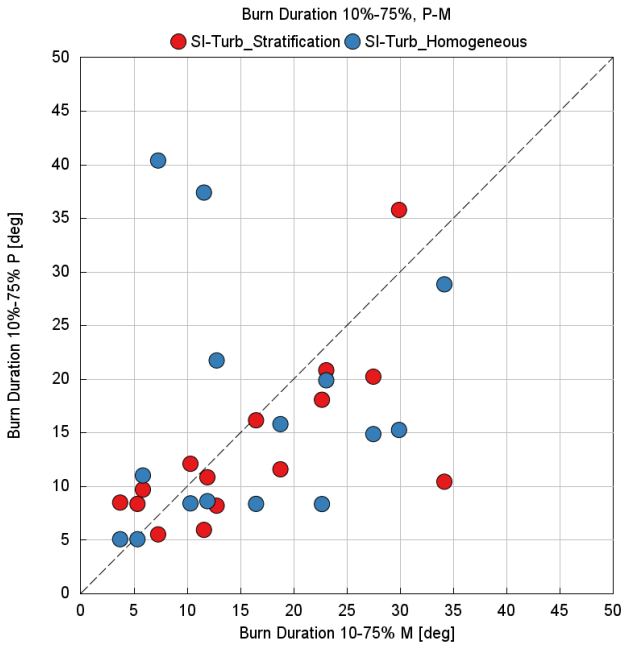

Figure 3.48: Burn Duration 10%-75% correlation plot, Predicted-Measured

The combustion duration shows the same trend as the MFB10 and MFB50, highlighting the little improvements obtained by adding the stratification command to the combustion model.

An overall summary can be made by analyzing the Root Mean Square Error (RMSE) values calculated for each of the two optimizations.

	RMSE w/o Stratification	RMSE w/ Stratification
Maximum Pressure [bar]	13.2	6.8
CA @ Max. Pressure [deg]	9.3	7.8
CA @ 10% Burned [deg]	3.9	1.8
CA @ 50% Burned [deg]	9.3	4.8
Burn Duration 10%-75% [deg]	13.1	7.5

Table 3.4: RMSEs of the models w/o and w/ Stratification on the five descriptive parameters of the combustion

The values in Table 3.4 highlight the goodness of the little improvements obtained with the calibration of the model with stratification imposed. Still, further refinements are needed to consider the model correctly predictive.

4 Conclusions and further developments

Climate change and environmental protection have become topics of crucial importance in the last decade. The importance of these topics has moved the OEMs to focus their attention on themes such as sustainability to comply with the current situation and the always more stringent legislations. In the transport sector, different technologies have been and are currently studied to try to enable its complete decarbonization. Among these technologies, one of the most promising ones is the hydrogen. This fuel can be exploited with different technologies such as Fuel Cells or ICE, both with a PFI or a DI configuration.

This thesis activity has focused on the study of a DI H_2-ICE. The aim of this work has been to develop a 1D-CFD predictive combustion model able to take into account the effects brought by the phenomenon of stratification introduced by the direct injection methodology. It has been necessary to develop a synergetic approach between 3D-CFD and 1D-CFD environments because of the lack of experimental data. At first, it has been necessary to analyze the 3D-CFD simulations provided in order to have a deeper understanding of the in-cylinder movements occurring during the injection event and the influence that the variation of SOI and λ had on the charge distribution at ST. Subsequently, during the combustion event, the λ - x_b profiles have been extrapolated for each case using two different approaches. Once all the needed data have been retrieved from the 3D-CFD environment, the activity has been moved to a 1D-CFD one. In GT-SUITE it has been decided to calibrate the *SI-Turb* model, which models the combustion process evolution starting from the turbulence levels, the laminar flame speed equation and an estimate of the turbulent combustion speed values. For this reason, a turbulence model has been created and the peculiar parameters of the turbulence have been calibrated and optimized to obtain the smallest possible errors of TKE and Normalized LS between the 3D-CFD and the 1D-CFD results. In the same way, a different model has been created to calibrate and optimize the turbulent flame speed characteristic parameters implemented in GT-SUITE; two different optimizations have been performed: a first one in which the profiles used to predict the stratification phenomenon haven't been considered and a second one in which they have. Eventually, it has been possible to make a comparison between these two optimizations. It has appeared that, in general, implementing the ϕ - x_b profiles extrapolated from the 3D-CFD results, helped in obtaining a better prediction

of the combustion process development. This has been noted at low-speed low-load working points, where the implementation of the stratification has helped in following in a better way the pressure and burn rate profiles of the cases analyzed, in particular for the combustion events that developed with a slower speed. Moving towards higher-speeds higher-loads cases, the prediction of the optimization with stratification imposed has returned better results with respect to the one without it in the majority of the cases. However, it has been noted a slight overestimation of these results considering the 3D-CFD ones used as reference. It must be concluded that the limited improvements obtained with the calibration of a predictive combustion model able to take into account the phenomenon of stratification with respect to one that doesn't consider it highlight the potentialities of the direct injection and the possibility of developing a fully functional and predictive combustion model able to predict the majority of the complex phenomena occurring in the combustion chamber.

Future studies will have the possibility to focus on specific topics that could improve the results obtained in this thesis activity such as:

- The injector placement to help the charge distribution into the combustion chamber;
- The number of injector holes to improve mixing;
- The implementation of a Miller cycle through a VVT system to improve the efficiency at specific loads;

Ultimately the potentialities of the direct injection as well as the complexity introduced by the stratification phenomenon have been faced and analyzed. It must, nevertheless, be highlighted that focusing on some criticalities and solving them will eventually bring to obtaining significant results.

5 Bibliography

[1] https://www.reuters.com/sustainability/eu-ministers-agree-watered-down-position-vehicle-emissions-2023-09-25/, accessed on 06 October 2023;

[2] https://single-market-economy.ec.europa.eu/system/files/2022-11/Euro%207%20factsheet.pdf, accessed on 28 August 2023;

[3] https://www.consilium.europa.eu/en/policies/green-deal/fit-for-55-the-eu-plan-for-a-green-transition/, accessed on 28 August 2023:

[4] Heid B., Martens C., Orthofer A., "How hydrogen combustion engines can contribute to zero emissions", McKinsey & Company 2021;

[5] https://www.hellonext.world/green-blue-and-grey-hydrogen-the-main-differences/, accessed on 28 August 2023;

[6] N. Matsubara, "A study of abnormal ignition in a hydrogen combustion engine", 10th International Engine Congress, Germany, February-March 2023;

[7] C. M. White, R. R. Steeper, A. E. Lutz, "The hydrogen-fueled internal combustion engine: a technical review", International Journal of Hydrogen Energy, January 2006;

[8] T. Wallner, A. M. Nande, J. Naber, "Evaluation of Injector Location and Nozzle Design in a Direct-Injection Hydrogen Research Engine", SAE International Powertrains, Fuels and Lubricants Congress Shangai, June 2008;

[9] T. Wallner, A. M. Nande, J. Naber, "Study of Basic Injection Configurations using a Direct Injection Hydrogen Research Engine", SAE International, 2009;

[10] V. M. Salazar, S. A. Kaiser, "An Optical Study of Mixture Preparation in a Hydrogen-fueled Engine with Direct Injection Using Different Nozzle Designs", Sandia National Laboratories, 2009;

[11] R. Scarcelli, T. Wallner, V. M. Salazar, S. A. Kaiser, "Modeling and Experiments on Mixture Formation in a Hydrogen Direct-Injection Research Engine", SAE International, 2009;

[12] R. Scarcelli, T. Wallner, N. Matthias, V. M. Salazar, S. A. Kaiser, "Numerical and Optical Evolution of Gaseous Jets in Direct Injection Hydrogen Engines", SAE International, December 2011;

[13] F. Pucillo, "Analisi numerica del processo di iniezione diretta e combustione in un motore alimentato a idrogeno", Master Thesis, Master of Science in Mechanical Engineering, April 2021;

[14] Zhang, Y., Mathieu, O., Petersen, E.L., Bourque, G. et al., “Assessing the Predictions of a NOx Kinetic Mechanism on Recent Hydrogen and Syngas Experimental Data,” Combustion and Flame 182 (2017): 122-141, https://doi.org/10.1016/j.combustflame.2017.03.019.

[15] GT-ISE Help, Reference Manual, Flow, Engine (GT-Power) References, Gamma Technologies